UNIVERSITY OF SOUTHAMPTON

# THE DEVELOPMENT OF HIGH POWER ND: LASERS AND THEIR APPLICATION TO STIMULATED RAMAN SCATTERING STUDIES IN GASES

by

David John Pratt

A thesis submitted for the degree of
Doctor of Philosophy

Department of Physics
Faculty of Science

September 1985

UNIVERSITY OF SOUTHAMPTON

ABSTRACT

FACULTY OF SCIENCE

PHYSICS

Doctor of Philosophy

# THE DEVELOPMENT OF HIGH POWER ND: LASERS AND THEIR APPLICATION TO STIMULATED RAMAN SCATTERING STUDIES IN GASES.

by David John Pratt

In the first part of this thesis we present work on Q-switched single longitudinal mode Nd: YAG laser operation, including an investigation of Fabry-Perot etalons, and experiments with a Nd: Glass laser as a potential source for tunable I.R. radiation. Both of these lasers were to be used as pump sources for Stimulated Raman Scattering (S.R.S.) experiments, to generate high power infra-red radiation.

For many applications, shorter pulses of around 100pS duration are required and in the second part of this thesis we present details of development work towards this aim. An actively mode locked (A.M.L.) laser was developed using an acousto-optic Bragg cell to perform the mode locking. A long pre-lase period is used to produce good mode locking, i.e. stable pulse durations and bandwidth limited pulses.

In the remainder of this thesis we consider the pumping of S.R.S in hydrogen and methane gas with 100pS pulses. The use of capillaries to confine the pump radiation and thereby lower the S.R.S. threshold is also investigated. We start by presenting a theoretical discussion of transient S.R.S. using tight focussing, capillary guiding and Stokes feedback. We then carry out experiments to confirm our calculations and investigate practical aspects. Reasonable agreement between theory and experiment is found. Finally we present details of S.R.S. pumped by a dye laser, itself synchronously pumped by a frequency doubled A.M.L. Nd: Yag laser. This system generated high power, tunable, infra-red radiation of high spatial and temporal quality.

CONTENTS

# 1. INTRODUCTION

Ever since the invention of the laser a quarter of a century ago research and development has been taking place to extend its wavelength coverage and increase its output power. In some regions of the spectrum this has been very successful. However, in the near and mid infra-red regions, (1-5$\mu$m), no completely satisfactory method of generating tunable laser radiation is presently available. One possible method of generating tunable near to mid infra-red radiation is stimulated Raman scattering (S.R.S.), from dye lasers. Consequently work has been and still is being carried out with the intention in improving this method as a technique.

The initial work, carried out as part of this thesis, was aimed at the development of single longitudinal mode (S.L.M.) Nd: Yag lasers with the particular aim of carrying out a careful study of S.R.S. in the gases hydrogen and methane. As part of this work capillaries would be investigated as a means for reducing S.R.S. threshold. This work would be a preliminary to using dye laser pumping. A single longitudinal mode laser would be necessary since only then can clean, reproducible results be obtained which can be compared with theoretical predictions for S.R.S.

As part of the exercise concerned with the development of an S.L.M. Nd: Yag laser, the technique of placing quarter wave plates around an etalon in order to allow its insertion at normal incidence was investigated. This technique, which is useful as it reduces tilt losses and allows the use of higher selectivity etalons, is described in chapter 2 after a brief outline of the methods used for obtaining S.L.M. Nd: Yag operation. In addition to the work on the Nd: Yag, Nd: Glass was examined since, unlike Yag, some degree of tunability, (a few hundred $cm^{-1}$), is obtainable. Nd: Glass can be used as a direct substitute for Nd: Yag and it was hoped that our S.L.M. techniques could be simply applied, just as with Nd: Yag. This work is also presented in

chapter 2, the conclusion however was not very favourable due to high thermally induced birefringence of the glass laser rod. It may be that in the future this work can be resurrected if an effective method of compensating for this birefringence, (e.g. using a slab laser), can be developed.

The S.L.M. work was a continuation of earlier work at Southampton and at a fairly early stage in the PhD programme the development of S.L.M. and its use in characterizing the S.R.S. process had reached a satisfactory conclusion. So, the decision was made to extend the Raman work to shorter pulses, (~100pS), with the longer term aim of pumping the Raman medium with tunable, synchronously pumped dye laser pulses. This laser would inturn be pumped by an actively mode locked, (A.M.L.), Nd: Yag laser. As a preliminary therefore this mode locked Yag laser has to be developed and then used, as the S.L.M. laser had been used, to characterise in detail the S.R.S. performance using these shorter pulses.

The bulk of this thesis is concerned with the development of the A.M.L. laser and the S.R.S. characterization using it, both with and without using a capillary waveguide. At a late stage in the PhD programme, J.K. lasers, (who sponsored this work in the form of a C.A.S.E. award), developed a synchronously pumped dye laser, pumped using an A.M.L. Nd: Yag laser. Consequently a visit to J.K. lasers was arranged in order to perform S.R.S. measurements using this laser. This work is also included in this thesis.

Chapter 3 of this thesis describes the theoretical and experimental work which was performed during the development of the A.M.L. Nd: Yag laser. Also described is the layout and performance of the synchronously pumped dye laser which was used in the work performed at J.K. lasers Ltd. Both of these laser systems produced well characterized pulses which contained sufficient energy for characterizing the S.R.S. process.

In chapter 4 we bring together the relevant theories which describe S.R.S. in hydrogen and methane using short pulses and with finite transverse beam profiles. The resulting theory predicts the S.R.S. threshold when under transient pumping conditions and either using tight focussing or a waveguide. These predictions are tabulated ready for comparison with the experimentally observed values given in chapter 5. Also in chapter 4 we consider briefly factors such as gas absorption, gas dispersion and efficiency considerations which affect the S.R.S. process. Papers containing details of some of the work carried out in chapters 4 and 5 are Hanna and Pratt, (1984) and Hanna, Pointer and Pratt, (1985), also enclosed as appendices 4 and 5 respectively.

In the last chapter of the main body of this thesis we describe the experimental measurements made on the transient S.R.S. process. In addition to simple measurements using tight focussing, we investigated the use of capillary waveguides and Stokes feedback as possible mechanisms for reducing the S.R.S. threshold energy. The use of a waveguide was particularly effective in this regard. To give an example, threshold for a 50pSec long pump pulse at 532nm was down to only 9$\mu$J. This brings S.R.S. as a technique for wavelength shifting within reach of dye lasers amplified using copper vapour lasers and the associated high repetition rates and average powers possible with this combination. Also in this chapter we compare the measured threshold values with those predicted in chapter 4. These values agree well and so allow successful conclusions and confident predictions of future work to be made in chapter 6.

## 2. LINE NARROWING AND SINGLE LONGITUDINAL MODE OPERATION

The usesof narrow linewidth laser sources are many, in particular the following are areas where they are extremely useful.

1. High power Nd: Glass amplifier chains: Here a single longitudinal mode is required since otherwise beating between modes will result in temporal structure and hence high intensity peaks which may cause optical damage in the amplifier chain. Consequently the whole system must be derated to operate at a lower power level. Alternatively where a fast electro-optic switch is being used to switch out a short ~1nS pulse then temporal structure will result in large amplitude fluctuations due to the random phase of this structure.

2. Non-linear optics experiments are much more satisfactory and easier to analyse theoretically if single frequency lasers are used. Lasers with temporal beating produce results which are not repeatable and this precludes accurate quantitive measurements. A simple example of this is second harmonic generation where temporal beating can result in an increased conversion efficiency. At Southampton we have used our $TEM_{oo}$, single frequency lasers to investigate accurately a variety of stimulated Raman and Brillouin scattering processes.

3. Holographic systems: When designed for illumination of large objects these systems require a laser source which has a coherence length larger than the dimensions of the object being pictured. Coherence lengths of a few meters are now needed for a number a holographic applications.

4. Tunable Lasers: Line narrowing is an integral part of the tuning process. Frequently, (e.g. for spectroscopy), it is required that the laser be line narrowed to a single longitudinal mode with a linewidth that is transform limited by the duration of the laser pulse.

This chapter describes work carried out on various aspects of line narrowing, some of which preceded the PhD program which is the subject of this thesis. A brief review of the entire field is

given in order to put in context the work which formed a part of this PhD program.

First we look at mode selection techniques in general, including a look at pre-lase Q-switching (Berry et al, 1981) and the use of electronic control (Hanna et al, 1983) to obtain a single longitudinal mode on every laser shot. Secondly we consider in some detail the use of etalons to select a single mode and a technique, using quarter wave plates, to improve their performance.

Finally we give a brief discussion of a Nd: Glass laser which was examined with a view to its potential as a source of tunable infra-red radiation.

## 2.1 A look at methods for line narrowing

In this section a brief description is given of the main devices used for line narrowing. The devices looked at are, gratings, prisms, etalons and resonant reflectors. Of these the first two are generally used for the initial stages of line narrowing with the later two used to complete the line narrowing, perhaps down to a single longitudinal mode.

In the later half of this section we discuss the most effective way of using these line narrowing devices. In particular we discuss increasing the build up time, suppressing any standing waves and other electronic methods for ensuring the laser operates on a single longitudinal mode on every shot.

### 2.1.1 Prisms, Gratings, Etalons and Resonant Reflectors

#### Prisms

Prisms provide a convenient method of tuning a laser medium over a large frequency range. They also have an inherently low insertion

loss if inserted at Brewsters angle and a damage threshold higher than most cavity elements. The disadvantage of prisms with respect to other methods of tuning a laser is the limited amount of line-narrowing obtainable and the need for a folded laser cavity.

When a light beam traverses a prism at or near minimum deviation one can derive the following equation (See Born and Wolf, 1980, p177).

$$\sin\left(\frac{\theta + \varepsilon}{2}\right) = n \sin\left(\frac{\varepsilon}{2}\right) \qquad 2.1$$

Where $\theta$ is the beam deviation through the prism, $\varepsilon$ the prism apex angle and n its refractive index relative to the surrounding medium. From this we can obtain:

$$\frac{d\theta}{dn} = \frac{2 \sin(\varepsilon/2)}{\sqrt{1-n^2\sin^2(\varepsilon/2)}} \qquad 2.2$$

which gives the angular dispersion as

$$\frac{d\theta}{d\lambda} = \frac{2 \sin(\varepsilon/2)}{\sqrt{1-n^2\sin^2(\varepsilon/2)}} \cdot \frac{dn}{d\lambda} \qquad 2.3$$

since we are working at Brewsters angle to minimize losses and at minimum deviation to minimise astigmatism we have $\varepsilon/2 = 90^{o} - \phi_B$ where $\phi_B$ is Brewsters angle.

Substituting this into equation 2.3 and using $\tan(\phi_B) = n$ gives

$$\frac{d\theta}{d\lambda} = 2 . \frac{dn}{d\lambda} \qquad 2.5$$

From experimental measurements on a laser with waist size 0.7mm an end mirror tilt of 0.5mRad was found necessary to introduce a loss of 50%. Using these figures and the value $\frac{dn}{d\lambda} = 2 \times 10^{-5} nm^{-1}$ appropriate to fused silica, we calculate that the half width half height linewidth to be,

$$\Delta\lambda = \frac{\Delta\theta}{2} \cdot \frac{d\lambda}{dn} = 12.5\text{nm} = 111\text{cm}^{-1} \text{ at } 1.06\mu\text{m}$$

Since the prism is normally used in a double pass arrangement this value will also correspond to the f.w.h.m linewidth of a single prism over a round trip.

This value is too large for most applications and so some means is needed to decrease this figure. Possible methods are:

a) to use multiple prisms in tandem
b) to use a larger spot size through the prism so decreasing the beam divergence and increasing the end mirror tilt sensitivity
c) to use a more dispersive prism material, (material with about 10 times the dispersion is available but is slightly lossy due to the close proximity of infra-red absorption lines).

Gratings

Gratings are capable of providing a very large degree of line narrowing. Their free spectral range is generally very large since the grating can be used at a low order while still maintaining a high selectivity. The reflection linewidth of a grating is given by twice the reciprocal of the depth of illumination on the grating, measured normal to the incident wavelengths. In a typical configuration this will be equal to about $1\text{cm}^{-1}$ which is significantly better than the figure obtained for a prism. The main disadvantages with gratings are their high insertion loss and poor damage thresholds.

The free spectral range of a grating is given by the grating equation,

$$2d \sin \alpha = m\lambda \qquad 2.6$$

where d is the groove spacing, m an integer, and $\alpha$ the beam angle of incidence relative to the grating normal. It follows that if m at the design wavelength is small then a very large change in $\lambda$ will be necessary before another diffraction order occurs at the same angle $\alpha$.

The linewidth of the main reflection peak can be estimated from Figure 2.1. In going from the main peak centre to the adjacent minima, the number of wavelength making up the distance L must change by half a wavelength. If this distance is 0.5cm, (a typical value) then this will correspond to a frequency change of $1cm^{-1}$

Figure 2.1

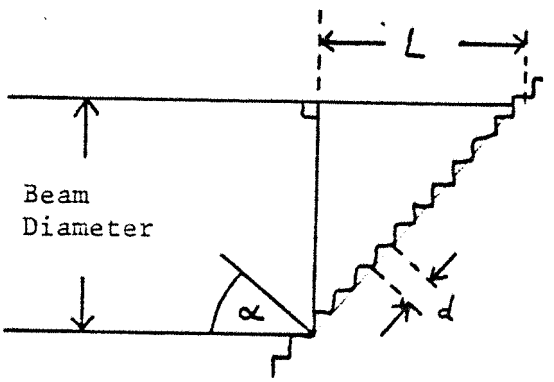


FIGURE 2.1 LIGHT INCIDENT ON A GRATING

It is because of this small linewidth that dye lasers with short cavity lengths can be made to operate on a single longitudinal mode using just a grating. In some circumstances the above linewidth may be too large, and in such cases beam expansion or grazing incidence techniques can be used to increase L. These techniques however, can also increase losses. An alternative is to use etalons and/or resonant reflectors.

## Etalons and Resonant Reflectors

In this section we take a look at the plane wave performance of etalons. A resonant reflector is simply an etalon used in reflection. The theory of etalons with plane waves is well known and is presented in many text books on optics, (e.g. Hecht and Zajak, 1974). The power transmission of an etalon is given by:

$$P_T = \frac{1}{1 + \frac{4R}{(1-R)^2} \sin^2(\delta/2)} \qquad 2.7$$

where R is the power reflectivity of the faces and $\delta$ the round trip phase shift given by $\delta = 4\pi nt/\lambda\cos(\theta)$ where n is the refractive index between the reflecting faces, $\theta$ the internal angle of incidence, and t the face separation. Similarily the power reflectivity of a resonant reflector is given by,

$$P_R = \frac{4R}{(1-R)^2} \cdot \frac{\sin^2(\delta/2)}{1 + \frac{4R}{(1-R)^2} \sin^2(\delta/2)} \qquad 2.8$$

Both of these equations are sketched in Figure 2.2 for a selection of face reflectivities. The etalon selects the wavelength at the peak of the transmission whereas the resonant reflector selects that wavelength with maximum reflectivity. From the figure we can clearly see that an increase in face reflectivity and hence finesse improves the etalon selectivity but for a resonant reflector the maximum selectivity is obtained with the smallest

FIGURE 2.2 THE FREQUENCY AND REFLECTIVITY DEPENDENCE OF ETALONS AND RESONANT REFLECTORS

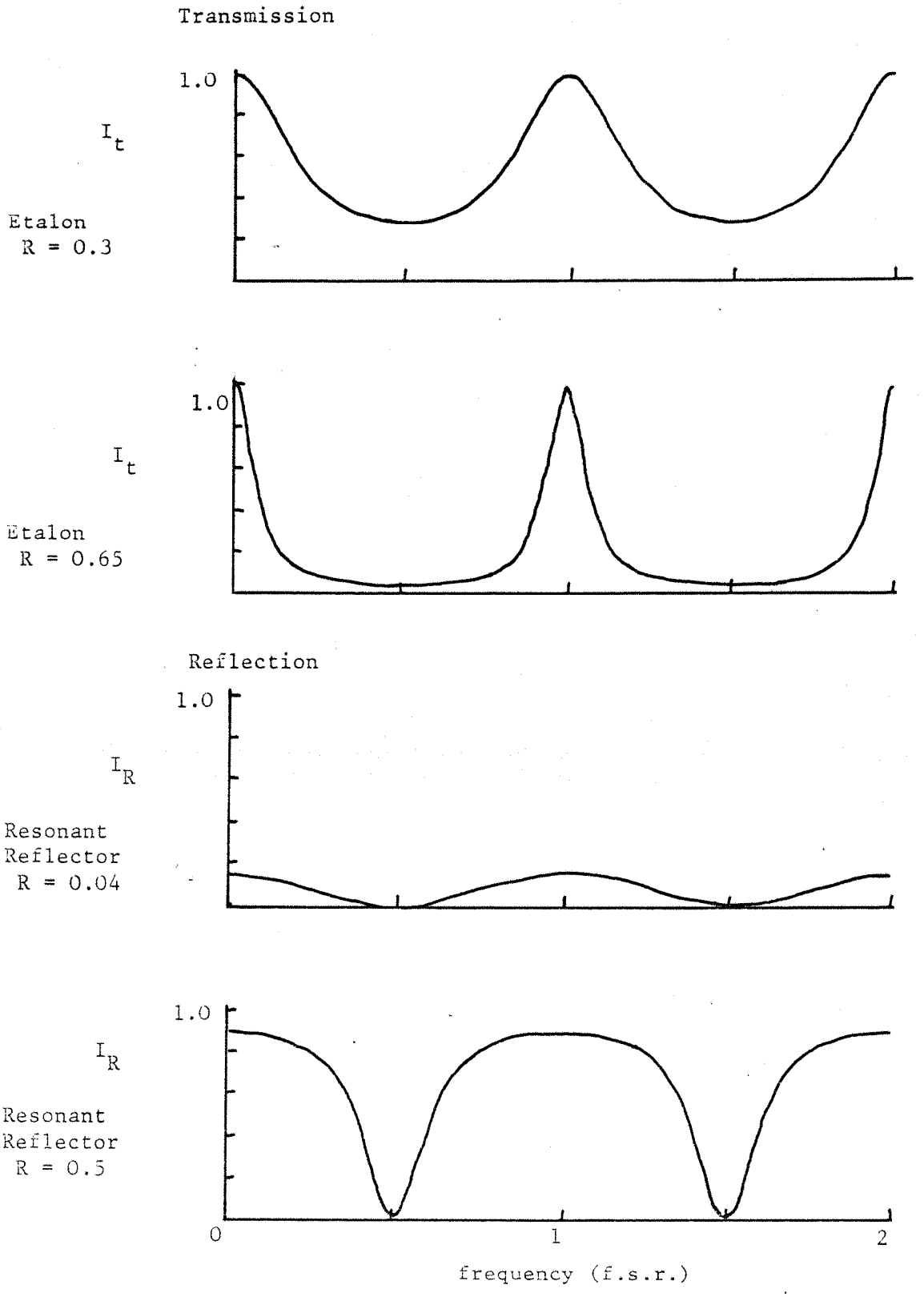


FIGURE 2.2

possible face reflectivity. The free spectral range of both devices (equal to 1/2nt) is the separation between adjacent peaks of the transmission/reflection profiles. For an etalon the finesse, defined as the ratio of the f.s.r. to the f.w.h.m. of the transmission peak, is given by $\pi\sqrt{R}/(1-R)$. These simple equations are sufficient to make initial estimates of etalon performance. In section 2.2 we analyse the etalon more thoroughly and predict effects due to tilt and finite beam geometry.

### 2.1.2 Practical aspects of using mode selectors

The choice of mode selectors required for any specific application depends on: the original laser linewidth, the insertion losses permissible, the damage susceptability of specific mode selectors, the cavity mode spacing, mode selector cost considerations and the degree of discrimination that is eventually required between any two cavity modes. The use of electronic and other techniques can assist the performance of the mode selectors chosen. For our Nd: Yag laser we require an intermode power ratio of at least $10^5$ (Berry et al, 1981) in order that no temporal ripple due to inter-mode beating can be observed, (i.e. less than 1% depth of mode beating). Using the technique of pre-lase q-switching described in section 2.1.3 we calculate that this can be obtained when the mode selectors introduce a round trip relative fractional loss between modes, $E_o$, of 2.5%.

#### An estimate of the probability of single mode operation in the presence of cavity length drift

Due to thermal fluctuations in the resonator cavity length, the cavity mode frequencies will be located randomly with respect to the centre of the etalon transmission profile. The general situation is depicted in Figure 2.3. The variable E is defined here as the round trip fractional loss due to the frequency

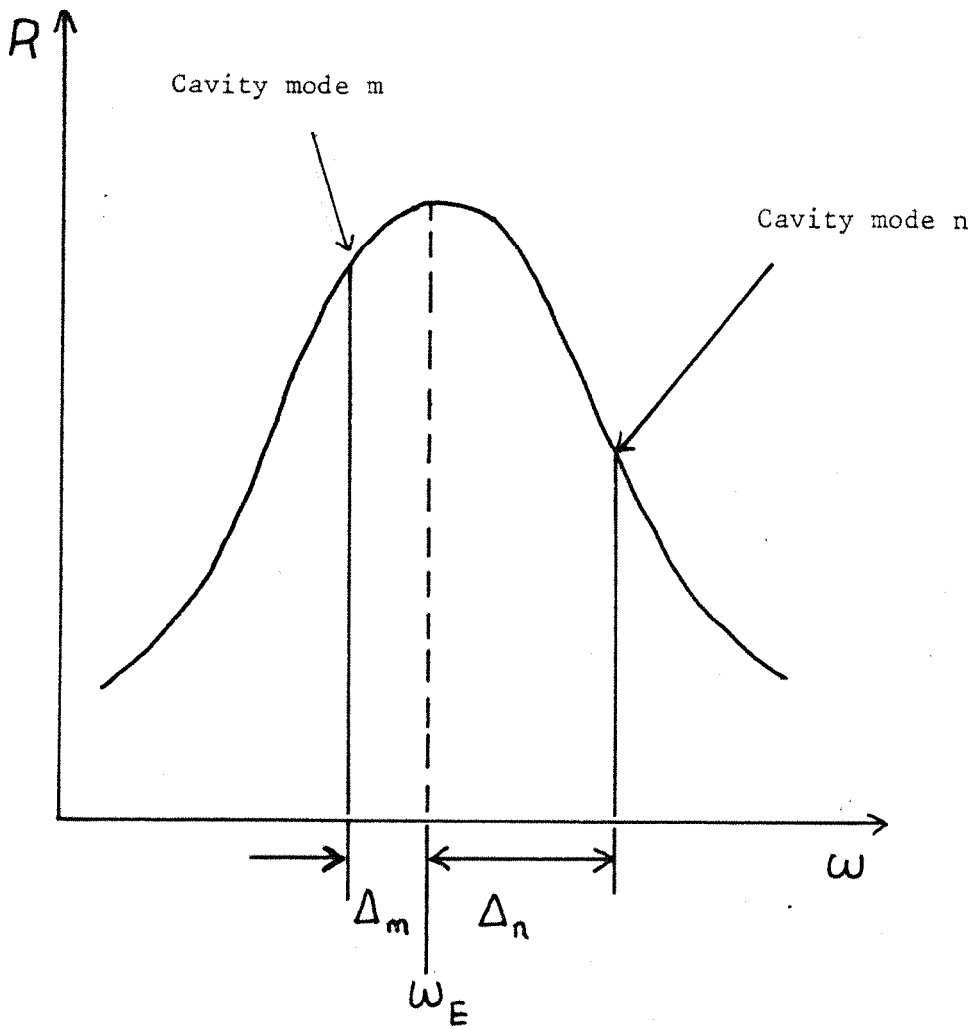


FIGURE 2.3: GENERAL LOCATION OF TWO CAVITY MODES m and n RELATIVE TO A REFLECTIVITY MAXIMUM OF A MODE SELECTOR.

selective elements, $E_m$, $E_n$ for the Mth and Nth modes respectively and $E_o$ the relative fractional loss requirement between the two modes. For small values of E we require,

$$\left| \frac{1 - E_n}{1 - E_m} \right| < 1 - E_o \qquad 2.9$$

to meet our definition of single mode operation. In Figure 2.3 we have marked $\Delta m$ and $\Delta n$, the spacings of the respective modes from the mode selector peak. The value of $\Delta m$ will drift randomly between zero and $\Delta/2$ where $\Delta$ is the cavity mode spacing ($\Delta = \Delta m + \Delta n$). If we expand the transmission profile about the peak as a Taylor expansion, we find all odd coefficients are zero. Neglecting 4th powers and higher (valid for small $\Delta m$, $\Delta n$) we can obtain values for $E_m$ and $E_n$ in terms of $\Delta m$, $\Delta n$ and the maximum possible discrimination, $E_{max}$, which are given by,

$$E_m = E_{max}\left(\frac{\Delta m}{\Delta}\right)^2 \text{ and } E_n = E_{max}\left(\frac{\Delta n}{\Delta}\right)^2 \qquad 2.10$$

Equation 2.9 can be rewritten using a binomial expansion as

$$\left|(1 + E_m - 1/2E_m^2 + .....).(1 - E_n)\right| < 1 - E_o \qquad 2.11$$

Substituting in equation 2.10, putting $\Delta n = \Delta - \Delta m$ and ignoring $E_n^2$ and greater terms we obtain:

$$\left(1 + E_{max}\left(\frac{\Delta m}{\Delta}\right)^2\right).\left(1 - E_{max}\left(\frac{\Delta-\Delta m}{\Delta}\right)^2\right) < 1 - E_o \qquad 2.12$$

which can be rewritten as

$$E_{max}(1-2\Delta m/\Delta) > E_o \qquad 2.13$$

if we neglect $E_{max}^2$ terms. Since $\Delta m$ has an equal probability of any value between zero and $\Delta/2$ we can write down a simple equation for $\rho$, the probability of a single mode shot, as,

$$\rho = 1 - \frac{E_o}{E_{max}} \qquad 2.14$$

Relative mode selector alignment

In addition to the frequency alignment of the cavity modes the mode selectors must be aligned with respect to each other and with respect to the gain medium so that one longitudinal mode has a gain larger, by at least the same factor $E_o$, than all other transmission peaks. With resonant reflectors this must be done by temperature tuning but with etalons angle tuning can also be used. In section 2.2 we show the calculated and measured values of tilt induced losses at typical tuning angles of 8 - 10m Rads. Some tilt is usually necessary in order to prevent parasitic lasing off the etalon faces, (see section 2.2), however, since additional tilt introduces more loss we want as small a tilt as posssible. For this reason it is best to align the etalon nearly orthogonal to the laser beam and to use temperature tuning as a mechanism for aligning the mode selector frequency peaks. In order to ascertain that the laser is operating on only one etalon mode selecting peak, the laser can be examined using a scanning Fabry Perot etalon external to the laser resonator, (see Sawyers, 1981, p126-127 for further details). The laser is fast Q-switched and frequency doubled so that a single frequency laser gives a single sequence of rings on a screen placed after the scanning Fabry-Perot etalon.

Increasing the buildup time

The linewidth of a laser depends on the selectivity of any line narrowing elements inside the cavity. It also depends however on the number of round trips that have occured since the amplification began from background noise. With fast q-switching

the gain in the laser is suddenly increased from zero to a factor, (in Nd: Yag), of about 5 per round trip. Since the background noise level is around $10^{-10}$W about 25 round trips will occur before the q-switched pulse emerges. The ratio of the output power in two competing modes is given by

$$\frac{P_L}{P_m} = \left(\frac{R_L}{R_m}\right)^n \qquad 2.15$$

where n is the number of round trips, and $R_L$, $R_M$ the effective mirror reflectivities for the respective modes. Using typical mode selectors $R_L/R_M = 0.95$ which gives for fast q-switching a ratio $P_L/P_M$ of 10. For the depth of modulation due to intermode beating to be less than 1% as required for our single mode laser we need a ratio $P_L/P_M = 10^5$ as mentioned earlier. From this it soon becomes apparent that a single mode laser, as defined, is impossible with fast q-switching unless line narrowing components of extremely high selectivity are used.

There are three commonly used methods of increasing the number of round trips so as to reduce the mode selector requirement.

A) Saturable absorber q-switching

This technique, also refered to as 'dye q-switching', consists of an optically bleachable dye placed in the laser cavity which initially prevents lasing. When the laser gain is just sufficient to overcome this additional loss, the circulating laser power slowly builds up until bleaching of the dye takes place. When this happens the dye loss rapidly decreases and the circulating power builds up into a short, high intensity q-switched pulse. During the initial slow build up of the circulating power around 500 round trips occur, resulting in a much more effective use of the mode selectors.

The problems of dye q-switching relative to electro-optic q-switching systems are as follows:

1. Dyes presently available for q-switching Nd: doped lasers are expensive and have a short lifetime making frequent dye changes necessary.

2. The time interval between the flashlamp trigger and the emission of the q-switched pulse shows a large jitter, typically of the order of 5-50$\mu$Sec. As a consequence of this the synchronous triggering of external components is difficult to accomplish.

3. Residual absorption remaining in the dye during the q-switched pulse emission results in a reduction of the output power.

B) Pre-lase q-switching

This technique, which is discussed further in the next section, was first reported by Hanna et al, (1972), 2 papers. The technique involves simulating a dye q-switch. A pre-determined voltage is applied to an intra cavity Pockels cell to almost prevent lasing resulting in the circulating power slowly building up over a number of round trips. This circulating power is monitored with a photodiode and when the "prelase" is detected the Pockels cell is opened resulting in the emission of a q-switched pulse.

C) Electronic feedback

If 500 round trips are insufficient then electronic feedback can be used to sustain the pre-lase for as long as the flashlamp pulse permits, (B. Luther Davies, 1979). In our work so far we have found 500 round trips to be sufficient and so this technique has not been pursued.

### 2.1.3 Pre-lase Q-switching

As stated earlier for single mode operation we require the power ratio between modes to be greater than $10^5$. Substituting this

value into equation 2.15 with n = 500 we find that E must now only be greater than 2.3%. This is a much easier criterion to meet than the 20% required when fast q-switching. Until now we have used the figure n = 500 for pre-lase q-switching without any justification. The aim of this section is to briefly go through the theory which gives rise to this value. Further details of the theory are to be found in Sawyers, (1981) and Hanna et al, (1972), 2 papers.

When the laser first reaches threshold the gain per round trip will continue to increase due to continued pumping from the flashlamp. During the small interval over which the pre-lase is building up from noise, this rate of increase in the gain can be considered constant since the flashlamp pumping will not change significantly during this period. After n round trips the effective gain per round trip for the pre-lase will therefore be given by $G_n = \exp(n\gamma T)$ where T is the round trip time (~7nsec) and the $\gamma$ rate of increase in gain per second, (the gain being expressed in a logarithmic format). From this we can obtain for the circulating power after n round trips the expression.

$$P_n = N_o \prod_{r=1}^{n} \exp\,(r.\gamma T) \qquad 2.16$$

where $N_o$ is the initial noise power from which the pre-lase originates. After some manipulation this can be written

$$P_n = N_o \exp\left(\frac{n.(n+1).\gamma\ .T}{2}\right) \qquad 2.17$$

which for reasonably large values of n can be re-written,

$$n \simeq \sqrt{\frac{2\ \mathrm{Ln}\ (P_n/N_o)}{\gamma.T}} \qquad 2.18$$

as an expression for the number of round trips that occur before the circulating power reaches $P_n$. Since a circulating power of

~100W is needed to trigger the photodiode, (and q-switch the laser), and the initial noise power, $N_o$, is around $10^{-11}$W, (smaller than the figure given earlier for fast q-switching due to the narrower final linewidth) we obtain:

$$n \simeq \sqrt{60/\gamma T} \qquad 2.19$$

In order to estimate $\gamma T$ we consider the gain pumped into the Yag rod over the entire flashlamp pulse. A gain of ~100, [=exp(4.6)], is pumped into the rod over a period of 200$\mu$S. Therefore over a cavity round trip time of 7nSec we obtain $\gamma T = 1.6 \times 10^{-4}$, which with equation 2.19 gives n = 610. With careful adjustment of the Pockels cells voltage it should be possible to obtain even higher values of n by ensuring that threshold is reached when the rod gain is nearly a maximum and $\gamma$ is consequently smaller.

Experimental work on pre-lase q-switching

The experimental work on pre-lase q-switching has been well covered elsewhere, (see Berry et al, 1981; Hanna et al, 1972, 2 papers; and Sawyers, 1981). As a result this section is just a brief summary of the recent work.

Most of the work on pre-lase q-switching in recent years has been carried out on a telescopic resonator which has the advantage of a large $TEM_{oo}$ mode volume whilst maintaining a cavity length of typically 1.3m. The mode selectors employed were either a 1cm thick etalon with 72% reflectivity faces or a 7.5cm thick uncoated resonant reflector, both devices made from fused silica. With the later device an additional thin uncoated etalon is required to ensure that only one resonant reflector peak dominates under the Nd: Yag gain profile.

Using the equation for the etalon finesse, $F = \pi\sqrt{R}/(1-R)$ we obtain an etalon transmission h.w.h.w. of $0.02cm^{-1}$. Since the cavity mode spacing is $0.004cm^{-1}$, we obtain using equation 2.7 the

maximum possible descrimination between two adjacent modes as $E_{max}$ = 4.2%. However, since the etalon is traversed twice this becomes 8%. A similar analysis of the resonant reflector yields $E_{max}$ = 9.5%.

Using the values $E_{max}$ = 9.5% and $E_o$ = 2.3% in equation 2.14 we find $\rho$ , the proportion of pulses which will have observable beating, to be about 25%. This is quite close to that observed experimentally using the following technique: A fused silica wedge with a wedge angle of a few degrees was inserted into the cavity, and the cavity then re-aligned. By moving the wedge laterally with a piezo-electric transducer the cavity length could be adjusted without misaligning the cavity. When scanning periodically through a range of lengths it was found that 25 in 140 pulses contained beating. Beating was monitored with an electric circuit which triggered a counter whenever a beating pulse was observed. The slight discrepancy between this measurement and theory could easily be acredited to uncertainty in the number of round trips occuring during the build up of the q-switched pulse.

### 2.1.4 Additional precautions needed for S.L.M. laser operation on every shot

This section describes a number of procedures which may be found necessary in order to obtain S.L.M. operation on every laser shot and which individually will improve the lasers performance in this respect.

a) Tilt of the laser rod

The end faces of the laser rod, although anti-reflection coated, can still introduce significant frequency selection since the rod acts as a gain enhanced Fabry-Perot etalon. If uncontrolled this frequency selection may act against the other mode selectors leading to two modes with equal gain and a non-S.L.M. output. To

eliminate this possibility the laser rod in our system is tilted to an angle of about 5mRad from the beam axis. This is sufficient to virtually eliminate any spurious mode selection from the rod faces.(for a more detailed account of gain enhanced etalons see Sawyers, 1981, section 4.2.5, part iii).

b) The use of quarter-wave plates around the rod to eliminate spatial hole burning

In a conventional standing wave resonator the standing wave pattern has differently positioned nodes for different longitudinal modes. As a result, when an S.L.M. laser is q-switched, inversion in the laser rod is not depleted at these nodes but remains to cause increased relative gain for other longitudinal modes. As a result of this a second q-switched pulse can emerge slightly after the first using this stored inversion. The effects of this can be minimized for adjacent modes by placing the rod near to one end mirror where for adjacent modes the standing wave patterns almost superimpose. An alternative method when using an isotropic gain medium is to place $\lambda/4$ plates around the rod. This eliminates the standing wave pattern as there are now two circular polarized, counter propagating beams in the rod, (Evtuhov and Seigman, 1965). This technique requires the optic axis of both $\lambda/4$ plates to be at $45^{o}$ to the cavity polarizer in order to ensure that both beams in the rod are circular polarized.

c) Elimination of the small remaining proportion of laser pulses which are not S.L.M

The technique of pre-lase q-switching is insufficient alone to obtain S.L.M. pulses on every shot since uncontrolled cavity length drifts and hence cavity mode frequency will always occasionally lead to two modes having approximately equal gains. This will happen less often if more powerful mode selectors are

employed, the possibility of it still happening however will remain. A number of techniques exist for eliminating the possibility of q-switching while two modes have roughly equal gains and hence intensities. These techniques have differing costs, capabilities and complexities and are outlined below.

1. Cavity length Stabilization; Invar steel or quartz cavity components together with temperature stabilization of the cavity elements works well but is a costly, cumbersome and elaborate way of overcoming this problem.

2. Cavity length control using a mechanically translatable silica wedge or piezo-electrically mounted mirror. This technique at its simplest involves translating laterally a wedge so as to alter the cavity length by $\lambda/4$ whenever a pulse with beats is observed on a fast oscilloscope. As a result one of the two modes with nearly equal gains will be shifted to near the top of the etalon profile and hence will dominate all other modes until the cavity length drifts by another $\lambda/4$. This technique only works if the mode selectors have high selectivity and the cavity length drift between successive laser shots is much less than $\lambda/4$. Limitations of this technique are that occasionally a pulse with beating occurs and that additionally an expensive, fast oscilloscope is continuously required to monitor the laser output. Both of these limitations are quite acceptable under some circumstances. A slight improvement in this technique is obtained if an electric beat detection circuit is used to mechanically translate the cavity length by $\lambda/4$ when beats are detected.

3. If it is required that no q-switched pulses with beating are allowed then the following technique can be used: An electronic circuit monitors the pre-lase as above and if beats are present also inhibits the opening of the Pockels cell q-switch, preventing the output of a q-switched pulse. This technique has the limitation that occasionally the laser misses a shot. The

technique which follows allows the S.L.M. operation of a laser with no beating and no missing pulses.

4. This technique involves monitoring of the prelase for beats during a sequence of initial relaxation oscillations. If the cavity length is swept by a suitable amount during these relaxation oscillations then one of the pulses will be found to be beat free and the laser can be q-switched.

This technique was first carried out at Southampton and further details can be found in Hanna and Koo, (1982). What is presented here is a brief outline of the technique together with its limitations. The technique applied at Southampton used the natural cavity length sweep induced in the Yag rod as a consequence of the pulsed flashlamp pumping. By setting the Pockels cell hold off volage slightly lower than usual for pre-lase q-switching it is found that 4 - 10 relaxation oscillations occur over a 10 - 20$\mu$s period. Consequently the natural cavity length sweep must be sufficient to sweep the cavity modes completely through the region where two mode operation occurs in this 10 - 20$\mu$s period. If this condition is not satisfied then occasionally none of the relaxation oscillations will be beat free and the laser will miss a pulse. Fortunately with Nd: Yag lasers this condition can be met provided a reasonable amount of mode selection is employed in order to narrow the region where two mode operation occurs. Using a 1cm long 72/72% reflectivity etalon and a 6mm uncoated resonant reflector a laser was built which gave a beat free, S.L.M. pulse on every shot. A diagram showing the block structure of the electronic circuitry employed is shown in Figure 2.4. The switch S was used to disable the beat detection circuit and hence allow performance comparisons with ordinary pre-lase q-switching.

FIGURE 2.4 BLOCK STRUCTURE OF ELECTRONIC SYSTEM FOR ENSURING A S.L.M. ON EVERY SHOT

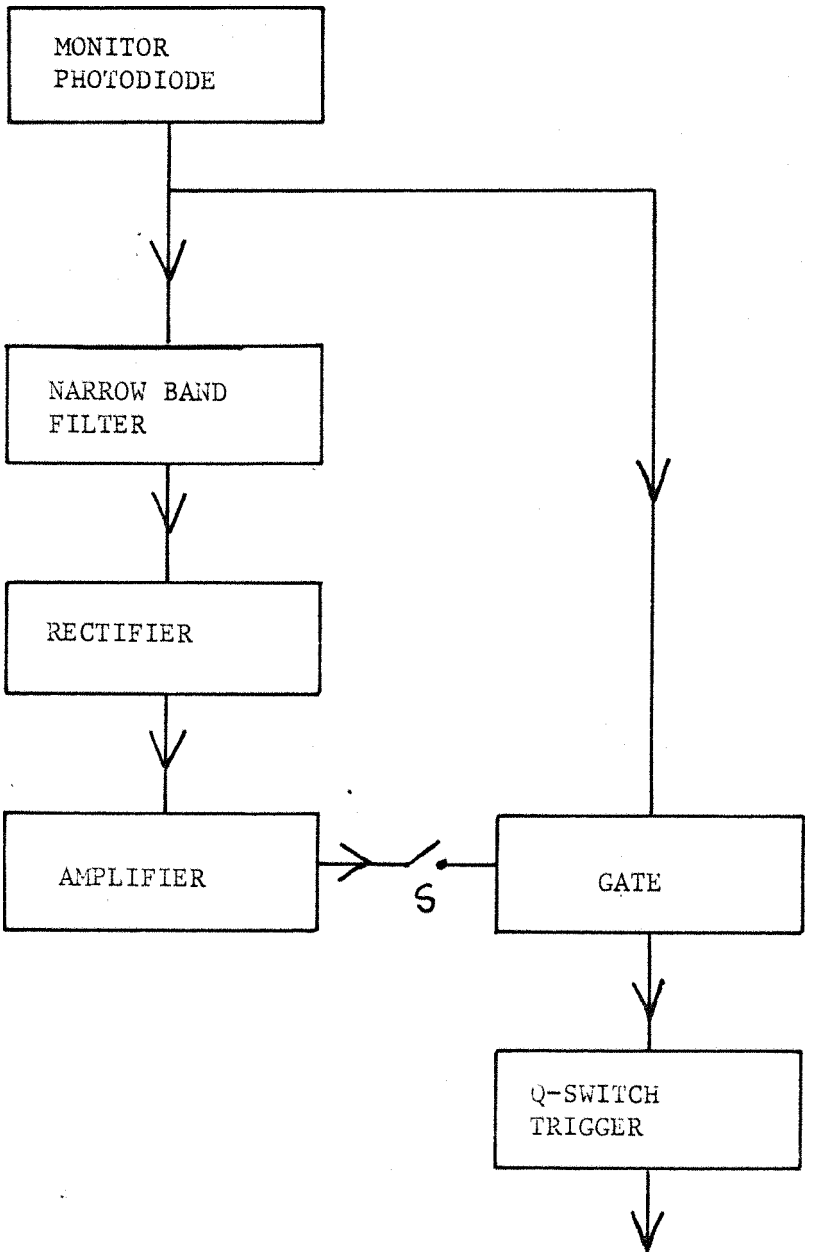


FIGURE 2.4

## 2.2 An investigation of etalon tilt losses and a method for using etalons at normal incidence

In section 2.2.1 we present the theory of etalon tilt losses and their degredation of finesse as a consequence of tilt. We then present in section 2.2.2 details of an experimental investigation of a technique allowing an etalon to be used with no tilt. In section 2.3 we give details of an experimental check to see that etalon losses agree with theory.

### 2.2.1 A theoretical analysis of etalon tilt losses

A limitation of the theory of plane waves with etalons occurs when the etalon is tilted since errors can be introduced as a consequence of lateral beam translation of the gaussian laser beam profile between successive reflections. In a laser cavity it is generally necessary to tilt the etalon to reject from the cavity the reflected laser beam. We therefore require an extended theory to take account of the Gaussian transverse beam profiles in our cavities.

Two references in the literature were found relating the problem of tilt, etalons and Gaussian beams. The first of these, (Arnaud, 1974), also includes the effects of diffraction in the analysis but only considers a single pass through the etalon. Leeb, (1975), considers a double pass but doesn't consider either diffraction or the degredation of finesse with tilt. In the remainder of this section we predict the double pass behaviour considering loss and finesse degredation using a similar technique to Arnaud and Leeb.

The performance of tilted etalons can be predicted by considering the interference of a Gaussian beam as it bounces back and forth inside the etalon. Figure 2.5 shows the situation with the various beams labeled. Since the etalon is generally employed in a double pass arrangement close to a cavity mirror, we also show the beams R which have passed twice through the etalon and also been reflected by the cavity mirror.

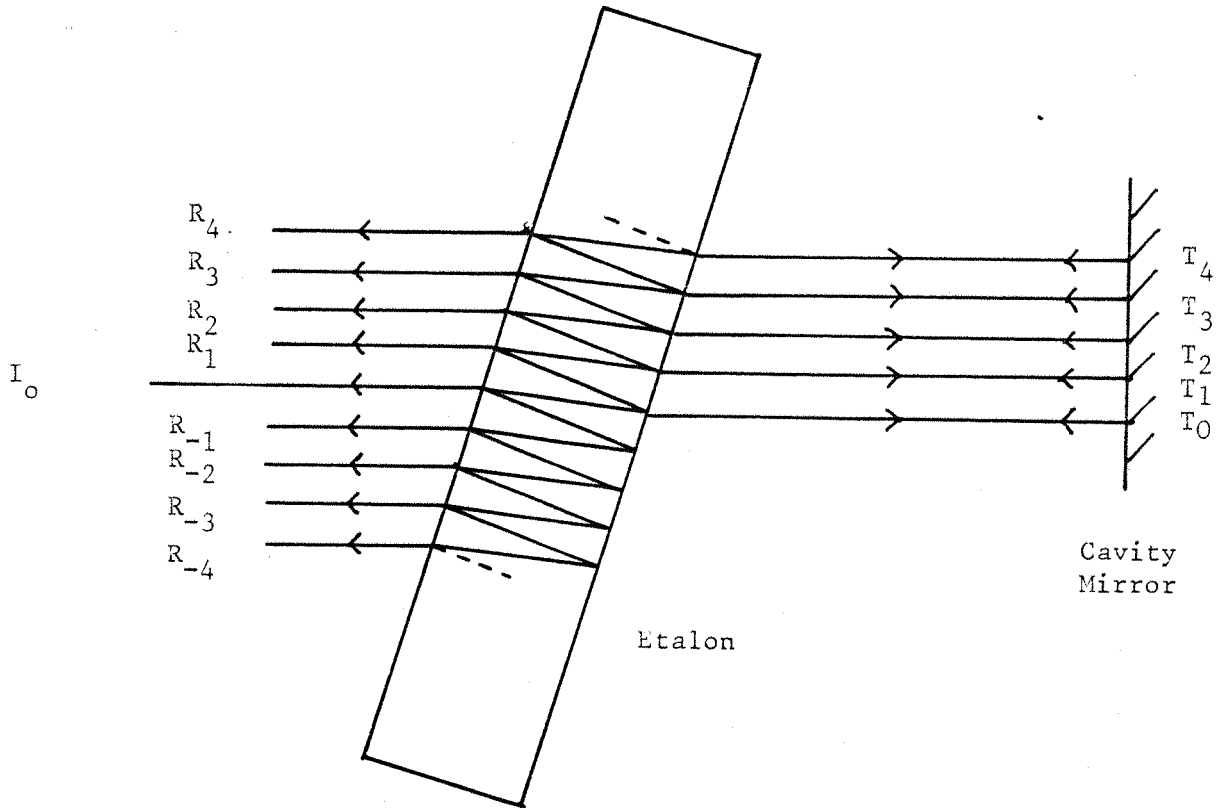


FIGURE 2.5 LABELLING NOTATION FOR BEAMS TRAVERSING A TILTED ETALON.

An incident Gaussian beam of peak amplitude, Eo, with a waist, W, will, upon traversing the etalon, be split into the various beams of amplitude $T_n$, (n>0). With the beams used in our resonator diffraction effects can be neglected over a few etalon round trips, hence we can consider all the beams $T_n$ to have the incident waist size W. The beam amplitudes $T_n$ can be written as

$$T_n = t^2 . r^{2n} . e^{in\phi} . E_o \qquad 2.20$$

where t, r are the amplitude transmission and reflection coefficients for the etalon surfaces and $\phi$ is the round trip phase shift of the etalon. At this stage the beams could be combined to give the total transmitted light. We however require the performance of an etalon used in a double pass arrangement with a plane mirror close by. Again we can neglect diffraction of the beams in propogating to and from the mirror and in passing a second time through the etalon. The beams of amplitude $R_n$ which are obtained after the second traversal of the etalon are given by:

$$R_n = t^2 \sum_{s=n}^{\infty} r^{2(s-n)} . e^{i(s-n)\phi} . T_s \; ; \qquad (n \geq 0) \qquad 2.21a$$

and

$$R_n = t^2 \sum_{s=o}^{\infty} r^{2(s-n)} . e^{i(s-n)\phi} . T_s \; ; \qquad (n < 0) \qquad 2.21b$$

If we substitute for $T_s$ we obtain after some manipulation

$$R_n = \frac{t^4 . r^{2|n|} . e^{i|n|\phi} . E_o}{1 - r^4 e^{2i\phi}} \; ; \text{ (for all n)} \qquad 2.22$$

To evaluate the round trip etalon transmission we consider the component of each returning beam which contributes to the incident Gaussian profile, i.e.

$$R_{TOTAL} = \sum_{n} K_n R_n \qquad 2.23$$

where $K_n$ is an amplitude factor given by:

$$K_n = \exp\left(\frac{-n^2 d^2}{2W^2}\right) \qquad 2.24$$

and is obtained from an overlap integral of the normalized Gaussian profiles of $R_n$ and $E_o$. The waist, W, is that originally incident and d is the lateral beam displacement due to tilt which can be expressed as $d = 2h.\sin\theta/\mu$, where h is the etalon thickness, $\mu$ its refractive index and $\theta$ the tilt angle of the etalon. Substituting equations 2.24. and 2.22 in 2.23 we obtain the total double pass amplitude reflectivity of the system to be

$$R_{TOTAL} = \frac{E_o(1-R)^2}{1 - R^2 e^{2i\phi}} \cdot \left[1 + 2 \sum_{s=1}^{\infty} R^s . e^{.is\phi} . \exp\left(\frac{-s^2 d^2}{2W^2}\right)\right] \qquad 2.25$$

where we have substituted r and t by the etalon surface intensity reflectivity R which is the parameter commonly used. As a check on the above calculation, with no tilt, i.e. d = 0, the term in square brackets becomes $(1 + Re^{i\phi})/(1 - Re^{i\phi})$, and direct comparisons can be made with equation 2.7 for an etalon with plane waves.

By multiplying equation 2.25 by its complex conjugate we obtain the total, double pass, intensity reflectivity which can be evaluated numerically. Equation 2.25 cannot be developed further analytically since no method exists to deal with the sum $X^s Y^{s2}$. In order to obtain the insertion loss of an etalon we set $\phi$ equal to zero in equation 2.25. Finesse degredation has been obtained by plotting equation 2.25 as a function of both tilt and $\phi$, however this work is not presented in this thesis. Figure 2.6 shows graphs of etalon tilt loss as given by various authors. The curve corresponding to equation 2.25 is identical to Arnaud's expression

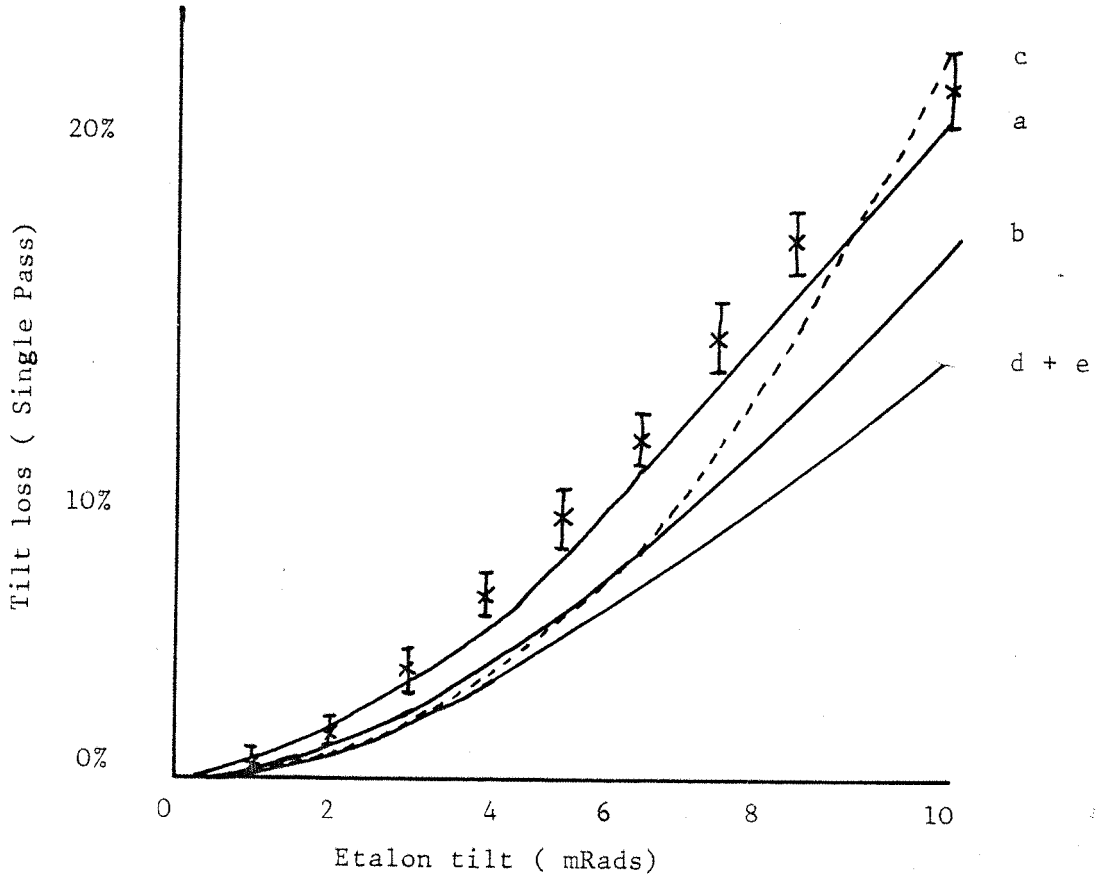


FIGURE 2.6 Additional single pass loss due to tilt as a function of tilt angle for the resonator configuration described in the text. Crosses represent experimentally measured values.

Full lines are theoretical predictions:

(a) Calculation following Arnaud et al, for transmission into the same Gaussian beam.

(b) Calculation following Leeb.

(c) Calculation using simplified expression due to Leeb.

(d) Calculation, following Arnaud et al for total transmitted power.

(e) Calculation, as detailed in text, single pass equivalent.

for the total transmitted power in a single pass. This is to be expected since our situation corresponds to Arnaud's repeated twice, the second time in the reverse order. Arnauds expression for the total transmitted power will also apply to the transmitted beam returning through the etalon and coupling into the incident beam as a consequence of reciprocity.

Also shown in Figure 2.6 are experimental measurements as described in section 2.23 and a simplified formula given by Leeb, valid for small angles, which is given by

$$L = \frac{8RC^2}{(1-R)^2} \quad \text{where } C = \frac{2.h.\cos\theta.\tan\theta}{\mu.W} \simeq \frac{2.h\theta}{\mu W} \qquad 2.26$$

All the curves given in Figure 2.6 correspond to the parameter values W = 0.7mm, R = 0.65mm, $\mu$ = 1.45 and h = 1.0cm.

Due to the divergence of the laser beam the amount of tilt that is generally required to prevent parasitic lasing is inversely proportional to the beam waist size. This in combination with equation 2.26 means that the loss typically introduced by using a tilted etalon is inversely proportional to the fourth power of the waist size. To give a typical example, a 0.7mm waist at 1.06$\mu$m wavelength requires a tilt angle of 3.5mRad at typical pump energies to prevent parasitic lasing of a 1cm thick 65/65% reflectivity etalon. This results in a calculated loss due to tilt of 9% per round trip in addition to any losses caused by absorption or unequal reflection coatings.

### 2.2.2 The use of $\lambda/4$ plates around the etalon to minimize tilt angle and hence insertion loss

In section 2.2.2 we mention that tilt is frequently used as a method of tuning etalons so that their tuning peaks coincide with each other and with the gain peak of the laser medium. With the use of temperature tuning some of this tilt can be avoided but still some tilt is required in order to decouple radiation

reflected by the etalon out of the cavity and to prevent parasitic lasing off the etalon faces. In a large number of situations this tilt requirement leads to significant additional insertion loss and a corrsesponding reduction in laser performance. Since the majority of lasing cavities employing etalons also use polarized light, we can use the technique of polarization rotation to decouple that radiation reflected from the etalon out of the cavity. By placing quarter wave plates on either side of the etalon, oscillation from etalon reflections is suppressed even when the etalon is aligned perfectly normal to the laser beam. At the same time oscillation is allowed, with minimum insertion loss, for light transmitted through the etalon and onto the laser resonator reflector. We shall now proceed to explain how this method works and the performance improvement achieved.

The principle of using a polarizer and quarter-wave plate to suppress feedback from reflections is well known in situations where the feedback arises from a component outside the laser (see Figure 2.7). A simple extension of this idea suggests an arrangement which ensures that the reflections from an intra-cavity etalon are suppressed while transmission through the etalon is unaffected. An example of such an arrangement is illustrated in Figure 2.8. The quarter-wave plates 1 and 2 are placed either side of the etalon and a polarizer separates this etalon assembly from the laser medium. The $\lambda/4$ plates can have their fast axes parallel to each other or perpendicular. In either case these are at $45^{o}$ to the plane of polarization transmitted by the polarizer. To simplify the discussion we shall assume the fast axes to be perpendicular, hence light which passes through both plates will have its polarization state restored.

Light which exits from the right hand face of the polarizer is horizontally polarized (in the plane of the page) and any reflections from the etalon will return as vertically polarized light, just as in Figure 2.7, and hence be rejected by the polarizer. Laser oscillation due to feedback between mirror 1 and

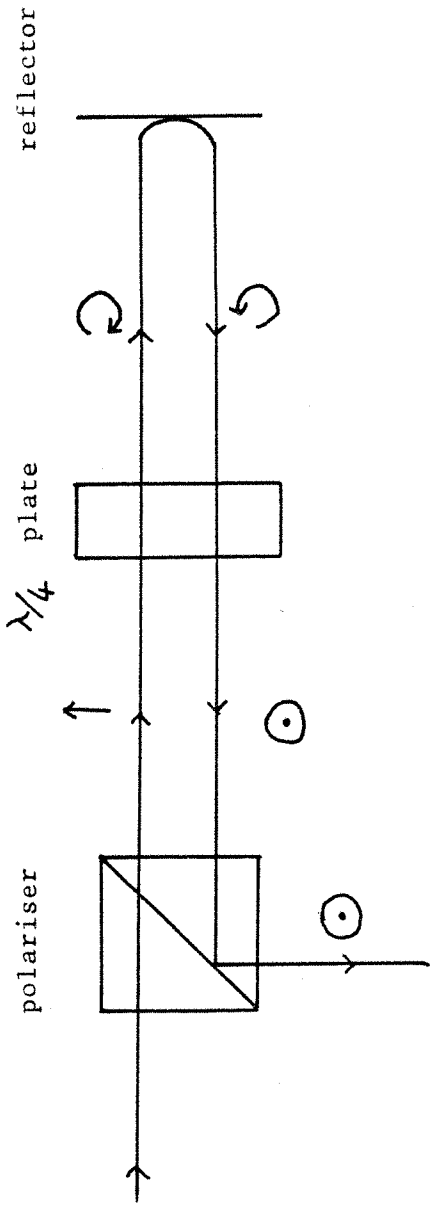


FIGURE 2.7 ARRANGEMENT TO SUPPRESS FEEDBACK FROM REFLECTIONS

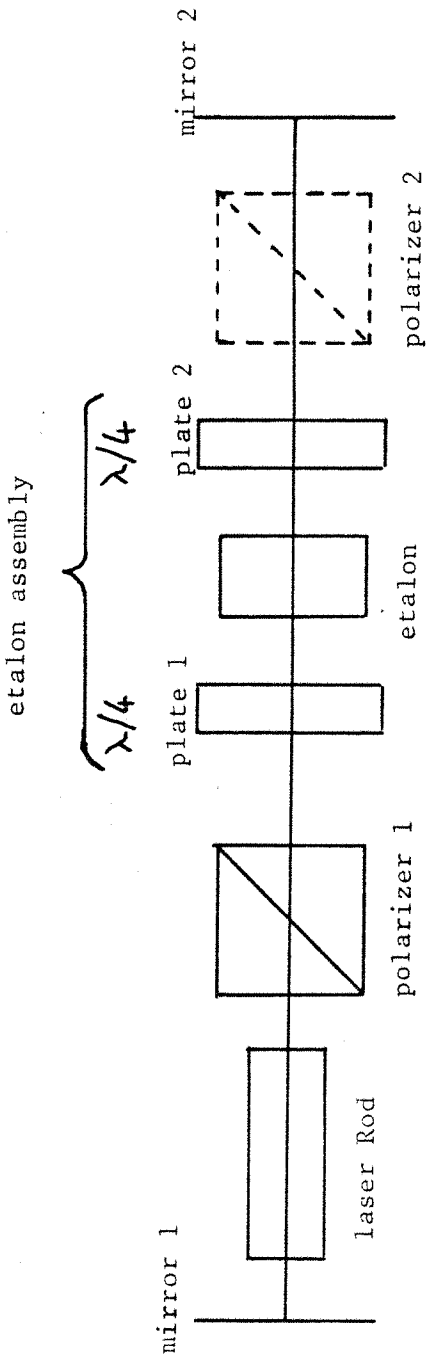


FIGURE 2.8 ARRANGEMENT FOR THE SUPPRESSION OF REFLECTIONS FROM AN INTRA-CAVITY ETALON

the etalon will therefore be suppressed. On the other hand light which continues through plate 2 will be restored to horizontal polarization and after reflection from mirror 2 and transmission again through plates 1 and 2 it remains horizontally polarized and hence transmitted by the polarizer. The laser is therefore constrained to oscillate on a feedback path which involves transmission through the etalon. This arrangement still allows the possibility of resonance effects due to reflections between the etalon and mirror 2 (although two round trips between them are needed to restore the polarization state and furthermore, those frequencies which have high transmission through the etalon will be only weakly reflected by the etalon). One could in principle eliminate this resonance completely by adding a second polarizer (polarizer 2, as shown in Figure 2.8). However in practice the effect of this resonance can be reduced to insignificant proportions by making mirror 2 the output mirror (hence having a low reflectivity) or by a very small tilt of the etalon, which has a negligible effect on the etalon performance. We have therefore dispensed with the second polarizer. Since passage through the etalon assembly produces no polarization change one can also use a Pockels cell Q-switch, in the usual quarter-wave configuration, placed adjacent to mirror 2.

A number of variations on this basic arrangement of components is possible. For example the role of the second quarter-wave plate could be taken by the Pockels cell Q-switch itself, with the closed condition corresponding to zero voltage and the open condition to quarter-wave voltage. Another possibility is to insert the quarter-wave plates as shown in Figure 2.9, enclosing the etalon and laser medium. In this way the same quarter-wave plates can serve the additional purpose of preventing spatial hole burning effects in the laser rod as described by Evtuhov et al, (1965). It should be added that this configuration relies on there being only minimal birefringence in the laser medium.

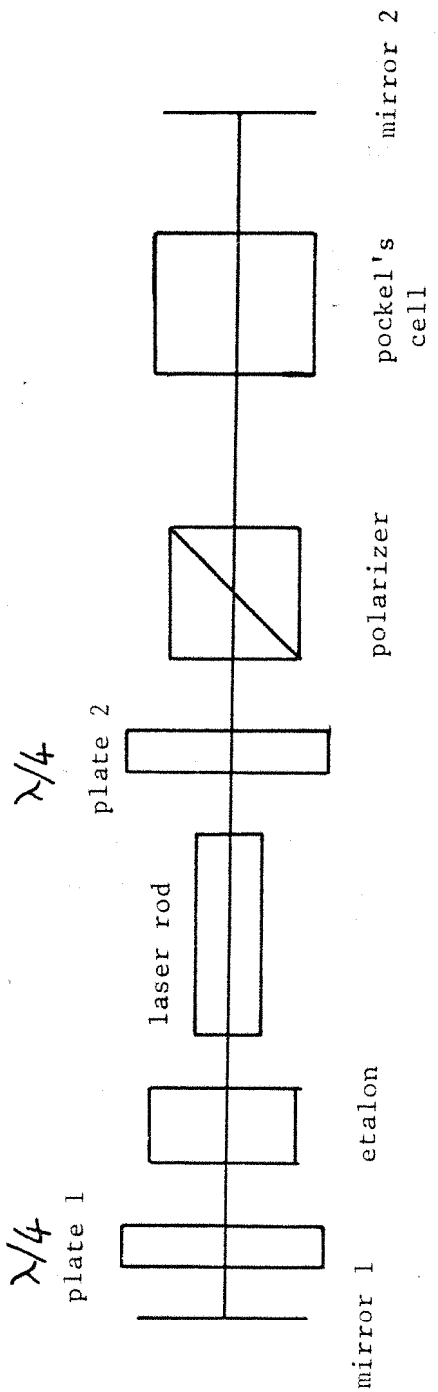


FIGURE 2.9 ALTERNATIVE ARRANGEMENT ALSO REDUCING SPATIAL HOLE BURNING IN THE LASER ROD.

### 2.2.3 Experimental work on etalon loss versus tilt and the technique allowing insertion at normal incidence

The experimental work on etalons involved measuring the effect of tilt on etalon loss and evaluating the improvement that could be obtained by using an etalon at normal incidence surrounded by $\lambda/4$ plates as described in the previous section. In testing the performance of the etalon in this new configuration we therefore had the following aims: (1) to confirm that normal incidence operation is possible without spurious oscillation due to etalon reflection. In fact at the maximum available flashlamp energies, ten times above threshold, oscillation due to etalon reflection could not be induced; and (2) to measure the insertion loss of the $\lambda/4$ plate assembly and compare this with measured additional etalon loss due to tilt.

The method of measuring the insertion loss is given in Hanna, Koo and Pratt, (1983), included as appendix 2. Essentially the technique involved measuring increases in threshold and comparing these with the increase induced by inserting a quartz flat into the laser cavity. The measurement accuracy was estimated to be better than a 1% single pass loss.

It was found that the combined loss of the two $\lambda/4$ plates was too small to be measured, however the etalon had a small but noticable loss even at normal incidence. This was measured to be 5% per round trip, a loss which is probably due to imperfect and unequal reflectivity faces on the etalon. When the etalon was tilted to prevent parsitic lasing this loss rose to 14% per round trip, i.e. a reduction in loss of about 9% per round trip can be achieved using our technique. We used a relatively low selectivity, 65/65% reflectivity, 1cm thick etalon, in our measurements. If etalons of higher selectivity are to be used, or if none $TEM_{oo}$ transverse beams are employed then walk of losses due to tilt will be even larger and the technique will be even more worthwhile. The major limitation with the technique at present is simply cost, £200 for

a pair of $\lambda/4$ plates with A.R. coatings, plus the cost of optically mounting the $\lambda/4$ plates. This limitation is relatively small compared with the cost for a 2cm long etalon with high reflectivity faces.

In conclusion, we have demonstrated a technique leading to improved performance of intracavity Fabry-Perot frequency selectors. Our measurements have shown that the etalon and quarter-wave plate assembly suppressed spurious laser operation with the etalon aligned normal to the laser beam and that under these conditions the insertion loss is reduced and mode selectivity improved when compared with a tilted etalon. These results suggest that considerably more mode-selectivity can now be achieved by using thicker etalons since walk-off effects are no longer a limitation.

## 2.3 A study of Nd: Glass as a potential tunable laser source

A large number of tunable laser systems exist i.e. dye lasers, colour centre lasers, optical parametric oscillators and vibronic lasers. Of these the latter and particularly alexandrite, have attractive features such as, high power, high repetition rate and that the tunability is achieved in a medium directly pumped by a flashlamp. In principle, the same line narrowing techniques as described earlier in this chapter for Nd: Yag could be applied, resulting in a tunable S.L.M. laser of very high power. Had alexandrite been available, this would have been actively persued in this PhD programme. However, it was felt that an alternative, which could have some merit, in particular some degree of tunability, was to use Nd: Glass in place of Nd: Yag as the laser medium. This medium has been looked at with regard to tunability by a number of authors (Lompre et al, 1977; Petite, 1975; Morellec et al, 1979), however none of these papers employ the techniques described in this chapter for line narrowing the Nd: Yag laser.

Graziuk and Zubarev, (1978), use a Tunable Nd: Glass laser as a pump source for Raman Scattering in Gases and liquids. This technique, extended with the use of capillaries and/or resonators, offers the possibility of easily obtaining a tunable, narrow linewidth, laser source, over certain regions of the mid-infrared spectrum.

Having decided to look at Nd: Glass as a potential tunable, S.L.M. laser, a particular problem which was forseen was narrowing from the initial linewidth of ~200cm$^{-1}$ to a single longitudinal mode. Some additional coarse line narrowing would be required as well as that used with Nd:Yag. In practise however, it was found that Nd: Glass was severely limited by thermally induced stress birefringence and our investigation was curtailed after the seriousness of the birefringence problem was established. A brief description of the Nd: Glass work is given here however, since it is felt that this approach may yet prove successful when used with a slab laser configuration in which birefringence problems are greatly reduced.

### 2.3.1 Anticipated problems with Nd: Glass

The problems which were anticipated with Nd: Glass involved its poor thermal conductivity, its resulting high thermally induced birefringence, and its low gain relative to Nd: Yag which is a consequence of its broader linewidth and hence smaller cross-section. The type of Nd: Glass chosen by us was the Q-100 laser glass manufactured by Kigre Inc. A data sheet on this glass is attached as appendix 2. This choice was made as a consequence of Q-100's high $Nd^{3+}$ doping concentration, a factor which results in a gain fairly close to that of Nd: Yag due to a higher pump absorption efficiency.

Thermally induced birefringence was anticipated to be a small problem during our experiments since the manufacturers data sheet on Q-100 states that birefringence is insignificant at pump levels of less than 40W per inch of rod length. (As will be seen

later this was not the case, and a 15% loss per round trip due to thermally induced birefringence was measured at a pump input power of 30W over the full 3" of rod length).

Due to thermally induced birefringence and associated rod fracture problems which occur at high pump powers, it was initially intended to operate at a 5Hz repetition rate instead of 10Hz as normal in our work with Nd: Yag. Later this had to be reduced to 2Hz in an attempt to reduce thermally induced birefringence losses sufficiently to allow a reasonably wide tuning range.

### 2.3.2 Preliminary tests on Nd: Glass

#### Gain

The gain of Q-100 Nd: Glass was measured by using a 3" x 1/4" rod in a J.K. Lasers, System 2000, Nd: Yag power supply and laser head. By changing the output reflector and measuring threshold the following results were obtained:

| Output Mirror Reflectivity | Threshold |
|---|---|
| 70% | 7.72J |
| 60% | 9.68J |
| 40% | 18.3J |

Table 2.10

At threshold we have the relation,

$$R_1.R_2 \exp(2\sigma N.L.) = 1 \qquad 2.27$$

Where $R_1$, $R_2$ are the effective mirror reflectivities and $\sigma$, N, L the emission cross-section, inversion density and rod length respectively. Since N is proportional to the pump energy, we can re-write equation 2.27 by taking natural logarithms to give,

$$\text{Ln}\ (R_1) + \text{Ln}\ (R_2) + K.E_{th} = 0 \qquad 2.28$$

or

$$E_{th} - A = K' \text{ Ln } (R_1) \qquad 2.29$$

where $A = \text{Ln}\ (R_2)/K$ and $K' = 1/K$. If we plot the values given in table 2.10 for our experimental measurements we find that all 3 points line on a straight line which is described by $K' = 12.5J$ and $A = 3.25J$. The term A is given here as a pump energy required to overcome cavity losses additional to the mirror $R_1$ and any initial priming energy required by the flashlamp, (flashlamps have a non-linear light output vs. pump energy relationship at very low pump energies). The gain coefficient obtained from these mesaurements ($K' = 12.5J$) agrees fairly well with the published data from Kigre Inc on Q-100 which is attached as appendix 2.

Energy Output

Measurement of the energy storage capability of Q-100 Nd: Glass is complicated since the proportion of the stored energy emitted in a q-switched pulse depends on the degree above threshold when q-switched . Additionally due to the presence of a polarizer when q-switching, birefringence losses introduce an alternative means for power loss from the cavity with a consequent reduction in the energy appearing in the main output beam. Predictions based on

the measured gain and the published cross-section give a stored energy of 66mJ in a 1.7mm spot size beam for every 12.5J of pump energy.

Using a telescopic resonator to give the required 1.7mm waist size in the laser rod the cavity threshold was 14.8J. This is substantially higher than expected from cavity losses and is due to birefringence losses. A 14.8J threshold corresponds to a round trip feedback factor of between 0.3 and 0.4. Since a 70% reflectivity output mirror was employed we can estimate the birefringence losses to correspond to a 50% transmission. Hence, about 40% of the circulating laser light will appear in the output beam, the rest being lost to birefringence. Svelto, (1982, p185), indicates that when q-switching with the stored pump energy being 18/14.8 above threshold, about 40% of this energy will appear in the q-switched beam. Hence, we obtain for the theoretically expected output power 0.4 x 0.4 x 95mJ = 15.2mJ. This agrees quite well with the 13mJ obtained and is well within the experimental error. Although this agreement was encouraging the actual magnitude of the result was not. Only 16% of the calculated stored energy appears in the output beam. This problem will get worse when tuning into the wings of the gain profile since the gain will reduce and losses from other than the output reflector will be even more dominant.

Birefringence

Throughout all the measurements on Nd: Glass it was noticed that a substantial increase in threshold was observed as soon as any polarizing element was inserted into the laser cavity. The manufacturer of Q-100 Nd: Glass (Kigre, Inc), states that birefringence is negligible at input powers of 40W per inch or less. They do not state however, with what diameter or length laser rod this is observed. Experimentally we can monitor birefringence in 2 ways, by noting a change in threshold at different flashlamp repetition rates, or by observing a collimated

He-Ne laser passing through the rod which is enclosed between crossed polarizing elements. Using the latter technique the familiar 'maltese cross' interference pattern, (see Born and Wolf, 1980), was easily visible with a pump energy of 8J at 2Hz, i.e. 16W over 3" of rod length. At 1.06$\mu$m this birefringence will result in a noticable loss as the rod is traversed twice per round trip and so significant depolarization will take place.

An alternative method of measuring birefringence is to compare the threshold pump energy immediately after switching on, with that obtained when the rod is in thermal equilibrium and birefringence has developed. Using this technique the threshold rose from 12.5J to 15.IJ. This 2.6J difference corresponds to a 20% loss, at a repetition frequency of 2Hz, a beam spot size of 1.7mm and a 75mm rod length.

Our measurements indicate that birefringence losses are very significant at the lowest pump powers and repetition rates. This is in conflict with the statements made in the manufacturers data sheet.

Tunability

The method chosen for tuning the Nd: Glass laser was a sequence of 4 prisms all at or near to Brewsters angle. Prisms were chosen due to their low insertion loss, (in the absence of rod birefringence), high damage threshold and absence of satellite transmission maxima. Neither gratings or birefringent filters are capable of meeting all these criteria. Four prisms are needed in order to have a transmission bandwidth much smaller than that of the laser medium and so allow effective tuning.

A simple stable resonator was employed during the tuning measurements as this was easier to align than a telescopic resonator. Initially it was also thought that sufficient energy would be obtained without having to resort to a telescopic

resonator. This view changed when the magnitude of the birefringence problem became apparent.

The main limitation on tuning range was found experimentally to be due to various resonator losses. These losses were due mainly to birefringence in the laser rod and slightly mis-aligned prisms. These losses together resulted in a higher threshold which, coupled with the lower rod gain in the wings of the gain profile, limited the tuning range. The actual tuning range obtained was of the order of $100cm^{-1}$. This however was asymmetric about the peak rod gain. The following results were obtained:

| Lasing Frequency | Threshold Energy | Input Energy | Output Energy |
|---|---|---|---|
| $\nu_o$ | 11.9J | 32J | 16mJ |
| $\nu_o+23cm^{-1}$ | 18J | 40J | 11.8mJ |
| $\nu_o-64cm^{-1}$ | 18J | 40J | 14.5mJ |

An output energy of 10mJ or greater was obtained over a tuning range of over $100cm^{-1}$. More energy could perhaps be obtained if a telescopic resonator had been employed but, due to the seriousness of the birefringence problem, this was not pursued further.

### 2.3.3 Conclusions on Nd: Glass

Our main conclusion on Nd: Glass is that this material is not suitable for use in medium to high repetition rate laser systems due to birefringence. This birefringence results in a loss which, due to the low gain of Nd: Glass relative to Nd: Yag, results in a higher pump energy requirement. These higher pump energies in turn produce more birefringence. In low repetition rate systems Nd: Glass still has potential as a means for generating tunable infra-red. However, since we were only interested in medium to high repetition rate systems, (5-10Hz), our programme of work on Nd: Glass was halted.

## 3. THE ACTIVELY MODE LOCKED ND: YAG OSCILLATOR

This chapter describes the design, construction and characterization of an actively mode locked, (A.M.L.), Nd: Yag oscillator as a source of short, stable pulses of around 100ps in duration. An A.M.L. system was chosen in preference to a passively mode locked system because of the following advantages.

1. Simple control of the output pulse length can be achieved using an A.M.L. oscillator by either inserting an etalon or varying the R.F. drive level to the acousto-optic modulator.

2. Better stability of the output pulse width and amplitude is achieved with an A.M.L. system.

3. Our experience with prelase operation to obtain S.L.M. Yag lasers should help in the design, construction and testing of an A.M.L. system. An additional advantage of the A.M.L. compared with a passively mode locked system is the synchronisation that is present in the A.M.L. between the output pulse train and the R.F. signal applied to the acousto-optic mode locker. This allows accurate synchronisation between the pulse train and external electronics which is much more difficult to achieve with a passively mode locked system.

As a result of all these advantages we decided to opt for the A.M.L. system despite the cheaper and simpler techniques involved in the operation of lasers passively mode locked and q-switched using a saturable absorber dye.

The design we chose for the A.M.L. oscillator was closely based on the theory presented in Kuizenga, (1977) and Kuizenga et al, (1981). A summary of this theory together with some additional calculations is presented in section 3.1 of this chapter. The

main conclusion to be drawn is that a large number of round trips are required to obtain short, bandwidth limited, modulation-free pulses. This same conclusion was also found from the work on the S.L.M. oscillator. Indeed there are some close similarities between the techniques required for frequency narrowing and mode locking, despite their opposite aims.

The build up time required to obtain the large number of round trips was initially obtained using the pre-lase technique as used in the q-switched S.L.M. oscillator. Later pre-lase periods longer than a few micro-seconds were required. For this a long pulse length power supply was obtained to drive the flashlamp for upto 5 milliseconds. This power supply was necessary in order to avoid the effects of relaxation oscillations which occur during the first millisecond of the prelase.

The laser was mode locked using a quartz acousto-optic modulator to modulate the cavity loss in resonance with the cavity round trip frequency. This acousto-optic modulator uses Bragg diffraction of the laser beam from two counter-propagating sound waves as the cavity loss modulating mechanism. The mode locker was driven by a stable quartz crystal oscillator together with a sequence of R.F. amplifiers supplying upto 15W of pulsed R.F. power at ~65MHz. The A.M.L. oscillator was independently q-switched using an electro-optic Pockels cell. This had a Brewsters angle configuration for minimum insertion loss and the elimination of spurious etalon effects which could effect the mode-locking process.

## 3.1 The theory of the A.M.L. Nd: Yag oscillator

### 3.1.1 The dynamics of active mode locking

The process of active mode locking can be considered as the independent effects of pulse shaping as a result of repeated

passes through the acousto-optic mode locker, together with pulse broadening and noise bandwidth reduction as a consequence of frequency selective elements present in the cavity. The theory relating to these processes is presented in Kuizenga, (1981, 1977 and 1970). In addition to the processes of pulse narrowing and bandwidth narrowing we must also consider the relaxation oscillations which interfere after the first few microseconds of the pre-lase. These are well discussed in the early laser literature, (Dunsmuir, 1961; Statz et al, 1965). The main conclusion of this theory is that the relaxation oscillations decay exponentially with a time constant similar to that of the upper laser level lifetime. In Nd: Yag this lifetime is 230$\mu$S so we can expect a steady prelase with no further relaxation oscillations after about one millisecond.

Pulse Shaping

Pulse narrowing occurs in the A.M.L. laser as a consequence of repeated passes through the acousto-optic mode locker. This has a single pass, amplitude transmission given by,

$$m(t) = \cos [\theta_m \sin (2\pi\nu_s t)] \qquad 3.1$$

(derived later, and appearing as equation 3.20). In this equation $\nu_s$ is the mode-locker modulation frequency and $\theta_m$ a factor related to the mode locker efficiency. Concurrently with the pulse narrowing, pulse broadening occurs as a result of bandwidth narrowing from the gain medium and any other frequency selective elements present in the cavity. The combination of these components gives rise to a frequency dependent round trip gain function,

$$G(\nu) = \exp (g_o) \exp [-\nu^2.L(o)] \qquad 3.2$$

which is obtained from a Taylor expansion of the gain function about the centre frequency with respect to $\nu^2$, neglecting $\nu^4$ and higher powers. This approach is described further in section 3.1.3 where frequency selection due to the rod gain function and intracavity etalons is considered. The factor L(o) in equation 3.2 is the value of $L(\nu)$ at the centre frequency of the rod or etalon. It describes the amount of line narrowing occuring at that frequency. We will derive an expression for L(o) in section 3.1.3, equations 3.24 and 3.25.

Using a self consistency approach where a gaussian pulse must reproduce itself after a complete round trip, Kuizenga; (1970), obtains a value for the steady state pulse duration which can be expressed as

$$\tau_{po} = \frac{[\ln(2)]^{1/2}}{\pi} \cdot \frac{1}{\theta_m^{1/2}} \cdot \frac{1}{\nu_s^{1/2}} \left(\frac{L(o)}{4}\right)^{1/4} \qquad 3.2$$

Having obtained a steady state value for the pulse duration we now require to know how rapidly the pulse duration approaches this value. For pulses much longer than $\tau_{po}$, line narrowing has no effect on the pulse shape, and hence we can write,

$$I(t) = [m(t)]^{4M} \qquad 3.4$$

where M is the number of round trips. (The factor 4 is needed since m(t) is an <u>amplitude</u> transmission and is traversed <u>twice</u> per round trip). For large M, Kuizenga expresses equation 3.4 in the form of a Gaussian profile with a full width half maximum given by

$$\tau_p = \sqrt{\frac{\ln(2).}{2M}} \; \frac{1}{\pi} \cdot \frac{1}{\theta_m . \nu_s} \qquad 3.5$$

The analysis for values of M covering the transition between equation 3.3 and 3.5 has been carried out, again by Kuizenga, by allowing a Gaussian pulse to change its duration during a round trip. He obtains

$$\tau_p = \tau_{po} \left[\tanh (M/M_o)\right]^{-1/2} \qquad 3.6$$

where $$M_o = \{\theta_m . \nu_s . [L(0)]^{1/2}\}^{-1} \qquad 3.7$$

This is our final expression for the pulse length of the A.M.L. oscillator which we shall use later in this section to make performance predictions.

Noise bandwidth reduction

This occurs in the A.M.L. laser due to successive passes through the amplifying medium and any other intra-cavity frequency selective elements. This process of bandwidth narrowing however occurs much more slowly than in the S.L.M. oscillator due to the elimination of virtually all frequency selective elements from the cavity. Fortunately the criterion for a bandwidth limited pulse is much less severe for the A.M.L. laser than for the S.L.M. laser. This is due to the inherent bandwidth of a 20nS pulse being 200 times smaller than the 100pS pulses produced by the A.M.L. laser. The transform limited bandwidth of a 100pS mode locked Gaussian pulse covers about 30 longitudinal mode spacings (4.4GHz, f.w.h.m). Our working definition of a bandwidth limited pulse is when the noise bandwidth, (i.e. that which would be obtained without mode locking), is less than a fifth of the pulse bandwidth. Accordingly we require a noise bandwidth of less than 6 longitudinal mode spacings, (900MHz).

From equation 3.2 we obtain for the pulse bandwidth after M round trips,

$$P(\nu) = R^M . \exp(Mg_o) \exp[-M.\nu^2 . L(o)] \qquad 3.8$$

where the factor R represents the effective mirror reflectivities. From this equation we can see that the laser noise bandwidth is proportional to $1/\sqrt{M}$. The f.w.h.m. noise intensity bandwidth after M round trips is infact given by

$$B_n(M) = \sqrt{\frac{4.\ln(2)}{M.L(o)}} \qquad 3.9$$

This is our final expression for the noise bandwidth which is used in the next section.

Pulse length and noise bandwidth predictions for the A.M.L. oscillator described in section 3.2

In our measurements on the A.M.L. oscillator a number of modifications were made during the period over which the work was carried out. These changes involved the R.F. power level to the mode-locker as well as spurious effects due to a plane-parallel output reflector. The calculations given here relate to an R.F. drive level of 7W and no spurious etalon effects. Under these conditions the following values are obtained from sections 3.1.2. and 3.1.3.

$$\begin{aligned} \nu_s &= 65.237\text{MHz} \\ \theta_m &= 1.7 \\ L(o) &= 5.6 \times 10^{-22}\ \text{Hz}^{-2} \end{aligned}$$

Substitution of these values into equation 3.3 gives a steady state pulse duration, $\tau_{po} = 87$pS. This corresponds to a steady state pulse bandwidth given by $B_{po} = 0.44/\tau_{po} = 5.1$GHz. For bandwidth limited pulses we require that the noise bandwidth be

reduced to less than a fifth of this, i.e. $B_n(M) < 1GHz$. Using equation 3.9 in conjunction with this inequality we obtain the requirement $M > 5,000$ for bandwidth limited pulses. For a 7.66nS round trip time this corresponds to a build up time of 40$\mu$S. The value of M required to obtain pulses of duration within a few precent of $\tau_{po}$ is given by the condition $M > 1.5xM_o$ where $M_o$ is defined by equation 3.7. For the resonator conditions defined above we obtain $M_o \simeq 380$ and hence $M > 570$.

From the above calculations it is apparent that, for the resonator configurations defined above, the time required for noise bandwidth narrowing is much larger than that required to generate short pulses. The technique of pre-lase q-switching is not a satisfactory method for increasing the build up time beyond about 10$\mu$S due to the onset of relaxation oscillations. The only method presently available for a prelase of 40$\mu$S or longer involves the use of a flashlamp pulse which can be extended to 5m sec. After the first millisecond the relaxation oscillations generally die away allowing a pre-lase which can extend over the remaining 4m sec. (If the R.F. drive frequency and the cavity round trip frequency differ by approximately the relaxation oscillation frequency then the R.O.'s may become actively driven and fail to die away). It is because the first millisecond of the pre-lase cannot be used that we require a laser power supply capable of driving the flashlamp for at least a few milliseconds.

If the technique of pre-lase q-switching is employed then the resulting 5$\mu$S pre-lase will result in pulses of duration within a few percent of $\tau_{po}$. The noise bandwidth however will be comparable to that of the mode-locked pulses themselves. As a consequence considerable ripple will sometimes be present in the structure of the pulse.

### 3.1.2 The Acousto-optic mode locker

#### General Details

The mode locker used in the A.M.L. oscillator was obtained from IntraAction Corp; of the U.S.A. The device was optimized to operate at around 67MHz, this corresponding to a convenient cavity length, (1.12 m optical), as well as being interchangeable with devices used at J.K. Lasers Ltd. Table 3.1 lists the pertinent specifications of the ML-67J mode locker used in our experiments.

The mode locker operates by using the Bragg diffraction of light by sound waves as shown in Figure 3.2 A standing acoustic wave is employed resulting in the transmitted beam being modulated at twice the acoustic frequency. It is this feature which results in mode locking of the laser.

A more detailed mathematical analysis of the mode locker's operation is given in the remainder of this section.

#### Efficient coupling of the incident R.F. energy

The incident R.F. electrical energy at 67MHz is coupled into the acousto-optic cavity with a piezo-electric transducer. On resonance a large standing wave is set up which, due to slight acoustic losses, results in the piezo-electric transducer representing a fairly low impedance of a few hundred ohms. An impedance matching transformer matches this effectively to the 50Ω transmission line ensuring minimum reflected power. Off resonance the piezo-electric transducer represents a high impedance due to a high proportion of the incident R.F. energy being reflected back down the driving transmission line. For good mode locking we require a large amplitude standing wave, consequently the R.F. drive frequency must be maintained on resonance with the mode locker. In our laser system this was obtained by stabilizing the

Table 3.1 Details of the ML-67J Mode Locker

length = 7.5cm
height = 1cm
transducer width = 3mm
estimated sound field width = 8mm
crystal width = 1cm
centre frequency = 67MHz
acceptible frequency range = 57-77MHz
Bragg angle = 5.95 mRad at 1.06$\mu$m
maximum incident power = 4W continuous
~ 15W pulsed
cooling : liquid - temperature stabilised
reflected power : less than 0.1% on resonance

Acousto-optic data on fused quartz

| | | |
|---|---|---|
| density | p | $2.2\times10^{3}$ kg/m$^3$ |
| acoustic velocity | $v_s$ | $5.97\times10^{3}$ m/s |
| refractive index | n | 1.46 |
| photoelastic constant | p | 0.2 |
| figure of merit | M | $1.51\times10^{-15}$ m$^2$/W |

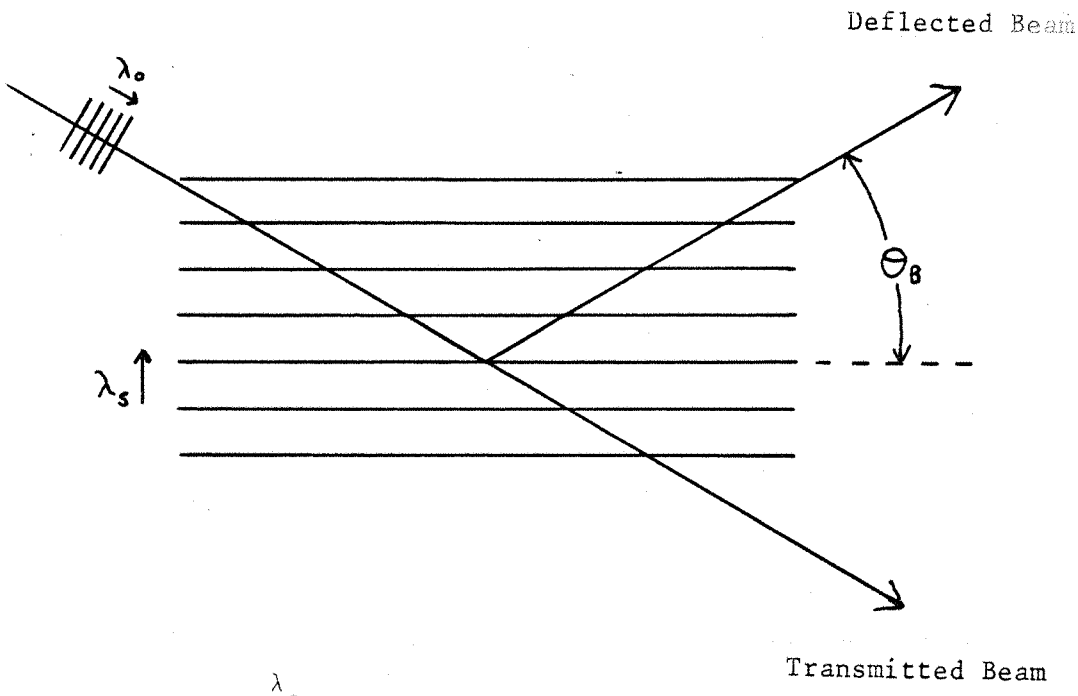


$\theta_B$ = Bragg angle = $\frac{\lambda_o}{\lambda_s}$

FIGURE 3.2 MODE LOCKER OPERATION

R.F. drive frequency and the mode locker temperature, (see sections 3.2.2 and and 3.2.1).

In order to work out the diffraction efficiency of the mode locker we need to know the refractive index variation due to the acoustic standing wave. The equations given in this section follow from the work presented in Yariv, (1975). There is however a factor of 2 difference from Yariv's equations which assume a travelling acoustic wave as opposed to the standing wave used here. Since the refractive index is directly related to the acoustic wave amplitude which is comprised of a standing wave, we have for the refractive index variation,

$$\Delta n\ (x,\ t) = A.\ \sin(k_s.x).\ \sin\ (2\pi.f_s.t) \qquad 3.10$$

In this equation $k_s = 2\pi f_s/V_s$, where $V_s$ is the acoustic velocity, and $f_s$ the acoustic frequency. The parameter A represents the peak change in refractive index which can be written in terms of a figure of merit M of the material and the acoustic intensity, $I_{AC}$, as

$$A = (2.M.I_{AC})^{1/2} \qquad 3.11$$

where

$$M = n^6.p^2/(\rho.V_s^3) \qquad 3.12$$

In equation 3.12, n is the equilibrium refractive index value for the material, p the photoelastic constant and $\rho$ the material density. The acoustic intensity used in equation 3.11 is that circulating the acoustic cavity. This intensity is related to the incident R.F. power, $P_{RF}$, by

$$I_{AC} = \frac{P_{RF}.Q.\alpha}{L.W.} \qquad 3.13$$

Where $\alpha$ is the piezoelectric transducer efficiency, L the transducer length, W the acoustic field width and Q the acoustic

cavity Q-factor. Estimates of Q using the characteristics of the reflected R.F. power versus frequency yield a value of about 5 for the cavity Q.

Substituting values into equation 3.13 from table 3.1 with 7W of incident power, $\lambda$=1.06$\mu$m and the piezoelectric transducer effficiency estimated as 50% gives,

$$I_{AC} = 2.92 \times 10^4 \text{ W/m}^2 \qquad 3.14$$

Substitution of this into equations 3.12 and 3.11 again using data from table 3.1 gives the peak refractive index, variation, $A = 6.6 \times 10^{-6}$.

The interaction of Light and Sound

This section describes the interaction of a laser beam with a refractive index distribution described by equation 3.10. If $E_i(Z)$ and $E_D(Z)$ are the incident and deflected beam amplitudes as a function of distance into the mode locker then Yariv, (1975) shows that

$$E_i(Z) = E_i(o) \cos(KZ) - i\, E_D(o). \sin(KZ) \qquad 3.15$$

$$E_D(Z) = E_D(o) \cos(KZ) - i\, E_i(o). \sin(KZ) \qquad 3.16$$

These equations indicate that the incident power oscillates back and forth between the two beams as a result of the induced refractive index grating set up by the acoustic wave. In our case the deflected wave at Z = o is zero with a resulting simplification of equations 3.15 and 3.16.

The factor K describes the rate at which power is transferred between the two beams. It can be written in terms of the periodic refractive index variation as

$$K = \cos(\theta).\ \omega_i.\mu\varepsilon_o.\ \Delta n(t)/2 \qquad 3.17$$

Since we can approximate $\cos\theta \simeq 1$ and $\omega_i\mu\varepsilon_o \simeq 2\pi/\lambda$ we obtain

$$K \simeq \pi.\ \Delta n(t)/\lambda \qquad 3.18$$

In the above equations, $\theta$ is the Bragg angle, $\omega_i$ the angular light frequency, $\lambda$ the corresponding free space wavelength and $\Delta n(t)$ is given by A sin $(2f_s t)$ since the spatial variation of $\Delta n(t)$ is taken into account when arriving at equation 3.18. Substituting equation 3.18 into 3.15 gives the following,

$$E_i(Z) = E_i(o).\ \cos\ [\pi.A.\ \sin\ (2\pi f_s t).\ Z/\lambda] \qquad 3.19$$

This equation is identical in form to that given by Kuizenga, (1981, etc) as $m(t) = \cos[\theta_m.\sin(\omega_m.t)]$. Rearranging equation 3.19 we obtain,

$$m(t) = \frac{E_i(L)}{E_i(o)} = \cos\left[\left(\frac{L.\pi.A.}{\lambda}\right)\sin\ (2\pi f_s.t)\right] \qquad 3.20$$

where we find $\theta_m = L.\pi.A/\lambda$ and $\omega_m = 2\pi f_s$. Substituting our value for A of $6.6 \times 10^{-6}$ into this equation for $\theta_m$ gives $\theta_m = 1.5$.

Experimental measurement of $\theta_m$

One possible method of measuring $\theta_m$ is to look at the time averaged, single pass, power diffraction efficiency. This is given by,

$$D = \frac{1}{\nu_s}\int_o^{1/\nu_s} \sin^2\ [\theta_m\ \sin\ (2\pi\nu_s t)]\ dt \qquad 3.21$$

which can be written in terms of the first order Bessel function $J_o(X)$ as

$$D = 1/2\ [1 - J_o(2\theta_m)] \qquad 3.22$$

Using a He-Ne laser at 633nm a time averaged diffraction efficiency of 21%, (corresponding to $\theta_m = 0.69$) was obtained with 0.42 Watts of incident R.F. power. The value of 0.69 at 633nm and 0.42W of R.F. corresponds to a value $\theta_m = 1.7$ at 1.06$\mu$m and 7W of R.F. This value agrees well with the value of 1.5 calculated and indicates that the estimated values used in equation 3.13 are fairly accurate. We have used the experimental value $\theta_m = 1.7$ in our calculations in section 3.1.1.

### 3.1.3 The effect of etalons in the A.M.L. Laser

In section 3.1.1 it was noted that a limitation on the minimum pulse width obtainable from the A.M.L. is due to the round trip linewidth of the Yag rod and the surrounding cavity. In Section 3.1.1 we used a factor L(o) to describe the effects of this line narrowing. It is the aim of this section to evaluate L(o) for a number of cavity configurations.

In the general case we will have two transmission profiles $G(\nu)$ and $T(\nu)$, representing respectively the transmission profiles of the laser rod and any etalon effects. The combination of rod and etalon can be represented by their product $P(\nu) = T(\nu) \times G(\nu)$ where we have assumed both profiles have coincident peaks since this represents the worse case condition from a pulse shortening point of view. If the minimum etalon transmission is instead coincident with the rod peak then frequency effects can cancel. This situation is discussed at the end of this section since the reduction of line narrowing at the peak may result in shorter mode locked pulses.

The contribution of the frequency selective elements to line narrowing is given by,

$$L(\nu) = \frac{1}{P(\nu)} \cdot \frac{dP(\nu)}{d\nu^2} \qquad 3.23$$

which represents the normalized curvature of the cavity round trip gain as a function of frequency. Substituting $G(\nu)$ and $T(\nu)$ we obtain,

$$L(\nu) = \frac{1}{G(\nu)} \cdot \frac{dG(\nu)}{d\nu^2} + \frac{1}{T(\nu)} \cdot \frac{dT(\nu)}{d\nu^2} \qquad 3.24$$

We shall come back to this equation after we have looked more closely at $G(\nu)$ and $T(\nu)$ and related them to better known parameters such as linewidth, finesse and free spectral range.

The transmission profile of the laser rod, $G(\nu)$ is given by its Lorentzian lineshape. This yields,

$$G(\nu) = \exp\left[g_o/(1 + \nu^2/\Delta\nu_R{}^2)\right] \qquad 3.25$$

where $g_o$ is the round trip intensity gain, (typically $\simeq 2$) and $\Delta\nu_R$ the h.w.h.m intensity linewidth, ($2cm^{-1}$ for YAG). The characteristics of this curve are such that the curvature at the peak increases with increasing $g_o$. This is why C.W. mode locked Yag lasers (with smaller $g_o$) generally produce slightly shorter pulses than pulse pumped Yag lasers. Differentating equation 3.25 with respect to $\nu^2$ we obtain,

$$\frac{dG(\nu)}{d\nu^2} = \exp\left[\frac{g_o}{(1+ \nu^2/\Delta\nu_R{}^2)}\right](-g_o).[1+\nu^2/\Delta\nu_R{}^2]^{-2}.\frac{1}{\Delta\nu_R{}^2} \qquad 3.26$$

which at the line peak ($\nu = o$) gives

$$\frac{dG(O)}{d\nu^2} = \exp(g_o).\ g_o/\Delta\nu_R{}^2 \qquad 3.27$$

The transmission function of an etalon is given by equation 2.7. This equation can however be re-written in the form,

$$T(\nu) = (1 + C.[1 - \cos^2(\nu/\Delta\nu_e)]/2)^{-1} \qquad 3.28$$

where $C = 4R/(1-R)^2$, the etalon contrast, $\Delta\nu_e = 1/2\pi$ times the etalon free spectral range and R is the power reflectivity of the etalon faces. Differentiating with respect to $\nu^2$, as with the rod gain function $G(\nu)$ , we obtain,

$$\frac{dT(\nu)}{d\nu^2} = \frac{-C}{2\Delta\nu_e^2} \cdot (1+\frac{C}{2}[1-\cos^2(\frac{\nu}{\Delta\nu_e})])^{-2} \cdot \text{sinc}\left(\frac{2\nu}{\Delta\nu_e}\right) \qquad 3.29$$

which at $\nu = o$ gives

$$\frac{dT(o)}{d\nu^2} = \frac{-C}{\Delta\nu_e^2} \qquad 3.30$$

where we have multiplied by two since the etalon is used in a double pass arrangement.

Substituting equations 3.30, 3.28, 3.27 and 3.25 into equation 3.24 gives

$$L(o) = \frac{g_o}{\Delta\nu_R^2} + \frac{C}{\Delta\nu_e^2} \qquad 3.31$$

The magnitudes of the two terms in this equation indicate whether etalon or rod effects will dominate the line narrowing process. In order to use the factor L(o) in Kuizenga's theory we note that in his work whenever $\Delta f_a^2$ appears it is divided by $g_a$. (The subscript a is used as Kuizenga uses an amplitude gain and linewidth). To use our term L(o) we simply substitute for $\Delta f_a^2/g_a$ in his work by 16/L(o). (Since $\Delta f_A = 2\sqrt{2} \times \Delta\nu_R$ and $g_o = 2 \times g_a$). Kuizenga's etalon terms can then be neglected as our term L(o) includes their effect.

Anti-Etalons

In the previous part of this section it was noted that an etalon could be used to partially eliminate the line narrowing effects of the laser rod. This is accomplished by aligning the etalon so that its transmission minimum coincides with the gain peak of the laser medium. With the correct choice of etalon the resulting combined round trip gain can be flattened as a function of frequency close to the rod gain peak.

Other authors have attempted this technique with a variety of solid state laser materials; Nd: Yag. Nd: Glass and Ruby, (see Graener, 1981; Von der Linde, 1972 and Graf, 1983; and McGeoch, 1973; respectively). In all of these attempts some degree of success was achieved, however, each time the technique of passive mode locking was used. It appears that the techniques of actively mode locking and suppressed natural mode selection have not previously been used simultaneously.

The theories presented in the above papers differ considerably as to the optimum etalon thickness and reflectively. We present here a procedure for choosing the optimum thickness for an etalon with a predetermined surface reflectivity. If the surface reflectivity can also be selected then even more suppression of natural mode selection will be possible by equating the second order derivative with respect to $\nu^2$ to zero as well as the first.

The transmission function of an etalon about its minimum transmission is given by, (from equation 3.28),

$$T(\nu) = \left(1 + \frac{C}{2}\left[1 + \cos^2\left(\frac{\nu}{\Delta\nu_e}\right)\right]\right)^{-1} \qquad 3.32$$

Using the technique presented with equations 3.28 through 3.30 we obtain the same result as 3.30 but with opposite sign, ie.,

$$\frac{dT(0)}{d\nu^2} = \frac{C}{\Delta\nu_e{}^2} \qquad 3.33$$

For minimum line narrowing we require L(o) given by equation 3.24 to be zero, i.e;

$$\frac{C}{\Delta\nu_e^{\,2}(1+C)} = \frac{g}{\Delta\nu_R^{\,2}} \qquad 3.34$$

Since g and $\Delta\nu_R$ are presumed fixed this equation prescribes an optimum relationship between C and $\Delta\nu_e$, or in component terms between the etalon reflectivity and thickness. Using the relationships $C = 4R/(1-R)^2$ and $\Delta\nu_e = (4\pi nt)^{-1}$, where t is the etalon thickness and n the refractive index of the medium separating the etalon faces, we can re-write equation 3.34 as

$$\frac{4R.(4\pi nt)^2}{(1+R)^2} = \frac{g}{\Delta\nu_R^{\,2}} \qquad 3.35$$

For our laser we have $g \simeq 2$ and $\Delta\nu_R \simeq 2cm^{-1}$, hence for an uncoated fused silicon etalon (R = 0.04), we obtain $t \simeq 1mm$.

To obtain operation at a transmission minimum, either temperature or angle tuning will be required. A consequence of operation at minimum transmission is that a significant loss will be introduced by the etalon. The silica etalon mentioned above will have a round trip insertion loss of ~27%. This is a large amount especially when using a long pulse power supply with its relatively low pump powers. Better results are likely to be obtained with a thicker etalon and lower reflectively faces, unfortunately no suitable device was available and so experimental tests of this theory were not carried out.

The effects of a plane/parallel output reflector

During the experimental work on the A.M.L. it was discovered that a plane/parallel, A.R. coated/30% reflectivity output coupler was causing the output pulses to be extended to 200pS in duration instead of the 100pS expected and obtained with a wedged output coupler. The remainder of this section presents an estimate of

the factor $\frac{1}{R(\nu)} \cdot \frac{dR(\nu)}{d\nu^2}$ which would appear in equation 3.24 as a consequence of this resonant reflector.

For the resonant reflector the minimum and maximum reflectivities obtained off and on resonance are 0.26 and 0.34 respectively if we assume a 1/4% reflectivity A.R. coating. Hence we can obtain

$$R(\nu) \simeq 0.34 - 0.04.(1-\cos(\nu/\Delta\nu_e)) \qquad 3.36$$

where we have approximated the reflectivity as varying sinusoidally over the free spectral range of the resonant reflector. This assumption is valid provided the reflectivity of the two surfaces is small and so multiple reflections between the two surfaces can be ignored. Differentiating equation 3.36 with respect to $\nu^2$ we obtain

$$\frac{dR(\nu)}{d\nu^2} \qquad \frac{0.04}{2\Delta\nu_e^2} \cdot \operatorname{sinc}\left(\frac{\nu}{\Delta\nu_e}\right) \qquad 3.37$$

Evaluating $\frac{1}{R(\nu)} \cdot \frac{dR(\nu)}{d\nu^2}$ which is the term contributing to equation 3.24 in place of $\frac{1}{T(\nu)} \cdot \frac{dT(\nu)}{d\nu^2}$ we obtain at $\nu = 0$

$$\frac{1}{R(o)} \cdot \frac{dR(0)}{d\nu^2} = \frac{0.02}{0.34 \times \Delta\nu_e^2} = 6.5 \times 10^{-21}\ \mathrm{Hz}^{-2} \qquad 3.38$$

since $\Delta\nu_e = 0.1\mathrm{cm}^{-1}$. The contribution to L(o) from the Yag rod linewidth is given in equation 3.31 as $g_o/\Delta\nu_R^2$ or $5.5 \times 10^{-22}$ $\mathrm{Hz}^{-2}$. From equation 3.38 we see that L(o) is dominated by the resonant reflector term which is 12 times larger. This means L(o) will be 13 times larger than if a wedged output reflector had been used. Consequently the laser pulse length, given by equation 3.3 as proportional to the fourth root of L(o), will be ~1.9 times longer. This agrees very well with that observed experimentally - the laser pulse length was approximately doubled.

Similar evidence of the effects of very weak etalon effects on the laser pulse duration was observed when a non-Brewster angled Pockels cell was employed. The very small etalon effects associated with the various surfaces (6) comprising this device resulted in a slight (~20%) increase in laser pulse length. No theoretical calculations on this effect were made since the various etalon parameters (i.e. spacings, reflectivities, tilt and wedge angles, etc), could not be estimated sufficiently accurately.

### 3.1.4 Frequency doubling the A.M.L. laser

In order to investigate the S.R.S. process at 532nm as well as at 1.06$\mu$m it was required to frequency double the output from the Yag laser. This section gives a brief account of the most important aspects of the frequency doubling process.

An analysis of frequency doubling the output of the A.M.L. laser must take into account the temporal and spatial profiles of the laser beam. For the A.M.L. laser the transverse profile is well approximated by a Gaussian. Similarily the temporal shape of each pulse in the train is well described by a Gaussian. The envelope of the energies of the individual pulses in the train can also be described as Gaussian without introducing significant error. Also needed in a description of the frequency doubling process are the characteristics of the frequency doubling crystal itself. These characteristics describe the acceptance angle and spectral linewidth for maximum 2nd harmonic conversion condition which is only exactly satisfied at one angle and frequency. In addition, for maximum conversion efficiency the coherence length of the two light frequencies must be larger than the length of the doubler crystal. Another factor affecting conversion efficiency is double refraction beam walkoff.

In our experiments a type I, KD*P doubler crystal was used. At a 1.06$\mu$m pump wavelength and at a temperature of 25$^{o}$C, Keochner,

(1976), gives the angular and bandwidth tolerances to be 1.7mRad.cm and 6.5nm.cm respectively. For a 2.5cm long crystal these values become 0.68mRad and 2.6nm. Since 2.6nm is much larger than the linewidth of the mode locked pulse train (~0.03nm) we can neglect any bandwidth limitations in the doubler. To assess the effect of the acceptance angle we need to consider the divergence of the pump beam. Some of the doubling carried out on the A.M.L. laser occured before the beam expanding telescope and so the beam waist was ~0.7mm corresponding to a beam divergence of 0.48mRad. This is barely within the 0.68mRad maximum but should not significantly affect doubling performance as very little pump energy propogates at an angle of 0.48mRad or greater. The beam walk off angle for KD*P, type 1 is 30mRad, again from data presented in Koechner. Over a 2.5cm long crystal this leads to a 0.8mm transverse separation of the two beams. This should have a negligible effect on the doubling performance if a 2mm pump spot size is employed, however, with a 0.7$\mu$m spot size significant fall off in performance is to be expected.

Due to the second order nature of the second harmonic generation process we can expect narrowing of the transverse and temporal pulse widths. The degree of narrowing depends on whether the doubling process saturates at the centre of the pulse. At low efficiencies no saturation occurs and all the Gaussian intensity envelopes will be reduced in width by a factor of $\sqrt{2}$. At efficiencies approaching 25% the centre of the pulse will become significantly saturated. Consequently the pulse shape will become slightly distorted and less pulse narrowing that the $\sqrt{2}$ mentioned above will occur. In our experiments efficiencies of typically 10-15% were achieved and so the $\sqrt{2}$ reduction in pulse width factors will be very close to that actually achieved. These $\sqrt{2}$ factors must be taken into account when evaluating the pulse parameters pertinent to the S.R.S. characterization experiments. Some parameters such as spot size and pulse train shape were re-measured after the doubler to check against significant departure from the $\sqrt{2}$ expected change and to ensure accurate experimental conditions for our S.R.S. measurements.

## 3.2 Experimental work on the A.M.L. System

In this section we describe the apparatus in more detail than at the begining of this chapter. Later in sections 3.2.4 and 3.2.5 we discuss our method for measuring the output pulse length and give the performance of the A.M.L. system in practice.

### 3.2.1 A description of the resonator, power supply and water circulator

#### The resonator

A very simple resonator configuration was used consisting of a stable 2 mirror cavity. The actual layout is shown in Figure 3.3. Initially the cavity length adjusting blocks were not present, instead the 30% reflectivity mirror was mounted on a precision translation stage. This was not quite satisfactory as cavity length adjustments slightly affected the mirror alignment and the precision translation stage made the mirror mount more sensitive to vibration and knocks. Apart from this the resonator remained the same throughout the experiments with the exception of the plane/parallel output reflector which was changed to a wedged device as soon as its effect on performance was noticed, (see sections 3.1.3 and 3.2.5). The resonator length in all cases corresponded to an optical length of 1.14m due to the fixed mode locker drive frequency. The resonator configuration used during the work at J.K. Lasers was based on a design developed independently from that at Southampton by J.K. Lasers. The J.K. Lasers layout is also shown in Figure 3.3.

Important features which must be borne in mind with the resonator are:

a) The mode locker must be located immediately adjacent to one of the resonator mirrors.

Southampton Design.

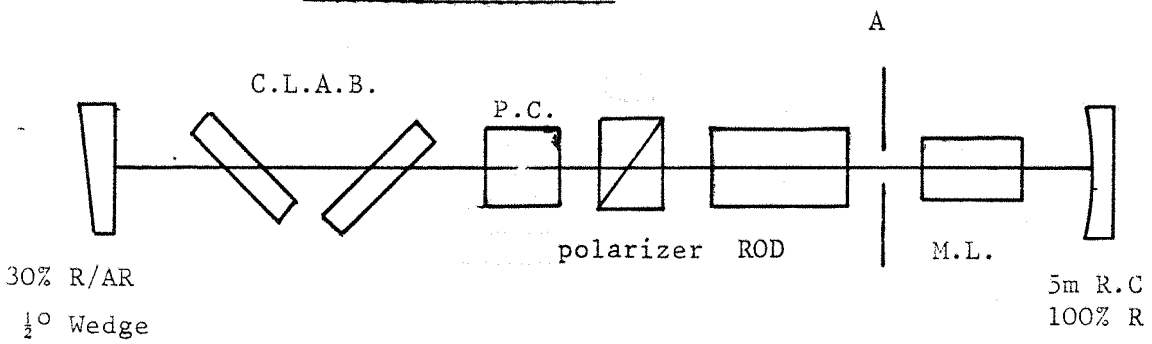


J.K.Lasers Design.

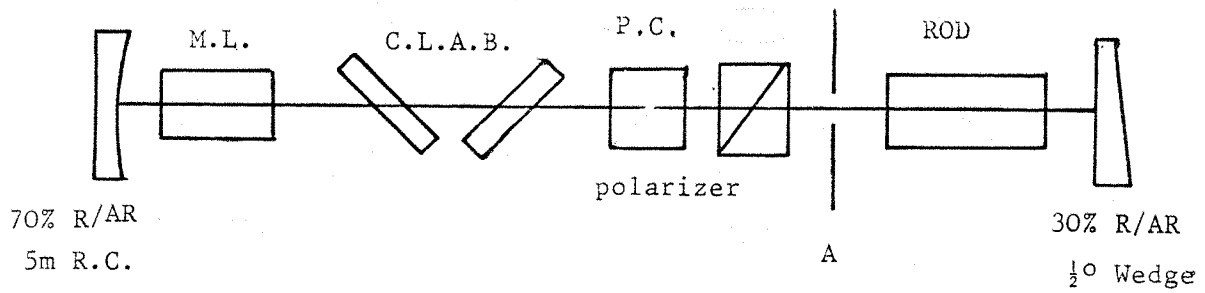


| | |
|---|---|
| C.L.A.B. | Cavity length adjusting blocks |
| P.C. | Pockels Cell |
| A | Aperture |
| M.L. | Acousto-Optic mode locker |
| R.C. | Radius of Curvature |

FIGURE 3.3 SCHEMATIC LAYOUTS OF SOUTHAMPTON DESIGNED AND J.K. LASERS DESIGNED A.M.L. OSCILLATORS

b) The aperture should be between the mode-locker and the Yag rod to prevent damage to the laser rod 'O' ring mountings caused by acoustically deflected beams.

c) Even very weak etalon effects must be completely eliminated. This means the Yag rod must be tilted and preferably wedged as must the Pockels cell crystal and the output reflector. In our system a tilted rod was used in conjunction with a Brewster angled Pockels cell.

d) The mode locker mount: Careful adjustment of both Bragg angle and crystal height must be made. In addition lateral position and angle of the mode locker must be adjustable in order to ensure the laser beam passes through the region of maximum acoustic intensity.

e) Room must be allowed for additional components used during the alignment process, (see section 3.2.3 and appendix 3).

The Power Supply

Most of the experiments on the A.M.L. were carried out with a long pulse power supply capable of pumping the Yag rod for up to 5 milliseconds. This has the advantage of eliminating the need for pre-lase control since after about half a millisecond the relaxation oscillations die to give a steady pre-lase. Near the end of the pump pulse the Pockels cell is opened and the laser Q-switched. Another advantage of the long pulse power supply appears when a photo-diode is used to monitor the pre-lase. By observing the relaxation oscillations with a slow oscilloscope it is possible to align accurately both the cavity mirrors and the cavity length (see section 3.2.3).

The disadvantages of the long pulse power supply are that it is more expensive, rod birefringence is higher due to more flashlamp power input, the Krypton flash lamps have a shorter lifetime, and

that the rod gain is less compared with that obtainable with a 200$\mu$s pulse power supply.

The water circulator

Initially the function of this unit was to supply the flashlamp and laser rod with a jacket of water containing sodium nitrite to provide cooling and prevent U.V. radiation from the flashlamp causing damage to the Nd: Yag rod. The coolant was maintained at just above room temperature by means of a temperature sensitive valve which allowed cooling water from the tap or an external cooling system to cool the closed loop coolant system.

In the A.M.L. system the coolant is also required to maintain the acousto-optic mode locker at a fixed temperature with a tolerance of about 1°C. Unfortunately the existing system was unsatisfactory since the coolant temperature varied significantly due to the inadequate stabilization process. In addition the long warm up time required before the mode locker reached its equilibrium temperature resulted in considerable flashlamp usage which, as stated earlier, have a limited lifetime and are expensive. Our solution to these problems was to plumb in extra pipe connections to the closed loop coolant holding tank and connect these to a Grants' water temperature stabilizer. This served the dual purpose of heating up the coolant before the flashlamp is fired, so saving on flashlamp lifetime, and acting as a thermal buffer to stabilized the coolant temperature. After the initial warm up the coolant temperature stayed within half a degree of optimum even when the laser was turned on and off.

The coolant temperature is adjusted by means of the dial on the Grants' temperature stabilizer in conjunction with the Danfoss valve on the cooler unit. The Danfoss valve opens slowly over a temperature range of a few degrees, consequently this valve adjusts the region over which the Grants temperature stabilizer

will operate satisfactorily. With the Danfoss valve either fully open or closed the stabilizers 2kW heater is incapable of maintaining the correct temperature.

The coolant temperature must be set so that the acousto-optic mode locker is on resonance with the crystal controlled R.F. drive signal. This is achieved by looking at the reflected R.F. signal from the mode locker which on resonance is a minimum. In addition the coolant temperature should be set slightly above room temperature so as to prevent the possibility of condensation on the mode locker or laser rod and the resulting optical damage possibility.

### 3.2.2 The mode locker R.F. drive

In order to obtain mode locked pulses which are short and stable it is essential to drive the acousto-optic modulator with a very stable, high power frequency source. Initially this was provided by a Hewlett-Packard model 3335A, frequency synthesizer together with an R.F. amplifier producing up to half a watt of continuous R.F. power. The disadvantages with this system were its cost (the system used was on a short term loan), and its inability to produce upto 20W of R.F. power, pulsed on for about 10mSec.

This section describes the design and construction of a quartz crystal based oscillator, its buffer/pre-amplifier, a second stage pulsed on pre-amplifier and the attachment of a commercial 20W R.F. power amplifier. Since about 80dB of gain is required between the oscillator output and the main amplifier output the entire system was built into 3 separate die-cast boxes in order to isolate the units and help prevent spurious oscillation. An important detail in the construction of the individual units was the keeping of parasitic inductances low by mounting the circuit components adjacent to a ground plane. This is a direct consequence of the high frequencies (70MHz) and low impedances,

(50Ω) employed. Efficient decoupling of the power supplies is also necessary in order to prevent spurious coupling between the units and hence oscillations. This was achieved by the liberal insertion of decoupling capacitors. The pre-amplifiers and oscillator were powered from a 15V regulator which obtained its power from the 24V smoothed supply used to drive the main 20W R.F. amplifier.

Figure 3.4 shows the circuit diagram of the quartz crystal based oscillator together with its two stage buffer amplifier. The frequency stability at the output was about 200Hz per hour or about 0.5 p.p.m. This is adequate so no attempts to temperature stabilize the quartz crystal were made. After the buffer amplifier the output level was about 10mW into a 50Ω load.

Figure 3.5 shows the pre-amplifier stage which also allowed the R.F. signal to be gated on and off. The three active transistors in this section boost the 10mW from the oscillator buffer to a level of 1.2W ready to drive the main 20W power amplifier. The gating action is implemented via transistors Q4 and Q5 which remove the bias from all three R.F. amplifying transistors so conserving power. In our system, Q4 was driven from a CMOS monostable with a time constant of 10mSec. This in turn was pulsed on by a signal from the A.M.L. power supply.

Due to the power amplifier requiring a load impedance close to 50Ω at both its input and output at all frequencies it was necessary to insert 3dB attenuators between the pre-amplifier, main amplifier and mode-locker. These prevented the main amplifier from spuriously oscillating as a result of the mode locker reflecting R.F. power at frequencies where the mode locker is off resonance.

### 3.2.3. The A.M.L. oscillator alignment technique

The alignment procedure for the A.M.L. oscillator is more complicated than for a simple stable cavity design since the

FIGURE 3.4 R.F. OSCILLATOR / BUFFER CIRCUIT

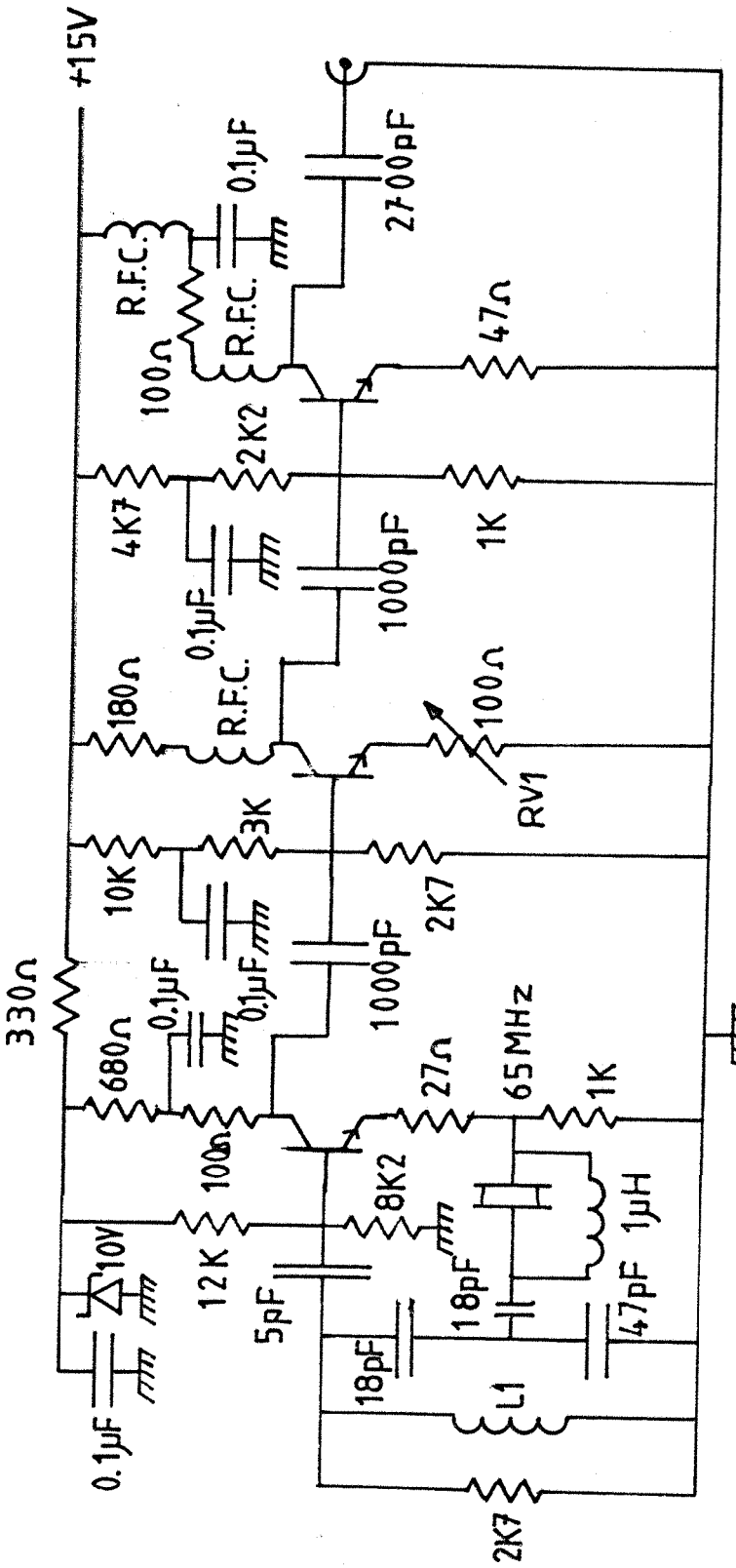


Notes: L1 = 8 turns, 8mm long x 5mm dia + tuning Stub.
Output level ≈ 10mW, Adjustable via RV1
All transistors 2N2222

FIGURE 3.4

FIGURE 3.5 R.F. PULSER AND PREAMPLIFIER

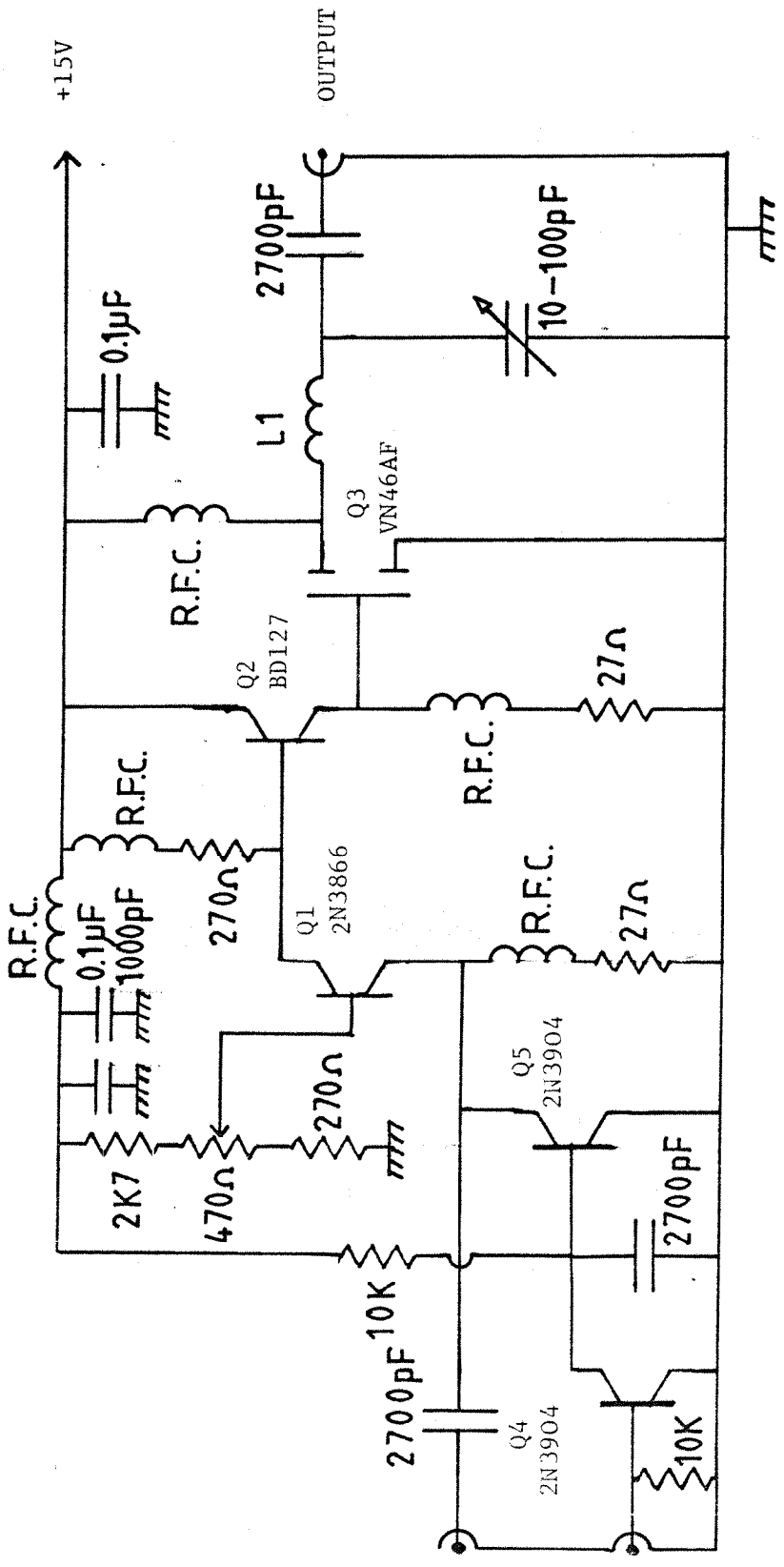


Note: L1 = 4 turns, 1cm long x 1cm diameter.

FIGURE 3.5

cavity length must be set correctly, to within a few microns, and the mode locker must be inserted into the cavity at the correct height and angle. In addition any etalon effects from the Pockels cell and laser rod must be eliminated if the minimum pulse width is to be obtained. In order to ensure that the diffraction efficiency of the mode locker is a maximum it is most effective to construct a sub-cavity which includes the laser rod but excludes the mode locker. The sub-cavity can be aligned with respect to the main cavity and then used to align the mode locker itself by monitoring its time averaged diffraction efficiency. In order to do this it is necessary to block off the reflection from the mirror which forms the cavity surrounding the mode locker. Failure to do this will result in mode-locking and spurious results as a consequence.

Having optimized the mode locker for optimum diffraction efficiency, replaced the outside mirror and removed the intracavity mirror, the cavity length can be optimised so as to coincide with the R.F. drive frequency. An easy way to do this is to monitor the oscillator threshold while varying the cavity length since the optimum cavity length also corresponds to the lowest threshold. The simplest method of monitoring the oscillator threshold is by observing the time of occurence of the first relaxation oscillation. Hence by minimizing this time the cavity length can be optimized.

When very close to the optimum cavity length the relaxation oscillations change in that they no longer die away but appear to become actively driven. This is most probably due to a coupling phenomena between the cavity round trip frequency, the R.F. frequency and the relaxation oscillation frequency. Since the R.O. frequency is 3 to 4 orders of magnitude smaller than the other two frequencies this coupling only occurs when the cavity length is very close to optimum. It has not been a part of the work of this thesis to investigate this phenomena further. The feature was however very useful as a check that a high diffraction efficiency from the mode locker was being maintained.

A step by step alignment procedure for the A.M.L. laser is presented as part of this thesis as appendix 3.

### 3.2.4 The pulse length measurement technique

When work first started on building the A.M.L. oscillator it was realized that an oscilloscope-photodiode combination would be too slow to monitor the short pulses that the laser was expected to produce. A photodiode with a rise time of 100pS was available, however, the only available oscilloscope had a rise time of 0.8nS. Since the use of sampling techniques to improve the frequency response are impractical with pulses of 10Hz repetition rate, an alternative means for measuring the laser pulse length was required. Since a streak camera was unavilable it was decided that some form of autocorrelation technique would be used to measure the pulse shape. The remainder of this section describes the design and construction of the autocorrelator used.

Figure 3.6 shows the autocorrelator which is essentially a modified Michelson interferometer followed by a frequency doubling crystal. As prism A is moved back and forth the pulses in the two beams move back and forth with respect to one another. If the two beams are incident upon the doubler at a slight angle to one another then by looking at the central frequency doubled beam a measurement of the pulse length can be made. This is because the central beam intensity is proportional to the intensities of both incident beams at the overlap region. A simpler way to look at this is that if the beams overlap a signal is produced, if they don't then no signal will result. The central beam is selected in preference to the two other second harmonic beams by use of a pinhole and the restricted acceptance cone of the doubler crystal.

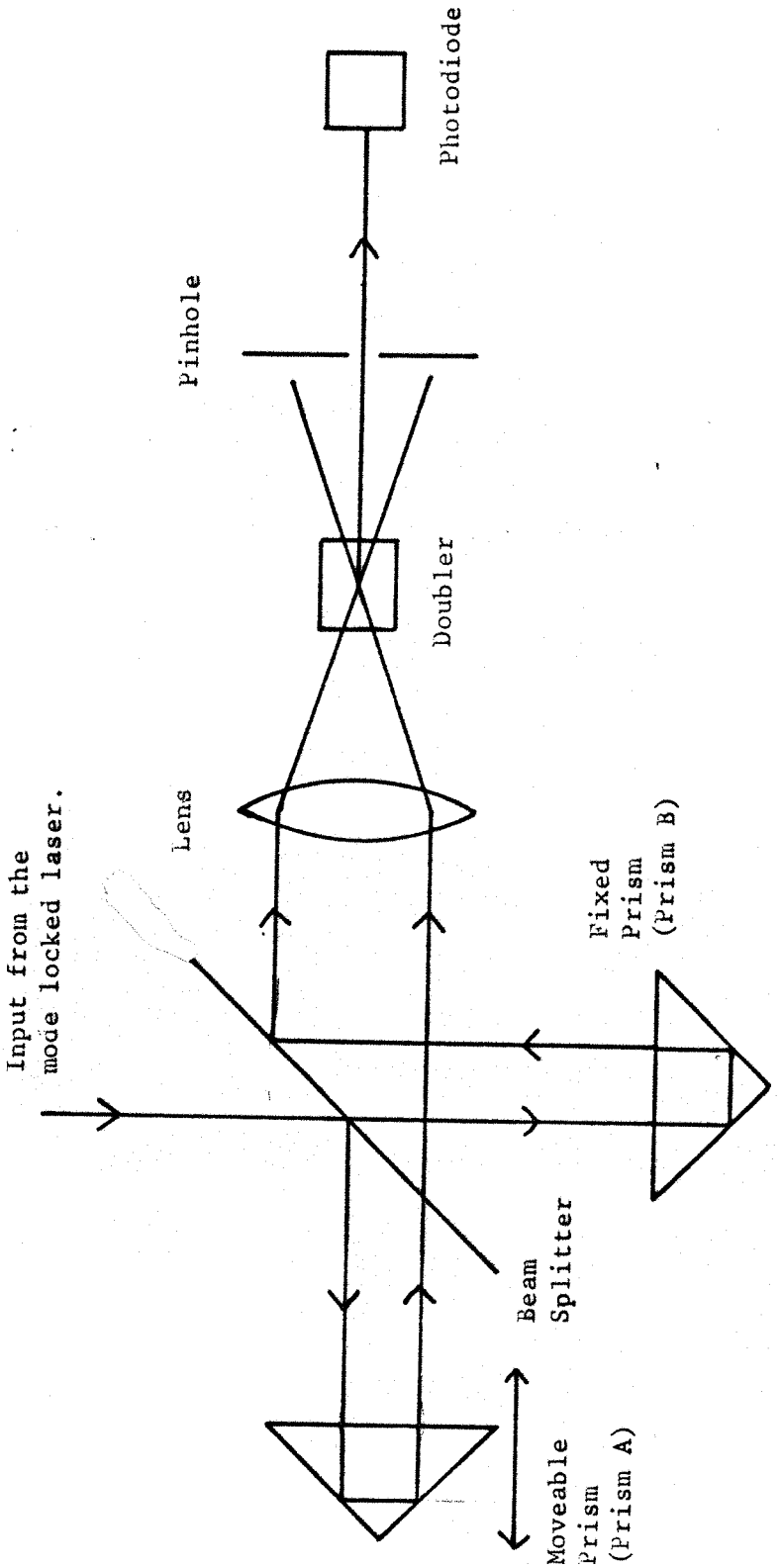


FIGURE 3.6 AUTOCORRELATOR OUTLINE

FIGURE 3.6

This method of autocorrelation has the advantage over other methods in that it is background free, i.e. no signal occurs when the pulses fail to overlap. The main problem is the need for both incident beams to overlap transversely in the doubler and remain stationary when prism A is moved back and forth. This is achieved by the use of a precision translation stage. We now present a brief mathematical treatment of the autocorrelation process.

The instataneous intensity in the central doubled beam is proportional to the product of the instantaneous intensities of the two incident beams. Therefore if a gaussian pulse with a 1/e, full width intensity duration of $2\tau$ is incident on the system the intensity in the central, doubled beam will be given by

$$I(t) = I_o \exp(-t^2/\tau^2) \exp[-(t+\Delta)^2/\tau^2] \qquad 3.39$$

where $I_o$ is constant provided the input beam amplitudes and transverse positions remain constant and $\Delta$ is the time delay between the two interferometer paths. If we look at the integral of I(t), (i.e. the beam energy), which can be obtained with a slow detector, we obtain,

$$E = \int_{-\infty}^{\infty} I_o \exp(-t^2/\tau^2) \exp[-(t+\Delta)^2/\tau^2]dt \qquad 3.40$$

Combining the two exponentials, completing the square and removing $\Delta^2/\tau^2$ terms from the integral we obtain

$$E = I_o \exp(-\Delta^2/2\tau^2) \int_{-\infty}^{\infty} \exp[-2(t+\Delta/2)^2/\tau^2]dt \qquad 3.41$$

or

$$E = I_o . K. \exp(-\Delta^2/2\tau^2) \qquad 3.42$$

Where K is a constant corresponding to the integral term. This equation gives us a value for $\tau$ by measuring E at two different values of $\Delta$. Comparing equation 3.42 with that for the intensity of the incident pulse, $I(t) = I_o \exp(-t^2/\tau^2)$, results in the conclusion that the function $E(\Delta)$ given by equation 3.42 will have a width which is $\sqrt{2}$ times larger than the incident pulse. If the f.w.h.m. of the detected pulse corresponds to a displacement of n centimeters of prism A, then equation 3.42 gives the pulse intensity f.w.h.m to be n x 47pSec.

Construction and Alignment of the Auto-Correlator

The alignment procedure for the autocorrelator is necessarily complicated and so full details are given here. Prism A needs to be mounted on a precision translation mount, in our case a travelling microscope base. The beam splitter is a 30% reflectivity mirror with a $1/2^{o}$ wedge which was A.R. coated on its rear surface. At $45^{o}$ it divided about 50% into each beam, with the wedge angle eliminating any confusion due to small reflections from the A.R. coating. Pinhole A was present to prevent any beams retro-reflected from the system interfering with the A.M.L. laser itself. The doubling crystal was of KDP, type I, suitable for doubling 1.06$\mu$m. The beam splitter mirror had to be placed in a specially constructed mount in order to allow access at acute angles over a reasonably large aperture.

What now follows is a description of the autocorrelator alignment procedure which is to be read in conjunction with figure 3.7 which shows the labelling notation of the various beams.

1) Beam b) must be made parallel to the direction of prism A's translation stage. Care must be taken to ensure that beam e) propagates through the beam splitter.

2) Prism A is mounted on the translation stage. Beam c) must be made parallel to b), about 0.5cm displaced horizontally, and

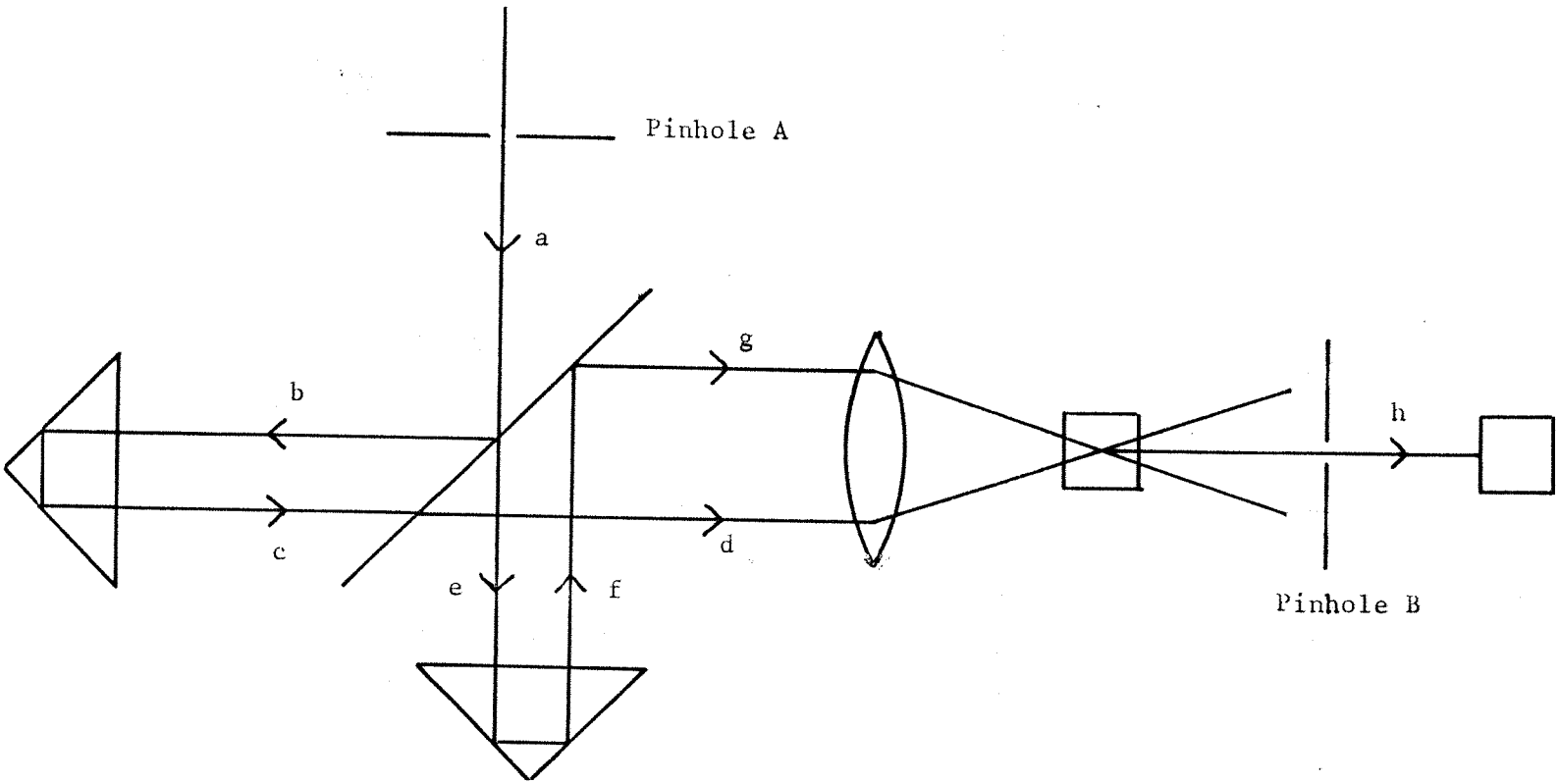


FIGURE 3.7 LABELLING NOTATION OF AUTOCORRELATOR BEAMS

FIGURE 3.7

continue through the beam splitter as beam d). None of these beams should move either in direction or transverse position as prism A is translated.

3) Prism B is mounted so that beam f) is retro-reflected parallel and displaced vertically about 0.5cm from beam e). Beam f) must be reflected by the beam splitter into beam g) which should be parallel to d) and about 0.7cm away. The beams must remain parallel and stationary when prism A is translated.

4) The lens (a 30cm focal length is suitable), is inserted and should cause both beams to focus down to the same point.

5) The K.D.P. crystal is inserted so as to contain this focus and aligned so as to phase match for second harmonic generation of the centrally generated beam h). If both second harmonic beams at d) and g) can be generated but not h) then the foci do not overlap. A small adjustment to the prisms should correct this. Note that to obtain beam h) with short pulses it is also necessary to have the path lengths in both arms of the autocorrelator similar.

### 3.2.5 A.M.L. Oscillator Performance

This section describes the performance of two different systems. The first was a system built as quickly as possible using components which were nearly all already present in the laboratory. The second system incorporated a number of improvements some of which were a consequence of discoveries made with the initial system and some of which were the result of equipment obtained after long delivery times preventing earlier instalation. The improvements are listed as follows:

1) With the construction of a high power, pulsed R.F. Amplifier the R.F. level was increased from 0.5W continuous to 7W in a 10 milli Second pulse.

2) The output mirror was changed from a plane/parallel to a plane/30' wedged reflector. This was to eliminate significant etalon effects caused by non-perfect A.R. coatings on the rear mirror surface.

3) The power supply was changed to a J.K. Lasers A.M.L. 'long pulse' type. As a consequence of this the prelase duration was increased from a few $\mu$Sec to upto 5mSec.

4) The coolant water was temperature stabilized using the Grants temperature stabilizer allowing more reliable matching of the R.F. drive frequency to the acousto-optic mode-locker resonance frequencies.

5) Cavity length adjusting blocks manufactured by J.K. Lasers were added to the cavity allowing finer control over the cavity length and preventing degredation of the output mirror alignment.

6) The whole system was mounted on a larger optical table with the availability of a 3" by 3/8" Yag amplifier rod. This allowed a much higher output energy to be obtained without optical damage problems. The larger optical table made alignment of the autocorrelator and the Raman experiments much easier.

Initial System Performance

The initial system produced an output of upto 5mJ in a train of pulses which were measured to be 470ps ($\pm$50pS) long. The pulse length, energy, envelope width and transverse profile all showed good stability ($\pm$10%), provided that the oscillator components were properly aligned. The output beam profile had a $TEM_{oo}$ profile due to a stable resonator configuration and an aperture present in the cavity. The limitation on output energy was due to the possibility of optical damage in the resonator. The laser

power supply itself was restricted to running at about half of its maximum possible output.

In order to compare the measured pulse duration with theory we must substitute the relevant values into equation 3.6 in order to obtain a predicted pulse duration. This was carried out in section 3.1.1. for the final resonator design described later in this section. For the earlier resonator designs however we must re-evaluate equation 3.6 using equations 3.3 and 3.7 and the relevant values for $\theta_m$, $\nu_s$, L(0) and M associated with this resonator.

With pre-lase q-switching we obtain M = 500, from section 3.1.2 we obtain $\theta_m$ = 0.45 at an R.F. level of 0.5W, the mode locker drive frequency, $\nu_s$, is 65.237MHz and L(o) is given at the end of section 3.1.3 as 7 x $10^{-21}$ $Hz^{-2}$ with the plane/parallel output reflector present. Substituting all of these values into equations 3.7, 3.3 and 3.6 gives

$$M_o = 410$$
$$\tau_{po} = 320pS$$
$$\tau_p = 350pS$$

This value for the predicted pulse length agrees fairly well with the 470pS measured experimentally and given at the begining of this section. The slight error is likely to be associated with estimates of $\theta_m$, and the effectiveness of the output reflector as a frequency selective element. Additionally the slightly longer pulses observed experimentally could be due to a non-optimally aligned mode locker which would be expecially likely to occur during the first measurements on the A.M.L. oscillator. This is likely to be more significant than on later measurements where an established alignment procedure had been adopted.

After 500 round trips the noise bandwidth given by equation 3.9 will be 780MHz. Since the transform limited pulse bandwidth is

given by $0.44/\tau_p$, or 980MHz for 450pS pulses, the pulses will be fairly close to being bandwidth limited. Consequently only a small amount of temporal structure should be present on the pulses. This was observed experimentally with the autocorrelator as no 'correlation spike', characteristic of this noise, could be seen when both arms of the autocorrelator were of the same length.

Performance of the improved system

After carrying out some initial experiments on S.R.S. in Gases in capillary waveguides using 450pS long pulses, (see A.J. Berry, 1984), the A.M.L. oscillator underwent a further period of development. During this time the major changes affecting the A.M.L. oscillator characteristics were the utilization of a long 5mS laser power supply and the increased R.F. drive power to the acousto-optic mode locker. The result of these modifications was a system producing pulses of 200pSec in duration which was about twice as long as expected. After some investigation it was discovered that the output mirror was a plane/parallel device whch theoretically should result in the approximate doubling of the pulse length as observed, (see section 3.1.3). When the output reflector was replaced by a similar but wedged device the resulting pulses were reduced in duration as expected by the factor of two. The resulting pulses of 100pS duration, ($\pm$20pSec depending on resonator component alignment), agrees very well with the value of 87pS predicted in section 3.1.1.

Throughout all the investigations on the A.M.L. oscillator the simple stable resonator configuration remained unchanged. Consequently the output beam comprised a diffraction limited, $TEM_{oo}$ mode with a spot size calculated to be 0.6mm which was confirmed experimentally using a photodiode array. The length of the pulse envelope was monitored with a vacuum photodiode and a transient digitizer which had a combined 1nSec rise time. The f.w.h.m. of the pulse envelope was typically 80nS but although consistent from shot to shot this varied significantly depending

on such factors as oscillator alignment, the age of the flashlamp and the Pockels cell voltage setting. Similarly the pulse train energy although consistent from shot to shot also varied on a long term basis from a typical value of 3mJ. The upper limitation on the value was due to the flashlamp power supply. This problem could have been alleviated slightly if a 4mm rod had been substituted for the 6.25mm rod actually present. Since only a 2mm rod diameter was needed to accomodate the laser mode, the smaller rod would have utilized the available flashlamp energy more effectively resulting in more output.

The output energy of the A.M.L. oscillator of only a few millijoules was insufficient for some of our S.R.S. experiments. As a result of this a beam expanding telescope and Yag amplifier rod were used to boost the available output energy. Details of these additions are given in section 5.1.3 together with the experimental work on S.R.S. Also described in that section are the results of frequency doubling the amplified A.M.L. oscillator output.

## 3.3 The synchronously pumped dye laser system

This section describes the operation and performance of a synchronously pumped dye laser, (S.P.D.L.) which was used to obtain some of the results presented in Chapter 5. Fuller details of the S.P.D.L. are to be found in Ure, (1984), following a design described by Wokaum et al, (1982).

Details of the layout of the S.P.D.L. system complete with the A.M.L. Yag oscillator, amplifier and frequency doublers are shown in figure 3.8. The whole system was mounted on a double width extruded laser base manufactured by J.K. Lasers. The components used in the S.P.D.L. system described here were drawn together from a number of sources, in a limited amount of time and with a limited financial budget. As a consequence a number of components were in a non-pristene condition. The resulting laser system produced upto 600$\mu$J of energy in a single 70pSec dye pulse, as opposed to 1mJ expected from a production system. Regular re-alignment was necessary due to a faulty mirror mount.

### Temporal and Spectral performance

Throughout the work at J.K. Lasers no accurate measurement of the A.M.L. pulse length was made. However, the Kuizenga theory predicts a pulse length of 100pS which we can confidently expect to be within about 10% of the experimental value. Using this value of 100pS we have a 532nm pulse length of 70pS and a dye pulse length of 50pS, increasing to about 70pS after the dye amplifier. This was confirmed experimentally, using an autocorrelator at J.K. Lasers, as being between 50 and 80pS. A better measurement was not possible due to jitter in the dye pulse amplitude and limited time with the system fully operational.

The spectral linewidth of the dye laser output has been measured by Ure, (1984) as 10.2GHz. This compared well with the bandwidth

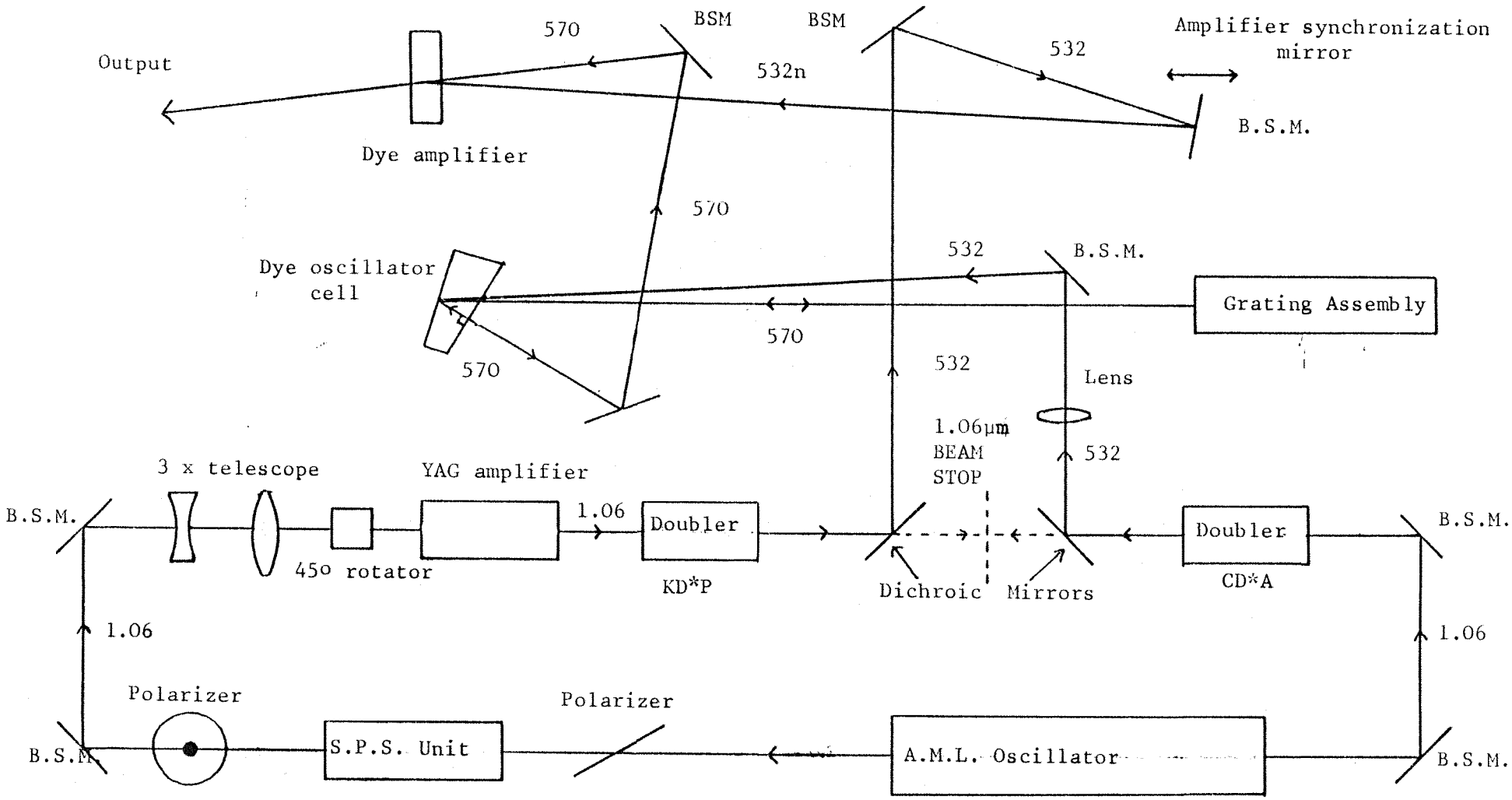


FIGURE 3.8 SCHEMATIC LAYOUT OF THE S.P.D.L. SYSTEM

(B.S.M. = Beam Steering Mirror)

limit for 50pS pulses of 8.8GHz and implies that the dye laser produced near bandwidth limited pulses. This is to be expected since the grating used to tune the dye oscillator was operated in a grazing incidence configuration with an illuminated depth of over 1cm. This corresponds to a spectral reflectivity f.w.h.m. of 7.5GHz.

The tuning range of the s.p.d.l. system was measured with a photodiode energy meter together with the calibrated tuning mechanism of the dye laser oscillator. The following results were obtained.

| Relative Energy Output | λ max | λ min |
|---|---|---|
| 1.0 | 558 | 558 |
| 0.75 | 562 | 556 |
| 0.5 | 568 | 554 |
| 0.25 | 570 | 553 |

From this data it is apparent that the tuning profile is asymmetric with a 14nm f.w.h.m. tuning range, ($450cm^{-1}$). The response of the photodiode energy meter was essentially constant over the entire tuning range.

# 4. THE THEORY OF TRANSIENT STIMULATED RAMAN SCATTERING WITH GAUSSIAN TRANSVERSE BEAM GEOMETRIES

Stimulated Raman scattering is an important non-linear optical process providing a method of extending the wavelength coverage of laser systems. Over a period of some twenty years various analyses have been made of the S.R.S. process. However, to the authors knowledge, the effect of Gaussian transverse beam geometries, has only been analysed for steady state S.R.S. and not with transient pump pulses. In this chapter we attempt a treatment of transient S.R.S. in situations where finite transverse profiles are involved. We consider a tightly focussed Gaussian beam in both free space and in a capillary waveguide. Firstly however we must collect together the preliminary analytical ideas and data before the combined treatment given in section 4.3.2 can be attempted.

## 4.1 The steady state, plane wave Raman gain coefficient

A steady state analysis of the growth of the Stokes intensity $I_s(z)$ over a length z of active material gives $I_s(z) = I_s(0) \exp(g_r.I_p.Z)$ where $g_R$ is the steady state, plane wave Raman gain coefficient. A derivation of this coefficient from the Raman cross-section is given by many authors, (e.g. Trutna and Byer, 1980; Hanna et al, 1979; and Kaiser and Maier, 1972) and a brief sumary of this calculation is given here.

We can write $g_R$ in terms of the Raman susceptability $\chi_R = \chi_R' + j\chi_R''$ (see Butcher, 1965) as

$$g_r = \frac{2\omega_s \chi_R''}{c^2 \varepsilon_o n_s n_p} \qquad 4.1$$

Similarily the imaginary part of the Raman susceptability can be written in terms of the differential cross section per unit solid angle, $d\sigma/d\Omega$, (Trutna and Byer, 1980) as

$$\chi_R'' = \frac{(2\pi)^3 n_p c^4 \varepsilon_o \Delta N}{\pi n_s \omega_p \omega_s^3 \hbar \Delta\omega_R} \cdot \frac{d\sigma}{d\Omega} \qquad 4.2$$

In both of the above equations the variables are as follows, $\Delta N$ is the population density difference between the initial and final states of the Raman transition, $n_s$, $n_p$ the refractive indicies at the Stokes and pump wavelengths, $\omega_s$, $\omega_p$ their angular frequencies, $\Delta\omega_R$ is the f.w.h.m of the Raman transition and $\frac{d\sigma}{d\Omega}$ is the Raman differential scattering cross-section. Combining equations 4.1 and 4.2 we obtain

$$g_r = \frac{4 \lambda_s^2 \Delta N}{n_s^2 \hbar \omega_p \Delta\omega_R} \cdot \frac{d\sigma}{d\Omega} \qquad 4.3$$

Note that the Raman differential scattering cross-section used above relates photon numbers of incident and scattered light and not intensity. Since most cross-section data relates to intensities, we must make the substitution

$$\left.\frac{d\sigma}{d\Omega}\right|_{\text{photons}} = \left.\frac{\omega_p}{\omega_s} \cdot \frac{d\sigma}{d\Omega}\right|_{\text{intensity}} \qquad 4.4$$

giving

$$g_r = \frac{4 \lambda_s^2 \cdot \Delta N}{n_s^2 \hbar \omega_s \Delta\omega_R} \cdot \left.\frac{d\sigma}{d\Omega}\right|_{\text{intensity}} \qquad 4.5$$

From now on we shall use just $\frac{d\sigma}{d\Omega}$ meaning the intensity definition. This is our final expression for the steady state plane wave Raman gain coefficient. We shall now obtain values for the parameters in this equation for the gases Hydrogen and Methane.

$\Delta N$ is given by the population difference per unit volume between the initial and final levels of the Raman transition. This is given by,

$$\Delta N = F(T).\ P/kT \qquad 4.6$$

where P is the pressure, k is Boltzmann's constant, T the temperature and F(T) a factor describing the proportion of active molecules.

For the Raman transitions of interest the final state population can be considered zero as it is many kT above the ground state. Consequently the factor F(T) is the proportion of atoms in the initial state. In hydrogen this factor is 0.66 at room temperature, (see Byer, 1976), whereas for methane F=1 since all molecules contribute to the Raman process, (Schrotter and Klockner, 1979).

The linewidth $\Delta w_R$ is obtained from experimental measurements reported by other authors. The results for Hydrogen and Methane differ substantially and depend on the pressure. For Hydrogen the Raman linewidth (f.w.h.m.) was found by Murray and Javan, (1972), to be described by

$$\Delta\omega_R = \frac{D}{P} + a.P \qquad 4.7$$

For pressures above about 10 atmospheres the first term (which corresponds to Dicke narrowing) becomes neglibible compared with the later. The linewidth then becomes a linear function of pressure. The value of a is given in Trutna and Byer, (1980), as, $a = 2.38 \times 10^8$ Rads. $Sec^{-1}.Atm^{-1}$.

For Methane the vibrational transition has a residual linewidth which at a few atmospheres pressure can be resolved into transitions corresponding to different initial rotational levels, (May et al, 1978). At higher pressures, Taira et al, (1982) obtained the following expression experimentally for the linewidth

$$\Delta\omega_R = 6 \times 10^{10} + 2.3 \times 10^{9}.P \qquad 4.8$$

where again P is the pressure in atmospheres. At low pressures it may be incorrect to use this expression in our equations for the Raman process as the $6 \times 10^{10}$ Rads/sec component is made up of the individual resolvable transitions. Due to a lack of better experimental data it was necessary to use this expression as given. At 30 Atmospheres pressure the error introduced should be sufficiently small.

The differential scattering cross section $d\sigma/d\Omega$ is calculated from tabulated measurements taken at various wavelengths. Schrotter and Klockner, (1979), summarize a large number of measurements taken by different authors for many gases at a number of wavelengths. The data relates to measurements at pump wavelengths other than those used in our experiments and it is therefore necessary to convert the data to 532nm and 1.06$\mu$m. The results of Schrotter and Klockner are quoted relative to $N_2$, for which

$$\left(\frac{d\sigma}{d\Omega}\right)_{N_2,514nm} = 4.3 \times 10^{-31} cm^2/sr \qquad 4.9$$

We also have at 514nm for the relative differential Raman scattering cross-sections which relate different gases to nitrogen, (given the symbol $\Sigma j$ by Schrotter and Klockner),

$$\Sigma j \text{ (Hydrogen)} = 3.4$$
$$\Sigma j \text{ (Methane)} = 9.0$$

Additionally there is a $\omega_s^4$ dependence of all the cross-sections which is not included in the $\Sigma j$ factor, hence we have

$$\left(\frac{d\sigma}{d\Omega}\right)_{H_2,514nm} = \left(\frac{d\sigma}{d\Omega}\right)_{N_2,514nm} \cdot \left(\frac{\nu_o - 4155cm^{-1}}{\nu_o - 2331cm^{-1}}\right)^4 \Sigma_j(\text{hydrogen}) \qquad 4.10$$

where $\nu_o$ is the frequency in $cm^{-1}$ corresponding to 514nm.

In methane the situation is similar leading to the following values,

$$\text{Hydrogen} : \frac{d\sigma}{d\Omega} = 9.4 \times 10^{-31} \text{ cm}^2/\text{sr}$$

$$\text{Methane} : \frac{d\sigma}{d\Omega} = 3.4 \times 10^{-30} \text{ cm}^2/\text{sr}$$

The relationship

$$\frac{d\sigma}{d\Omega}_{(\lambda=\lambda_p)} = \frac{\omega_s^4(\lambda_p)}{w_s^4(514)} \cdot \frac{\left[\frac{1}{\Omega_{ig}-W_p} + \frac{1}{\Omega_{ig}-W_s}\right]^2_{(\lambda=\lambda_p)}}{\left[\frac{1}{\Omega_{ig}-\omega_p} + \frac{1}{\Omega_{ig}-\omega_s}\right]^2_{(\lambda=514)}} \frac{d\sigma}{d\Omega}_{(\lambda=514)} \qquad 4.11$$

gives the cross section value for different wavelengths (Hanna et al, 1979). The terms is square brackets describe the dispersion of the Raman susceptability with $\Omega_{ig}$ being the dominant intermediate level in the Raman process. In hydrogen this level is at 90,000$cm^{-1}$ and so at worst a 20% error would be introduced by ignoring these terms in going from wavelengths of 500nm to the longest wavelength. In Methane the situation is similar. The results obtained using these equations for Hydrogen and Methane at 30Atms and at the wavelengths used in the experiments are given in table 4.1. Also given is some other useful data such as Stokes wavelengths and frequencies.

| Raman Medium | Pump | 1st Stokes | $\frac{d\sigma}{d\Omega}$ ($cm^2/sr$) | $g_r$ (cm/W) | $T_2$ (pS) |
|---|---|---|---|---|---|
| $H_2$ | 1.06um ($9361cm^{-1}$) | 1.91um ($5236cm^{-1}$) | $1.2x10^{-32}$ | $1.3x10^{-9}$ | 280 |
| shift = $4155cm^{-1}$ | 0.53um ($18782cm^{-1}$) | 0.684um ($14627cm^{-1}$) | $7.9x10^{-31}$ | $3.7x10^{-9}$ | |
| $CH_4$ | 1.06um ($9391cm^{-1}$) | 1.54um ($6474cm^{-1}$) | $7.0x10^{-32}$ | $3.25x10^{-10}$ | 16 |
| shift = $2917cm^{-1}$ | 0.53um ($18782cm^{-1}$) | 0.630um ($15865cm^{-1}$) | $2.7x10^{-30}$ | $8.6x10^{-10}$ | |
| | 0.57um ($17500cm^{-1}$) | 0.686um ($14583cm^{-1}$) | $1.95x10^{-30}$ | $7.9x10^{-10}$ | |

TABLE 4.1 S.R.S. DATA IN HYDROGEN AND METHANE

## 4.2 The effects of Gaussian transverse beam geometries

When carrying out stimulated Raman experiments with laser beams, the theories of plane wave S.R.S. cannot be applied directly. This is as a result of variation in the intensity of the pump beam in the transverse plane. The problem is further complicated by diffraction of the Stokes wave which introduces losses, and broadens the Stokes transverse profile. This broadening will be balanced somewhat by gain focussing introduced as a result of the Gaussian transverse profile of the pump.

The three parts of this section consider the effect on threshold of three different beam geometries; tight focussing, using a waveguide, and using a resonator.

### 4.2.1 Tight focussing

In all our tight focussing experiments the pump beam was comprised of a $TEM_{oo}$ mode which was tightly focussed to the centre of a cell of length L. Cotter et al, (1975), consider a steady state analysis of this problem but find that the resulting progagation equation for the Stokes wave cannot be solved analytically. What follows is a summary of their work which included approximations allowing an analytical solution to be obtained which agrees closely with the numerically obtained solution for the exact analysis.

The pump beam is given by the following equations for a tightly focussed pump beam.

$$I_p(r,z) = I_{po}(z).\ \exp\{-2r^2/w_p^2(z)\} \qquad 4.12$$

where

$$w_p^2(z) = W_{po}^2.\ (1 + \varepsilon^2) \qquad 4.13$$

$$I_{po}(z) = 2.P_p[w_{po}^2\ (1 + \varepsilon^2)]^{-1} \qquad 4.14$$

$$\varepsilon = 2.(z - z_f)/b_p \qquad 4.15$$

$P_p$ is the pump power, $w_{po}$ is the beam spot size at the waist (focus), $z_f$ the position of that focus and $b_p$ the confocal parameter of the pump beam ($=2\pi w_{po}^2/\lambda_p$). The transverse profile of the pump intensity, given by equation 4.12 results in gain focussing of the Stokes wave. The Stokes wave therefore will tend towards a beam whose diffraction and gain focussing balance each other. It has not proved possible to obtain an analytical solution for the Stokes beam profile from equation 4.12. However, by making a parabolic approximation for the on axis pump intensity,

$$I_p = I_{po}(z)\ [\ 1 - 2r^2/w_p^2(z)\ ] \qquad 4.16$$

an analytical solution can be found if the Stokes profile changes slowly with respect to its equilibrium value given by diffraction and gain focussing. The analytical solution is found by substituting an arbitary Gaussian profile for the Stokes wave:

$$E_s(r) = A \exp[\ -j(\phi + Qr^2/2)\ ] \qquad 4.17$$

where $$\frac{Q}{k_s} \equiv \frac{1}{q} \equiv \frac{1}{R_s} - \frac{2j}{k_s W_s^2} \qquad 4.18$$

into the wave equation for the Stokes radiation,

$$\frac{1}{r} \cdot \frac{\partial}{\partial r}\left(r.\frac{\partial E_s}{\partial r}\right) - 2jk_s.\frac{\partial E_s}{\partial z} + jk_s.g_r.I_p(z,r).E_s = 0 \qquad 4.19$$

Separating terms with equal powers of r we obtain two equations

$$\frac{Q^2(z)}{K_s} + \frac{\partial Q(z)}{\partial z} + j\,\frac{2\tilde{P}_p}{k_s W_p^4(z)} = 0 \qquad 4.20$$

and $$\frac{1}{A(z)} \cdot \frac{dA(z)}{dz} = \frac{\tilde{P}_p}{2k_s W_p^2(z)} - \frac{1}{R_s(z)} \qquad 4.21$$

where $\tilde{P}_p = 4g_r P_p/\lambda_s$ and $P_p$ is the pump power.

Obtaining an approximate solution to equation 4.20, Cotter et al substitute this into equation 4.21 and integrate to obtain the following equation relating the Stokes amplitude gain and pump power for a cell of length L with a pump waist at the cell centre.

$$\frac{A(L)}{A(o)} = \exp\left\{ [(\tilde{P}_p - 2\sqrt{\tilde{P}_p})/2\kappa]\arctan(L/b_p) \right\} \qquad 4.22$$

Where $\kappa = \omega_s / \omega_p$

Re-arranging equation 4.22 to obtain a predicted threshold power for a given Raman gain requirement we obtain,

$$P_{pth} = \frac{\lambda_s}{4g_r}\left\{1 + \left[1 + \frac{\kappa}{\arctan(L/b_p)}.\mathrm{Ln}\left(\frac{P_s(L)}{P_s(o)}\right)\right]^{1/2}\right\}^2 \qquad 4.23$$

Normally $\mathrm{Ln}\left(\frac{P_s(L)}{P_s(o)}\right)$ is set equal to 30 for threshold to be reached since this is a typical difference between detector threshold and the quantum noise power $P_s(0)$. The expression above has been used to predict threshold for pump pulses of ~20nSec where the Raman process is steady state. The threshold values obtained are in good agreement with experimentally measured threshold powers.

In our later treatment of transient S.R.S. we shall need to make use of equation 4.23. Before introducing our transient analysis however, we shall examine the steady state analysis relating to waveguide and oscillator configurations.

### 4.2.2 The use of a waveguide

The threshold powers for S.R.S. are typically quite high which means for many low power laser sources S.R.S. is not a suitable technique for frequency shifting as threshold cannot be reached. In order to lower the threshold we must maintain tighter focussing over a longer length so increasing the intensity-length product in $G_s = \exp(g_r.I_p.L)$. The problem is worst at longer wavelengths since not only is $g_r \propto \lambda_s^{-1}$ but the intensity-length product when tight focussing with a fixed input power is proportional to $\lambda_p^{-1}$.

One method of increasing the interaction length is to use a resonator and repetitively reflect the Stokes beam through the gain region. With a mode locked pump beam an additional complication arises since the Stokes pulses have to be synchronized with incoming pump pulses. Alternatively, if only a single mode locked pulse is available, for example if a single mode locked pulse switchout system is employed, then the use of a resonator is impossible unless both pump and Stokes beams are repetitively reflected and refocussed. This idea has been used with some success (Herriot et al, 1964; Trutna and Byer, 1980), but the multiple pass cell arrangement is critical in its alignment and has mirror damage limitations. A theoretical analysis of resonators is presented in section 4.2.3.

An alternative method of increasing the intensity length product is to use a small bore capillary waveguide, (Rabinowitz et al, 1976; Hartig and Schmidt, 1979). This technique has achieved threshold reductions of well over an order of magnitude, (Berry and Hanna, 1983), but apart from the results reported by May and Sibbett, (1983), these measurements have all been made with pulses long enough (>10nSec), to satisfy steady state conditions. The use of a capillary waveguide for S.R.S. requires careful consideration as coupling losses, waveguide losses, and the degree of transience, all need to be taken into account. The remainder

of this section evaluates these factors in order that an optimum choice of capillary length, capillary bore and focussing conditions can be made.

The problem of guided radiation in hollow cylindrical dielectric waveguides has been treated by many authors including Marcatilli and Schmeltzer, (1964), and Adams, (1981). The essential result obtained is that the lowest loss mode is the $EH_{11}$ mode which has an intensity loss coefficient $\alpha_{11}$ given by

$$\alpha_{11} = \left(\frac{2.405}{2\pi}\right)^2 \frac{\lambda^2}{a^3} \cdot \frac{n^2 + 1}{2(n^2-1)^{0.5}} \qquad 4.24$$

where a is the capillary bore radius, $\lambda$ the wavelength of the light propagating through the waveguide and n the refractive index of the capillary. From this equation we can see that the losses increase with increasing wavelength and decreasing bore radius. Figure 4.2 shows the dependence of losses on wavelength and capillary bore for a 1 metre long waveguide. This figure, taken from Berry, (1984), also shows the theoretically expected bending losses.

An analysis of bending losses in capillary waveguides is given in Marcatilli and Schmeltzer, (1964), and summarized in Berry, (1984). The final result for the $EH_{11}$ mode, valid for small amounts of bending, is given by

$$\alpha_{11}(R) = \alpha_{11}(\infty) + \frac{a^3}{\lambda^2 R^2} \; 15.5 \; [1 + 0.246 \cos(2\theta_o)] \qquad 4.24b$$

In this equation $\alpha_{11}(R)$ is the $EH_{11}$ attenuation coefficient, a the bore radius and R the bend radius of curvature. The angle $\theta_o$ is the angle between the $EH_{11}$ polarization and the plane containing the bent capillary. A 1m long capillary which is bent so that its

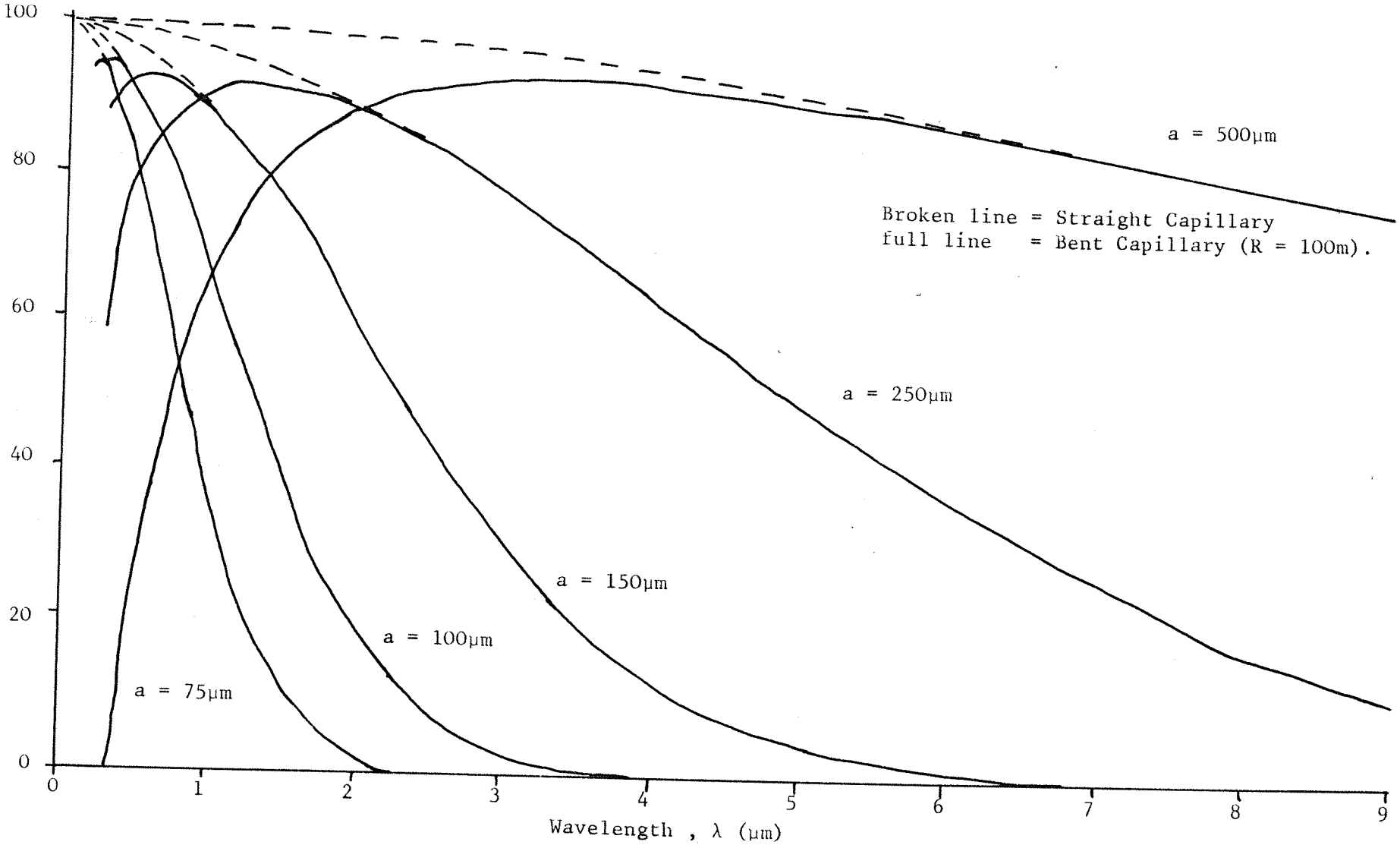


FIGURE 4.2 CAPILLARY LOSSES

FIGURE 4.2

centre is displaced 0.5cm has a bend radius of 25m. The resulting attenuation coefficient contribution is around $0.04m^{-1}$ and so the effect of this loss can generally be neglected.

Fortunately the lowest loss $EH_{11}$ mode and the $TEM_{oo}$ free space mode have almost identical profiles resulting in a high coupling between the two modes given the correct matching conditions. Abrams, (1972), calculates that the coupling between the two modes is a maximum when the $TEM_{oo}$ waist size, $w_o = 0.644a$ at the entrance to the capillary. With this matching condition he calculates a 98% coupling efficiency between the two modes.

A rough idea of the degree of improvement a capillary waveguide will bring can be obtained by comparing the length of the capillary to the confocal parameter corresponding to a beam of waist 0.644 a. This gives only a rough estimate and more accurate method of calculating the S.R.S. threshold power in a waveguide is required.

In a capillary the pump intensity profile is well described by the $EH_{11}$ mode. Additionally the Stokes intensity profile will have a profile very similar to this mode since in a waveguide gain focussing has a negligible effect compared with guidance from the capillary. Since both pump and Stokes can be well described by the $EH_{11}$ mode, we can with very little loss of accuracy use the almost equivalent $TEM_{oo}$ free space mode to estimate threshold. The theories given in Boyd et al, (1969), consider the interaction between the Stokes and pump waves when both are defined by $TEM_{oo}$ Gaussian modes. They obtain over a length L an increment in the Stokes power $\Delta P_s$ given by

$$\Delta P_s = -\mathrm{Im}\left\{ \frac{\omega_s}{2} \int_0^L \oint_{-\infty}^{\infty} E_s^{*} P_s \, dx.dy.dz \right\} \qquad 4.25$$

where $P_s$ is the non-linear polarization given by,

$$P_s = -i.\chi_R".\varepsilon_o.E_p.E_p^*.E_s \qquad 4.26$$

where $\chi_R"$ is the imaginary part of the non-linear susceptability which is related to the Raman gain coefficient and is given by equation 4.2. Equation 4.25 contains an overlap integral in which the term $E_s^*$ acts as a projection operator picking out the contribution that the polarization makes to the Stokes field $E_s$. In order to obtain a value for $\Delta P_s$ we must substitute in the pump and Stokes fields with the appropriate radial profiles i.e.

$$E_{p,s}(r) = E_{po,so} \exp(-r^2/W_o^2) \qquad 4.27$$

Subsituting these in equation 4.25 via 4.26 we obtain,

$$\Delta P_s = \frac{\omega_s}{2} \int_0^L \int_0^\infty [\chi_R".\varepsilon_o.E_{po}^2.E_{so}^2.\exp\left(\frac{-4r^2}{W_o^2} - 2\gamma_p z\right)$$

$$-2.P_s.\gamma_s.Z]r.dr.2\pi.dz \qquad 4.28$$

where we have changes to polar co-cordinates and allowed for pump and Stokes losses of the form $\exp(-\gamma z)$ by introducing the terms $\gamma_p$ and $\gamma_s$. For a $TEM_{oo}$ beam the relationship between the electric field and the instantaneous power is given by,

$$E^2 = \frac{4P}{\pi W_o^2} \sqrt{\frac{\mu_o}{\varepsilon_o}} \qquad 4.29$$

hence substituting for pump and Stokes into equation 4.28 and re-arranging we obtain

$$\int_{P_s(o)}^{P_s(L)} \frac{\Delta P_s}{P_s} = \frac{\omega_s}{2} \int_o^L \int_o^\infty [\chi_R" .\mu_o. \frac{16.P_p}{\pi^2 W_o^4}. \exp\left(\frac{-4r^2}{W_o^2} - 2.\gamma_p.Z\right)$$

$$-2.\gamma_s.Z]\ r.dr.2\pi.dz \qquad 4.30$$

where $P_p$ and $P_s$ are the pump and Stokes powers corresponding to $E_p$ and $E_s$. Performing the integrals and substituting for $\chi_R''$ with $g_r$ given by equation 4.1 we obtain

$$\text{Ln}\left(\frac{P_s(L)}{P_s(o)}\right) = \frac{g_r . L_{eff} . P_p}{\pi W_o^2} - 2.\gamma_s.L \qquad 4.31$$

where the variable $L_{eff}$ corresponds to an effective length to take into account the effect of pump losses. This is given by

$$L_{eff} = [1 - \exp(-2\gamma_p L)]/2\gamma_p \qquad 4.32$$

Re-arranging equation 4.31 to obtain a required pump power given a required Raman Stokes gain, we obtain,

$$P_p = \frac{\pi . W_o^2 \; [\; \text{Ln}\; \{P_s(L)/P_s(O)\} + 2.\gamma_s.L]}{g_r . \; L_{eff}} \qquad 4.33$$

This equation can be used to predict S.R.S. threshold by substituting for $P_s(L)/P_s(O)$ with the ratio between the detector threshold and the Stokes noise power. Using $EH_{11}$ profiles rather than Gaussian profiles gives a slightly different result, (Ibison, 1982).

$$P_p' = 0.885 . P_p \qquad 4.34$$

With the theoretical predictions of this section and the gain coefficients evaluated earlier we are now in a position to make predictions of the pump power required to reach steady state S.R.S. threshold. Transient predictions will be dealt with in section 4.3.2.

### 4.2.3 The use of synchronous pumping

If the pump consists of more than one pulse there is no reason why the full exp(30) gain must be obtained in a single pass through the medium. Instead, mirrors can be placed around the Raman cell and part of the Stokes beam reflected so that it coincides with later pump pulses as they propagate through the medium. The use of a resonator has been tried using long input pulses of around 20nS, (Trutna and Byer, 1980; Berry , 1983). A synchronously pumped short pulse Raman resonator has (apart from a few recent instances in optical fibres), to the authors knowledge only been published by Colles, (1971), who used very short pulses, (~5pSec), with benzene as the Raman medium. The resonator used in this instance was primarily to compensate for dispersion in the benzene and consequently produce shorter pulses rather than to reduce the threshold power. The aim of this section is to give a rough idea of how much threshold reduction should be expected using a typical resonator configuration.

The threshold reduction expected in using a resonator will depend on the round trip Stokes losses. These will be comprised of the following; mirror losses, uncoated window and lens losses, mirror alignment losses, imperfect spot size matching, and imperfect synchronisation of the pump. Another factor determining the degree of threshold reduction that may be obtained with a resonator is the number of pulses in the pump train.

The overall gain of a train of pump pulses can be obtained by adding together the single pass effective gains of each pulse in the train, where by single pass effective gain we mean that the gain allowing for round trip Stokes losses but not being less than unity. At threshold this product will be equal to $P_s(L)/P_s(0)$ which is approximately equal to exp (25). A numerical approach must be used in order to find the peak single pass gain since the solution is needed to work out how many pulses contribute to the product.

To estimate the expected threshold reduction for a resonator we consider the conditions applicable to our pump laser. As a rough estimate of the Stokes losses we can assume a round trip intensity attenuation factor of exp(-4). The pulse train has a Gaussian envelope with a f.w.h.m. of 45nSec or 6 pulse spacings. We can therefore describe the gain resulting from a single pulse, to be given by

$$G(n) = G(o).\ \exp\left(\frac{-n^2.\ Ln(2)}{9}\right) \qquad 4.35$$

where n is the separation in numbers of pulses from the centre pulse and G(O) is the centre pulse gain. In our experiments on synchronous pumping, the overall Stokes gain requirement was approximately exp(25). Numerically we find that this gain is reached when the centre pulse gain reaches or exceeds exp(10). In a single pass the centre pulse gain would be required to provide a gain of exp(25), hence we can expect a threshold reduction of, between 2 and 3 from the use of the synchronous pumping.

If a capillary waveguide is also used in the resonator then additional Stokes round trip losses will be introduced as a consequence of launching inaccuracies and waveguide attenuation. Typically these will result in an extra Stokes attenuation of exp(-3), making exp(-7) in total. We now find that for a total Stokes gain requirement of exp(25) we require a centre pulse gain of exp(14). Hence for a capillary waveguide resonator with our laser we expect a threshold reduction of only 45%.

## 4.3 Transient S.R.S.

Until now our theoretical investigations of S.R.S. have only considered the steady state Raman process where the pump pulse duration, $\tau_p$ is much greater than the Raman transition dephasing time $T_2$. Later in this section we shall show that the Raman

process is steady state only if $\tau_p \geq 20T_2$. The value of $T_2$ is obtained from the homogeneous linewidth of the Raman transition $\Delta\nu_R$ which varies with pressure as given by equations 4.7 and 4.8. At the pressures used in all our experiments the homogeneous linewidth dominates the inhomogeneous linewidth and so we have used the relation,

$$T_2 = \frac{1}{\pi} \cdot \frac{1}{\Delta\nu_R} = \frac{1}{\pi . c . \Delta\tilde{\nu}_R} \qquad 4.36$$

where $\Delta\nu_R$ is the f.w.h.m. of the Raman linewidth. We obtain for $T_2$ the following results.

| Pressure (Atmospheres) | $T_2$ Hydrogen pSec | $T_2$ Methane pSec |
|---|---|---|
| 20 | 442 | 18.9 |
| 30 | 295 | 15.6 |

From these figures we can clearly see that with pump pulses of around 100pS in duration, S.R.S. in Hydrogen gas is highly transient. In Methane the pulse length $\tau_p$ is about 5 times $T_2$. Nevertheless, the effects of transience will be readily noticeable since $\tau_p < 20T_2$.

In the remainder of this section we shall firstly describe a treatment of transient S.R.S. assuming a plane wave geometry. We then extend this theory to cover Gaussian beams when tight focussing and when using a waveguide. Finally we substitute into our solution the parameters used in our experiments so as to obtain predictions for transient S.R.S. threshold which we can compare with experiment in Chapter 5.

### 4.3.1 A plane wave analysis of transient S.R.S.

A mathematical treatment of transient S.R.S. with plane waves has been performed by many authors including Carman et al, (1970) and Penzkofer et al, (1979). The problem is generally simplified somewhat by neglecting pump depletion and assuming no saturation of the Raman medium population takes place. What follows is a brief summary of the theory presented by Carman et al.

The initial equations for the S.R.S. process including the time dependence of the Raman excitation Q are given by,

$$\frac{\partial Q^*}{\partial t} + V_{ph} \cdot \frac{\partial Q^*}{\partial Z} + \Gamma . Q^* = i . K_1 . E_S . E_L^* \qquad 4.37$$

$$\frac{1}{V_s} . \frac{\partial E_s}{\partial t} + \frac{\partial E_s}{\partial Z} = -i\, K_2 . Q^* . E_L \qquad 4.38$$

where $V_{ph}$, $V_s$ are the group velocities of the vibrational and Stokes waves respectively and $\Gamma$ is related to the Raman linewidth $\Delta\nu_R$ and the Raman transition dephasing time $T_2$ by $\Gamma = 1/T_2 = \pi . \Delta\nu_R$. The variables $K_1$ and $K_2$ are related to the Raman gain coefficient $g_r$ by,

$$K_1 . K_2 = \Gamma . g_r . (\varepsilon_o/\mu_o)^{1/2}/4 \qquad 4.39$$

and

$$K_2/K_1 = 4\pi . \omega_R . k_s \qquad 4.40$$

where $\omega_R$ is the Raman shift frequency and $k_s = 2\pi/\lambda_s$.
To solve equations 4.37 and 4.38 we introduce the new co-ordinates $t' = t - z/V_s$ and $z' = z - V_{ph} . t$. Typically $V_{ph}$ is small enough to be ignored during the small time interval of interest, i.e. $z' \simeq z$. The quantity $t'$ is a variable representing "local time" relative to the arrival of the pump pulse at any point in the Raman medium. Substituting for these new co-ordinates we obtain,

$$\frac{\partial Q^*}{\partial t'} + \Gamma \cdot Q^* = -i.\ K_1.E_S.E_L^* \qquad 4.41$$

$$\frac{\partial E_s}{\partial z'} = i.\ K_2.E_L.Q^* \qquad 4.42$$

The solution of these equations is given in Carman et al, (1970) as:

$$E_s(z'.t') = E_{so}(t') + (K_1.K_2.Z')^{1/2}.\ E_L(t').$$

$$\int_{-\infty}^{t'} \{\exp\ [-\Gamma.(t'-t")]\ \frac{E_L^*(t").E_{so}(t")}{[W(t')-W(t")]^{1/2}}.\ I_1(F)\}dt" \qquad 4.43$$

where $$F = \{2.K_1.K_2.Z'[W(t')-W(t")]\}^{1/2} \qquad 4.44$$

where $$W(t') = \int_{-\infty}^{t'} |\ E_L(\tau)\ |^2.d\tau \qquad 4.45$$

and $I_1$ is a modified Bessel function of first order. In the limit of strong transient interaction, i.e. $t_p << T_2$ and $g_r.I_p.L >> 1$ the approximation $I_1(x) = (2.\pi.x)^{-1/2}.e^x$ is valid and one obtains,

$$Ln[|E_s(L,t')/E_s(0,t')|^2] = 4\ [K_1.K_2.L.W(t')]^{1/2} \qquad 4.46$$

From this we obtain the approximation that the transient Stokes gain is proportional to the square root of the accumulated pump energy.

Equation 4.43 is our final expression for the plane wave Stokes transient growth. It allows us to obtain the final output Stokes field, (and hence intensity), in terms of the input Stokes field, (noise in our case), and the pump field. Various authors have

produced graphical data calculated from equation 4.43 for a pump pulse with a Gaussian temporal profile, (e.g. Penzkofer, (1979), figure 17 and Carman, (1970), figure 3). The data we want however is a plot of, the equivalent steady state gain for the peak pump power, $G_E$, against the ratio of $\tau_p$ to $T_2$, for a range of transient Stokes gain requirements. The equivalent steady state gain is defined as the gain that would be produced under steady state conditions with the given peak pump power. Figure 4.3 shows such a graph plotted, on a BBC microcomputer using a series of programs written by Pointer, (1984). To obtain a predicted transient threshold power the ratio $\tau_p/T_2$ and the required gain are substituted into figure 4.3 to give an equivalent steady state gain. The ratio of this equivalent gain to the required gain gives the relative increase in threshold power for the transient case compared with the steady state case. It can be seen from figure 4.3 that transience causes a significant decrease in gain from the steady state case unless $t_p > 20T_2$.

### 4.3.2 The extension of transient S.R.S. to Gaussian transverse beam profiles

In our measurements, both guided and unguided tightly focussed beams are involved. As a result the assumptions of a plane wave geometry made in the previous section are clearly unsatisfactory and further consideration is required.

#### Transient S.R.S. with tight focussing

The approach of Cotter et al, (1975) outlined in section 4.2.1 gives an increase in the threshold power as a result of Stokes losses which arise through diffraction. This theory cannot be readily applied to cover the transient situation due to the difficult problem of a non-uniform transverse gain profile undergoing a transient evolution. However by making some further well founded approximations we find that the approach of Cotter et al can be extended to give transient S.R.S. predictions using

FIGURE 4.3: RAMAN THRESHOLD vs. PULSE DURATION

for $G_T$ = 20, 30, 40, 50 and 60

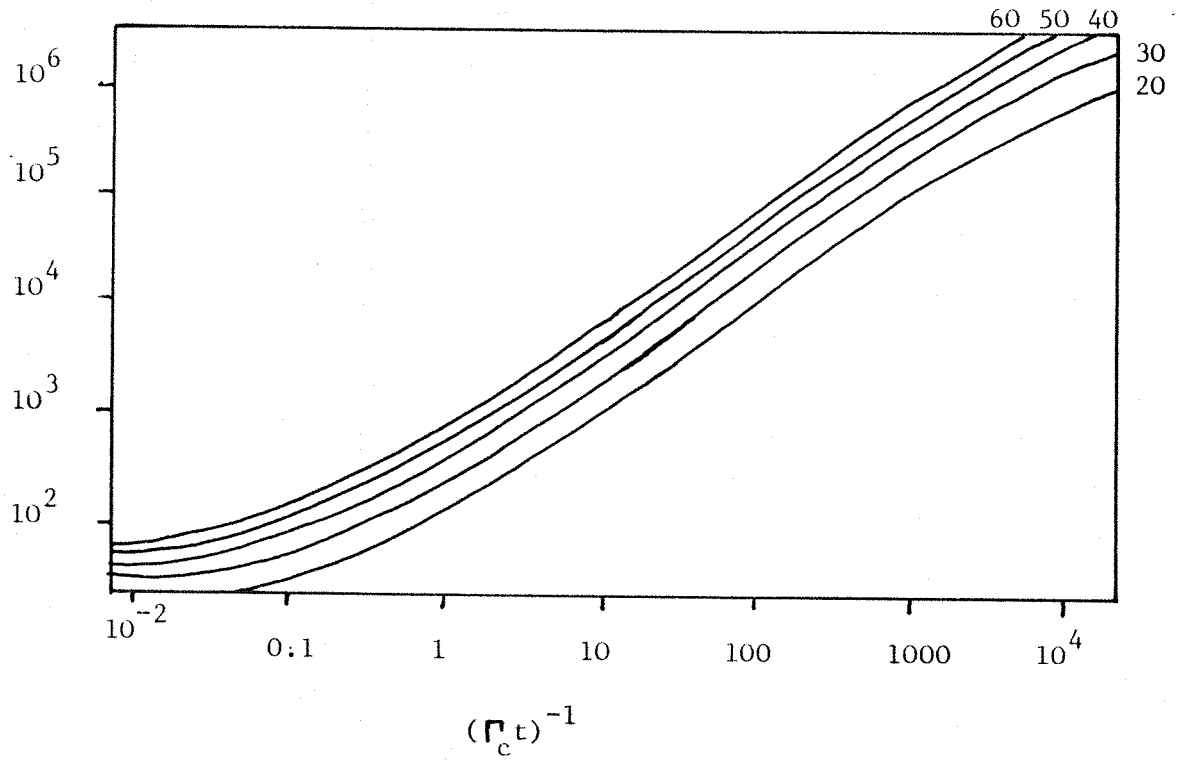


Figure 4.3

tight focussing. These predictions give good agreement with our experimental results to within expected errors.

The analysis of Cotter et al leads to a matched ratio for the Stokes to pump spot sizes which is given by

$$\frac{W_s^2}{W_p^2} = \frac{2}{(W_p^2.g_r.I_{po}.k_s)^{1/2}} \qquad 4.47$$

where $W_p$ and $W_s$ are spot sizes and $I_{po}$ is the on-axis pump intensity. The variables $g_R$ and $k_S$ take their usual meanings as defined in section 4.1. It is interesting to note that since $W_p^2.k_S = b_p.k_s/k_p$, where, $b_p$ is the confocal parameter, the term in brackets on the right hand side is proportional to the gain requirement for threshold. Substituting typical values into this equation, $W_p$=60$\mu$m, $k_s$=2$\pi$ x $10^6$ $m^{-1}$ and $g_r.I_p$=$10^3 m^{-1}$, we obtain $W_s^2/W_p^2$ = 0.42. This is an approximate value since in addition to the approximations made in Cotter et al we have also neglected the effect of transience on gain focussing. Since the Stokes spot size is smaller than that of the pump, the Stokes will experience a Raman gain close to that appropriate to the on-axis pump intensity. This is significantly larger than the gain required to reach steady state threshold since considerable diffraction losses attenuate the Stokes. In order to obtain a transient threshold prediction we evaluate the magnitude of this on axis gain requirement at threshold since, from figure 4.3 it is apparent that the degree of transience depends on this Stokes gain requirement.

The on-axis steady state gain, $G_{A,ss}$, for a tightly focussed Gaussian beam is given by,

$$G_{A,ss} = \int_{-L/2}^{L/2} g_r.I_{po}(z).dz \qquad 4.48$$

where

$$I_{po}(z) = \frac{2P}{W_{po}^2} \cdot \frac{1}{1+(2z/b_p)^2} \qquad 4.49$$

where $W_{po}$ is the pump spotsize at the focus, P the peak power in the pump beam, and $b_p = 2\pi.W_{po}^2/\lambda_p$ is the confocal parameter of the focussed pump beam. Substituting and integrating we obtain,

$$G_{A,ss} = \frac{4.g_r.P.\ \arctan\ (L/b_p)}{\lambda_p} \qquad 4.50$$

The steady state threshold prediction of Cotter et al is given as equation 4.23. Substituting this into equation 4.50 for the peak pump power allows us to relate the on-axis gain to the actual Stokes gain required for threshold, $G_R$. We obtain

$$G_{A,ss} = \frac{\arctan(L/b_p)}{K}\left[1 + \left\{1 + \frac{K.\ G_R}{\arctan(L/b_p)}\right\}^{1/2}\right]^2 \qquad 4.51$$

Substituting typical values from our experiments into this equation we obtain the results presented in table 4.4 where we have used the value $L/b_p = 20$ as this was the case in all our experiments. The lower values of $G_R$ are also included since for our 532nm and 570nm pumped experiments, the actual Raman gain requirement differed considerably from exp(30), (see section 4.4.1). As can be seen from table 4.4 the ratio of on-axis to actual Stokes gain is consistently around 1.7 despite considerable variation in the pump wavelength, Stokes wavelength and gain requirement. From this we can deduce that the actual transient S.R.S. gain will differ very little from that predicted.

Table 4.4 The evaluation of typical on-axis gains using tight focussing

| Gas | pump wavelength $x10^{-6}m$ | $G_R$ | K | $G_{A,ss}$ | $G_{A,ss}/G_R$ |
|---|---|---|---|---|---|
| $CH_4$ | 1.06 | 30 | 0.69 | 51.3 | 1.71 |
| $CH_4$ | 0.532 | 30 | 0.84 | 48.7 | 1.62 |
| $H_2$ | 1.06 | 30 | 0.56 | 54.3 | 1.81 |
| $H_2$ | 0.532 | 30 | 0.78 | 49.7 | 1.66 |
| $CH_4$ | 0.532 | 24 | 0.84 | 41.3 | 1.72 |
| $H_2$ | 0.532 | 26 | 0.78 | 44.7 | 1.72 |
| $CH_4$ | 0.570 | 30 | 0.83 | 48.9 | 1.63 |
| $CH_4$ | 0.570 | 27 | 0.83 | 45.5 | 1.69 |

Having obtained a value for the on axis transient gain requirement using equation 4.51, we can substitute this into figure 4.3 to give an equivalent steady state on axis gain $G_E$. Equation 4.50 enables us to relate this steady state gain to the threshold power requirement since by re-arranging we obtain,

$$P_{th} = \frac{\lambda_p . G_E}{4. g_r . \arctan(L/b_p)} \qquad 4.53$$

This is our final equation used in predicting the transient S.R.S. threshold power. In section 4.4.2. we obtain numerical values for the predicted threshold power using the analysis just described.

Transient S.R.S. in waveguides

In a waveguide the factor $g_r.I_{po}$ is much smaller than when tight focussing due to the much longer interaction length and hence lower intensity required to reach threshold. As a consequence the Stokes spot size will tend to be defined by capillary guidance rather than gain focussing and will be well described by the $EH_{11}$ mode. As a result, the Stokes losses will be given by the normal capillary transmission losses for the $EH_{11}$ mode at the wavelength in question. The transient Stokes gain requirement will therefore by given simply by that required to reach detector threshold from noise plus any capillary guiding losses. This value for the transient Stokes gain can be used with figure 4.3 to give an equivalent steady state gain. This in turn can be be substituted into equation 4.34, which can be re-written,

$$P_{th} = \frac{0.885.\pi.W_o^2.G_E}{g_r.L_{eff}} \qquad 4.54$$

to give our final value for the predicted transient threshold power in a capillary. Section 4.4.3 evaluates these predicted transient threshold powers for the experimental conditions described in chapter 5.

## 4.4 Theoretical threshold calculations

This section evaluates theoretical threshold predictions for the experimental arangements described in chapter 5. First however it is necessary to take a closer look at the initial and final Stokes power levels in order to work out the Raman gain requirement at threshold. This parameter has a greater effect on threshold for short pulse S.R.S. than with steady state S.R.S. This is due to the square dependence of the pump power on the Raman gain for highly transient pump pulses as expressed by equation 4.46. We need a value of $P_s(L)/P_s(O)$ that is within an order of magnitude for threshold predictions to be accurate to within ~15%.

### 4.4.1 The Stokes gain requirement

Our equations for S.R.S. threshold require a value for $P_s(O)$, the initial radiation power in the Stokes mode at the Stokes wavelength. This value is given by pump induced spontaneous Raman emission as this is many orders of magnitude larger than the black body radiation level. Assuming a pumped region in the Raman medium corresponding to a single transverse mode, the Stokes noise power is given by, (Hanna et al, 1979),

$$P_s(O) = h.\nu.\Delta\nu \qquad 4.55$$

where h is Planck's constant, $\nu$ the Stokes frequency and $\Delta\nu$ the linewidth of the Stokes radiation produced by the S.R.S. process.

Typical results obtained using this equation are presented in table 4.5. In all cases the value $\Delta\nu = 0.25cm^{-1}$ was used as this corresponds approximately to the transform limited linewidth of the Stokes output for pulses of length, $t_s = 50ps$. Also shown in table 4.5 is an estimate of the required Stokes output at threshold. The variation is due to the differing methods used to detect the Stokes radiation depending on its wavelength. Since this work was carried out, an alternative definition of threshold has been adopted at Southampton, and is used in our recent paper (see Appendix 5). Threshold is now defined as being when the 1st Stokes energy is equal to 1% of the pump energy. In this work threshold is defined as being when 1st Stokes is observable. We now present calculations giving the final 1st Stokes power levels in our experiments at threshold. With 1.06$\mu$m pumping a pyroelectric detector was employed with a detection threshold of 1$\mu$J. Since the Stokes radiation typically comprised a train of 3 pulses a single pulse threshold energy of 0.3$\mu$J is used as the final Stokes energy requirement at threshold. With 532nm and 570nm pumping threshold was determined according to whether first Stokes was visible on a piece of white card after separating out the pump light. Measurements of the eyes sensitivity under these conditions where made at 532nm using our pump laser, a disc calorimeter and a selection of neutral density filters. It was found that an energy of 2.5nJ at 532nm corresponded to the same brightness as first Stokes threshold. After correction for the eyes sensitivity as a function of wavelength and multiplication by 0.3 due to 3 pulses being in the train, the final Stokes energies presented in the table were obtained. The pulse length $t_s$ used to obtain threshold power from the threshold energy given in table 4.5 was 50ps, a consequence of the choice of $\Delta\nu = 0.25cm^{-1}$ for the noise linewidth. Since both $P_s(L)$ and $P_s(O)$ depend in the same way on $t_s$, the actual value of $t_s$ will not affect our predictions for the required Stokes gain.

Table 4.5 Estimates of the initial and final Stokes power levels and the resulting Raman gain requirement

| Gas | Pump Wavelength | $P_s(O)$ W | $E_s(L)$ nJ | $P_s(L)$ kW | $Ln[P_s(L)/P_s(O)]$ |
|---|---|---|---|---|---|
| $CH_4$ | 532nm | $2.36x10^{-9}$ | 3 | 57W | 23.9 |
| $H_2$ | 532nm | $2.2x10^{-9}$ | 30 | 0.57 | 26.1 |
| $CH_4$ | 1.06um | $9.6x10^{-10}$ | 300 | 5.7 | 29.4 |
| $H_2$ | 1.06um | $7.8x10^{-10}$ | 300 | 5.7 | 29.6 |
| $CH_4$ | 570nm | $2.2x10^{-9}$ | 100 | 1.9 | 27.2 |

The actual values given in table 4.5 for the Raman gain requirement are used in the threshold predictions. The use of an arbitrary choice of exp(30) for the Raman gain will result in errors greater than 20% in the actual gain requirement. The non-linear dependence of the gain on the pump power for transient S.R.S. will serve to make the resulting error in the threshold prediction even larger.

### 4.4.2 Predictions: Tight focussing

In all our tight focussing experiments the exact value of $L/b_p$ caused little change in the predicted threshold due to the nature of the $\arctan(L/b_p)$ function. The steady state data on the Raman transitions needed in an evaluation of transient threshold has

been given in table 4.1. The predicted threshold values are obtained using the technique described in section 4.3.2. The stages necessary to obtain a predicted value are summarized as follows.

a. Obtain the required on-axis transient gain, $G_{A,ss}$, from table 4.4 or equation 4.51 and the required Stokes gain, $G_R$, given in table 4.5.

b. Evaluate the ratio of the pump pulse length to the Raman dephasing time $T_2$ given in table 4.1.

c. Using the on-axis transient gain and the above ratio, obtain the equivalent on-axis steady state gain, $G_{E,ss}$, from figure 4.3.

d. Substitute $G_{E,ss}$ into equation 4.53 to obtain the threshold power required for this gain.

The predicted threshold powers obtained using these steps for the experiments described in chapter 5 are given in table 4.6.

Table 4.6

| Gas | Wavelength | $G_R$ | $G_{A,ss}$ | $t_p$ | $\ln(\Gamma t_p)$ | $G_{E,ss}$ | $P_{th}$ |
|---|---|---|---|---|---|---|---|
| $CH_4$ | 1.06$\mu$m | 30 | 50 | 117ps | 2 | 128 | 6.85MW |
| $H_2$ | 1.06$\mu$m | 30 | 54 | 125ps | -0.8 | 1340 | 18MW |
| $CH_4$ | 532nm | 24 | 41 | 83ps | 1.65 | 115 | 1.17MW |
| $H_2$ | 532nm | 26 | 45 | 83ps | -1.2 | 1340 | 3.16MW |
| $CH_4$ | 570nm | 27 | 45.5 | 70ps | 1.5 | 155 | 1.84MW |

### 4.4.3 Predictions: Using a waveguide

To obtain a predicted threshold power for S.R.S. in a waveguide a large number of experimental parameters must be known. These are, a) the capillary effective length which is given by equation 4.32 and is dependent on the pump transmission as well as the true capillary length, b) $g_R$, $\lambda_p$, $\lambda_s$ etc. from table 4.1, c) the bore radius of the capillary, a, which leads to an effective spot size in the guide given by $W = 0.664\ a$ , d) the overall Stokes gain requirement inside the capillary from section 4.4.1, but also including the Stokes guide losses, and e) the ratio $t_p/T_2$ as used in section 4.4.2 for tight focussing. Having obtained these parameters the following steps lead to a prediction for the transient S.R.S. threshold power using a capillary.

a. Use the overall Stokes gain requirement as obtained at d) above, together with the ratio $t_p/T_2$ in figure 4.3, to obtain an equivalent steady state gain requirement $G_{E,ss}$.
b. Substitute this into equation 4.54 to obtain the threshold power required for this Stokes gain.

Using data from the experimental work described in chapter 5 we obtain the threshold predictions given in table 4.7. All the capillaries used in the experimental work had a bore radius of 100$\mu$m and a length of 82cm. Their pump transmissions however differed considerably leading to different values for their effective length. The effective lengths obtained from the experimental measurements of pump transmission are also given in table 4.7.

Table 4.7

| Gas | Wavelength | $L_{eff}$ | $t_p$ | $\ln(\Gamma t_p)$ | $G_E$ | $G_{E,ss}$ | $P_{th}$ |
|---|---|---|---|---|---|---|---|
| $CH_4$ | 1.06$\mu$m | 0.38m | 110ps | 2.0 | 34 | 74 | 720kW |
| $H_2$ | 1.06$\mu$m | 0.44m | 110ps | -0.9 | 33 | 600 | 1.27MW |
| $CH_4$ | 532nm | 0.57m | 67ps | 1.4 | 25 | 60 | 147kW |
| $H_2$ | 532nm | 0.57m | 53ps | -1.7 | 27 | 812 | 467kW |

## 4.5 Additional factors

Other factors which may influence the use of S.R.S. as a means of generating tunable infrared radiation are gas absorption, gas dispersion and the many factors which affect conversion efficiency. This section takes a brief look at these aspects.

### Gas absorption

In order to obtain a good conversion efficiency it is required that the medium be as transparent as possible at both the pump and Stokes wavelengths. Homonuclear, diatomic molecules such as hydrogen have no serious absorption bands since they have no electric dipole moment. Consequently $H_2$ gas is sufficiently transparent for good transmission from the visible to the far infrared region. When the density of $H_2$ molecules is sufficiently large, i.e. in liquid $H_2$, collision induced absorption occurs at wavelengths corresponding to the Raman shift, (2.4$\mu$m). In a 1m long cell filled to 30 atmospheres this absorption is only a few percent in $H_2$, (Watanabe and Welsh, 1965) and consequently can be neglected at all wavelengths. In methane there exists significant absorption bands at 7.7$\mu$m, 3.3$\mu$m and 2.3$\mu$m, even at low pressures. Additionally, small overtone absorptions introduce significant absorptions between about 1$\mu$m and the first main absorption at 2.3$\mu$m. Absorption spectra for $CH_4$ at low pressures are readily available, (Partridge, 1984). From these it is apparent that almost total extinction will occur in a 1m long cell filled to 30 atmospheres in the regions 2.2-2.4$\mu$m, 3.1-3.5$\mu$m and 7.2-8.3$\mu$m. These wavelengths must therefore be avoided when using S.R.S. in Methane as a means of generating infrared radiation.

### Gas dispersion

In S.R.S., parametric processes play an important part, providing starting radiation for higher order Stokes generation, and as a mechanism for anti-Stokes generation. The effectiveness of 4-wave

mixing is complicated by the requirement for phase-matching between the 4 beams. The result is that the radiation produced by 4-wave mixing appears in cones, so as to maximise the interaction length which is limited by both the finite transverse profile of the pump beams and the phase matching criterion. In general, parametric processes work better in media with low dispersion as this allows a smaller cone angle and hence a longer interaction length. We now present data on refractive index and dispersion in hydrogen and methane.

Data on the refractive index of Hydrogen from 0.4$\mu$m to 1.7$\mu$m is given in Peck and Huang, (1977). For Methane however, the only data that could be obtained after an extensive computer assisted literature search, was for the visible region from 0.4$\mu$m to 0.68$\mu$m, (K. Kerl, 1982). In the infrared region the absorptions at 2.3, 3.3 amd 7.7$\mu$m make extrapolation of this data unreliable beyond about 0.8$\mu$m. To make comparisons of phase matching in $H_2$ and $CH_4$ in the visible we can use the Cauchy formula given in Born and Wolf, (1980), page 95,

$$n - 1 = A_1(1+B_1/\lambda^2) = A_1(1+B_2.\tilde{\nu}^2) \qquad 4.56$$

where $A_1$, $B_1$ and $B_2$ are constants and $\tilde{\nu}$ the optical frequency in $cm^{-1}$. The values of $A_1$ and $B_1$, given in Born and Wolf for Hydrogen and Methane, are:

| Gas | $A_1 \times 10^5$ | $B_1 \times 10^5$ cm$^2$ |
|---|---|---|
| $H_2$ | 13.6 | 7.7 |
| $CH_4$ | 42.6 | 14.41 |

If we consider the process of co-linear 1st anti-Stokes generaton we have the phase matching condition

$$k_a + k_s = 2.k_p + \Delta k \qquad 4.57$$

where $k = 2\pi.n(\lambda)/\lambda$ or $2.\pi.\tilde{\nu}.n(\tilde{\nu})$ and $\Delta k$ is the phase mismatch. Using the Cauchy formula given by 4.56 for $n(\tilde{\nu})$ and substituting in equation 4.57 we obtain,

$$\tilde{\nu}_a.\ A_1(1+B_2.\tilde{\nu}_a^{\,2}) + \tilde{\nu}_s.A_1(1+B_2.\tilde{\nu}_s^{\,2}) + \tilde{\nu}_a + \tilde{\nu}_s$$

$$= 2\tilde{\nu}_p + 2\tilde{\nu}_p\ A_1(1+B_2\tilde{\nu}_p^{\,2}) + \Delta k/2\pi \qquad 4.58$$

where we have divided throughout by $2\pi$. Substituting $\tilde{\nu}_a = \tilde{\nu}_p + \tilde{\nu}_R$ and $\tilde{\nu}_s = \tilde{\nu}_p - \tilde{\nu}_R$ gives

$$A_1.B_2.(\tilde{\nu}_p+\tilde{\nu}_R)^2 + A_1.B_2.(\tilde{\nu}_p-\tilde{\nu}_R)^2 = 2.A_1.B_2.\tilde{\nu}_p^{\,2} + \Delta k/2\pi \qquad 4.59$$

and hence we can see that the phase mismatch is given by

$$\Delta k = 4.\pi.A_1.B_2.\tilde{\nu}_R^{\,2} \qquad 4.60$$

Since the product $A_1.B_2$ is 6 times larger for $CH_4$ in the visible than $H_2$ we expect about 3 times as much phase mismatch, (due to the larger Raman shift in $H_2$). This in turn will lead to approximately 1.7 times the phase matching angle for the anti-Stokes due to the $\theta^2$ dependence of the 1-cos ($\theta$) term which gives the on-axix wave vector change. As a consequence of this phase matching angle being 1.7 times smaller, $H_2$ should perform significantly better than $CH_4$ at anti-Stokes and higher order Stokes generation. This was observed experimentally provided that both gases where pumped at the same level above threshold.

Efficiency considerations

There are a large number of factors which all act independently to reduce the efficiency of the S.R.S. process from an ideal 100%. What follows is a description of the various mechanisms that reduce conversion efficiency.

a) Quantum efficiency

Since a pump photon has a higher energy than a Stokes photon, ($E=h\nu$), for 100% photon conversion the energy conversion will only be $\nu_s/\nu_p$. Clearly this factor gets worse further into the infra-red.

b) Transverse modes

Due to gain focussing, the Stokes beam as it propogates has a spot size that is generally smaller than the pump beam, (equation 4.47). As a consequence even for 100% on-axis conversion efficiency the overall conversion efficiency will be less. In a waveguide this mechanism will not be relevant since both the pump and Stokes are well described by the $EH_{11}$ waveguide mode.

c) Temporal pulse narrowing

The Stokes pulse generated by transient S.R.S. is significantly reduced in duration compared with the pump pulse, (see for example, Lowdermilk and Kachen, 1975). This is to be expected since for unsaturated, steady state S.R.S. the Stokes pulse length will be reduced from the pump pulse length by a factor equal to the square root of the Raman gain requirement, (i.e. about 5). Saturation may reduce this effect slightly.

d) Pulse train envelope shortening

The Stokes pulse train envelope will suffer from the same narrowing process as the pulse length. Again saturation of the centre pulses will allow slightly larger conversion efficiencies.

e) Conversion to higher Stokes orders and to anti-Stokes

When operating well above threshold the gains of parametric and further cascade Raman processes are high resulting in depletion of

the 1st Stokes in order to generate higher order Stokes and anti-Stokes. The actual conversion efficiency expected has been calculated numerically by Von der Linde et al, (1969), for both plane waves and Gaussian beams. These curves essentially indicate that maximum 1st Stokes conversion efficiency occurs at about twice the threshold power. Above this an increase in pump power causes very little increase in the 1st Stokes power. One possible method for increasing the first Stokes conversion efficiency is to use a resonator. The lower pump powers required, result in less parametric interaction and consequently less higher order Stokes and anti Stokes generation.

f) System losses

Reductions in efficiency also result as a consequence of limitations in the availability of suitable optics, for example:

1. Non A.R. coated lenses and cell windows at the pump and Stokes wavelengths.

2. Unoptimized resonator mirrors when using feedback to reduce S.R.S. threshold.

3. Waveguide coupling and transmission losses.

4. Losses introduced while separating the Stokes and pump after the Raman cell system.

If we make rough estimates of the magnitudes of these mechanisms for conversion efficiency reduction, we obtain an overall expected conversion efficiency of about 10% at twice threshold. This is in reasonable agreement with our experimental results presented in the next chapter.

# 5. EXPERIMENTAL INVESTIGATIONS OF TRANSIENT STIMULATED RAMAN SCATTERING

In this chapter we present experimental measurements of S.R.S. in the gases hydrogen and methane using short pump pulses. These measurements were made in order to establish the performance of S.R.S. for use as a widely tunable, U.V. and I.R. picosecond source. Performance features to be investigated include threshold and conversion efficiency as well as the number of Stokes orders, etc.

In the long term this tunable radiation would be achieved using a synchronously pumped dye laser (S.P.D.L.) as the pump source. An intermediate aim however was to establish the performance, (especially with regards to threshold), using a pump laser such as the A.M.L. Yag oscillator which has near perfect pump characteristics. These measurements would be used to develop and test the quantitative theories (given in chapter 4), describing the transient S.R.S. process so that reliable predictions of S.P.D.L. pumped S.R.S. performance can be made.

So far a quantitative theory has only been developed for threshold since conversion efficiency calculations are considerably more complicated. Accordingly the measurements have concentrated on threshold with only sufficient measurements of conversion efficiency to confirm that the technique is a practical, tunable, U.V. and I.R., picosecond laser source.

Most of the measurements given in this chapter were made using the output from an A.M.L. Nd: Yag laser at 1.06$\mu$m and its second harmonic. This laser, described in chapter 3 of this thesis, is the near ideal laser source mentioned above which is required to accurately characterize the S.R.S. process. In addition to this work carried out at Southampton University, some measurements were made using a S.P.D.L. at J.K. Lasers as part of a C.A.S.E. Studentship industrial visit. These measurements are described near the end of this chapter.

## 5.1 The experimental arrangement

A diagram of the general layout for all the experiments is shown as figure 5.1. The actual layout of components varied somewhat from this depending on the pump wavelength and/or whether a resonator/waveguide was employed. On occasion extra components were inserted or perhaps removed depending on the experimental requirement. In all experiments however, the general layout remained the same. The remainder of this section describes in detail the reasons for choosing this layout, together with the variations used for different experiments.

### 5.1.1 A general description

The experimental layout required for the experiments is necessarily complicated since a large number of measurements need to be made at the same time. These measurements are, the pump pulse length, the pump energy incident on the Raman cell, and details of the output into the various wavelengths after the Raman cell.

Immediately after the A.M.L. oscillator a small proportion of the output energy is split off and sent to the autocorrelator described in chapter 3. This allowed continuous monitoring of the duration of pulses in the pump train and hence a check on the A.M.L. performance. A beam expanding telescope and 3" x 3/8" Nd: Yag amplifier were inserted after this point in the later experiments as it was required to make measurements with pump energies larger than could be supplied by the A.M.L. oscillator alone. Variation of the pump energy was obtained either by varying the flashlamp energy to the Nd: Yag amplifier or by attenuating the beam using the Fresnel reflections from two tilted, self compensating optical flats, (see section 5.1.3 for further details). After frequency doubling a dichroic filter was used to separate the harmonic. The small amount of residual 1.06$\mu$m transmission was allowed for in our measurements of the 532nm energy made after this point.

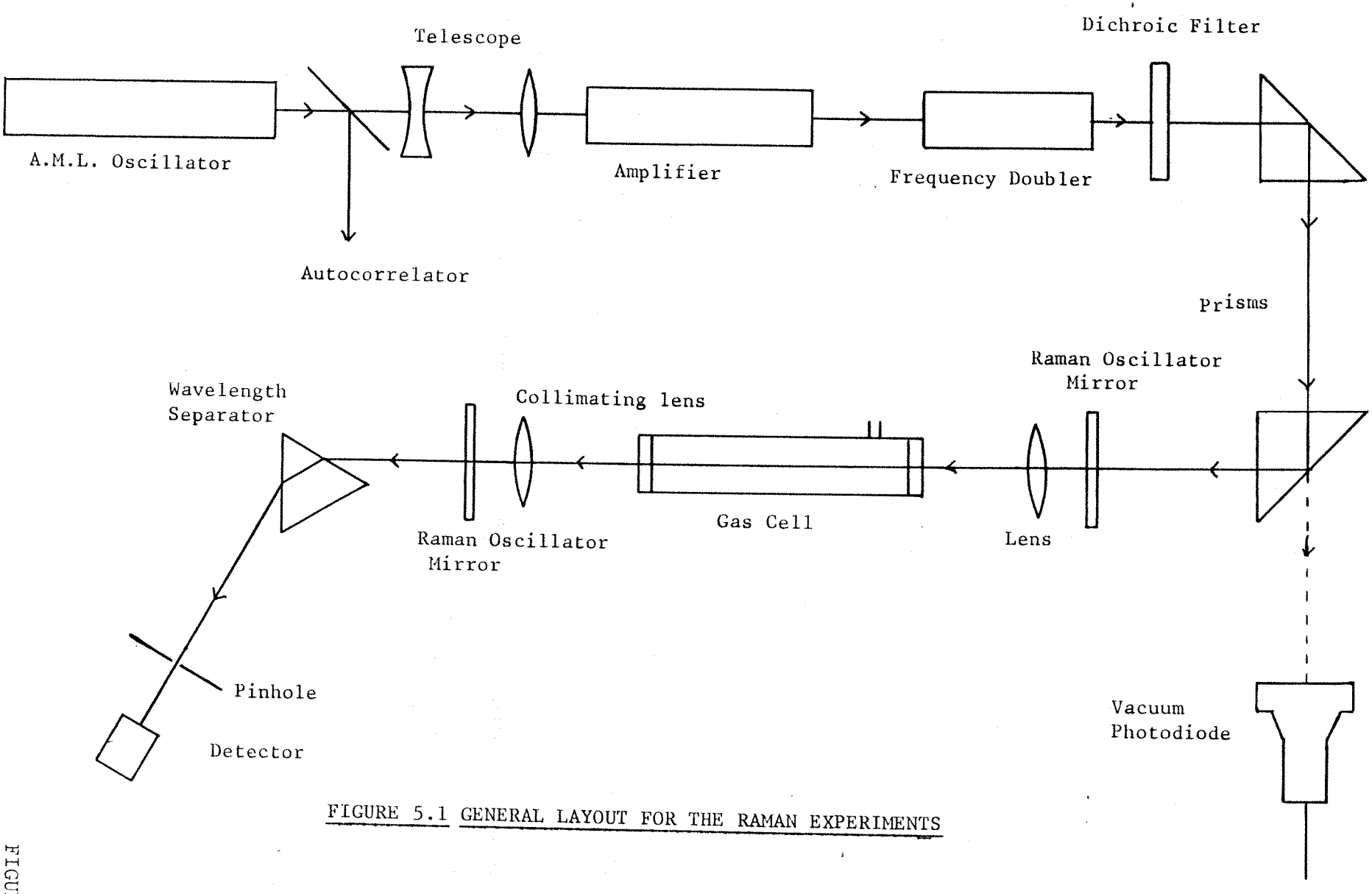


FIGURE 5.1 GENERAL LAYOUT FOR THE RAMAN EXPERIMENTS

FIGURE 5.1

Due to the high conversion efficiency to 532nm this represented a small fraction of the 532nm energy. The frequency doubler and the dichroic filter were removed for 1.06$\mu$m pumping of the Raman cell.

The turning prisms were needed as the optical table length was limited. Scattered light from these prisms was used as a source for a vacuum photodiode (Si photocathode) used to continuously monitor the pulse train envelope duration.

The Stokes oscillator mirrors could be removed but for convenience were frequently left in place since they represented a negligible pump loss. When not in use the Stokes oscillator mirrors were miss-aligned so as to prevent damage caused by reflections of 1.06$\mu$m propogating back down the Nd: Yag amplifier chain, and to prevent erronously low, single pass threshold results due to Stokes feedback. The Stokes oscillator mirrors were separated by the same optical spacing as the A.M.L. oscillator mirrors, to within a few millimetres, in order to ensure synchonism of the Stokes feedback.

Beam focussing

The focussing lens used just before the Raman cell was chosen to either produce a suitable tightly focussed pump beam, or to match the pump beam with the entrance to the capillary waveguide. A suitable tightly focussed pump beam can be defined as one which satisfies 3 conditions.

1. Cell window damage will not occur at the highest pump powers likely to be used.

2. Gas breakdown at the beam focus will also not occur at this same power.

3. The ratio of the cell length to the beam confocal parameter ($L/b_p$) is at least 5 and preferably 20. (Tight focussing).

If these three conditions can not be met then a longer gas cell should be used. When using a capillary the beam must be focussed to give a waist of $W = 0.644a$, (where a is the bore radius of the capillary) at the capillary entrance. At the same time condition 1 above relating to window damage must be satisfied. This can generally be done by ensuring a sufficient distance between the capillary entrance and cell window.

Frequently it was found that the required beam matching was impossible without using a focussing lens with a very long focal length (a few metres). Since lenses with focal lengths over 1m are difficult to obtain and would cause problems due to the distance from the lens to the focus, an alternative method was required. A convenient method adopted in our experiments was to use the beam expanding telescope before the amplifier rod as a method of changing the spot size at the main focussing lens.

The collimating lens located after the gas cell is not critical unless Stokes oscillator mirrors are in use. In the single pass experiments the collimating lens was usually chosen to provide a slightly converging beam. This allowed easier differentiation between the different wavelength components after the wavelength separator.

Wavelength separation and energy monitoring

One or more prisms were used after the final Stokes oscillator mirror in order to separate the various wavelength components generated in the Raman cell from each other and the pump wavelength. Additionally high and low pass filters were sometimes used to assist in the separation process. A pyro-electic energy meter (Laser Precision Corp, Model RKP335) was used on most occasions to monitor the energies in the various Stokes and anti-Stokes components emerging from the Raman cell. Due to low threshold energies obtained for S.R.S. with short pulses, this was the only energy monitor suitable since energies were as low as

1$\mu$J. The only other available energy monitoring system sufficiently sensitive was a silicon photodiode based system. This however has the disadvantage of requiring re-calibraton at every wavelength at which it was used. In addition it failed to respond to wavelengths longer than 1.1$\mu$m.

In order to measure the pump energy incident on the Raman cell an energy monitor, (usually a small disc calorimeter), was placed between the focussing lens and the cell window. This was capable of measuring the average incident pump energy to within a few microjoules. Better accuracy could be obtained using the pyroelectric energy meter mentioned above.

### 5.1.2 Construction details of the Raman gas cell and the gas handling system

During the experiments pressures of upto 30 Atmospheres of the gases hydrogen and methane were required. Consequently a well designed and built gas system was needed.

The gas system can be considered to comprise two parts; the gas cell itself and the gas handling system required to fill and empty it. Details of these two parts are given in figures 5.2 and 5.3. Construction of the gas filling system was with 1/4" outside diameter, soft copper tube together with Hoke "Gyrolock" fittings. These can all be used safely at pressures well above 1000 p.s.i. (70 Atmospheres). An automatic relief valve set to 40 Atmospheres was present in the filling system to prevent the gas cell from being overfilled. Pressure regulation was achieved with the pressure regulator supplied with the gas cylinder. The gas cell itself was constructed from "Aminco" stainless steel 'T' fittings together with a 1/2" O.D. connecting pipe. Special fittings were made to attach the cell to the gyrolock pipe fittings. A short piece of flexible nylon tubing attached the cell to the gas handling system allowing easy optical alignment of the Raman cell.

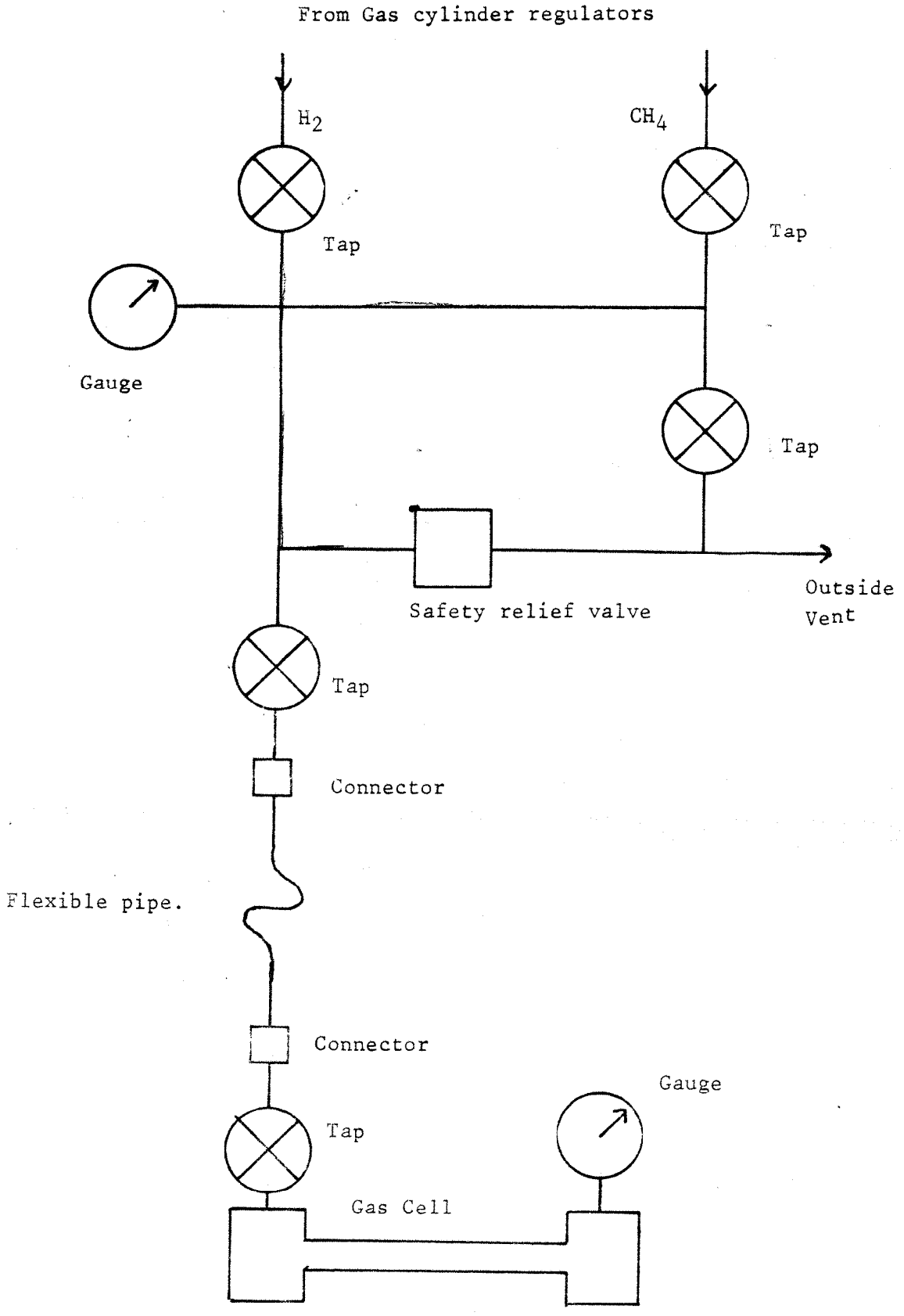


FIGURE 5.2 THE GAS FILLING SYSTEM

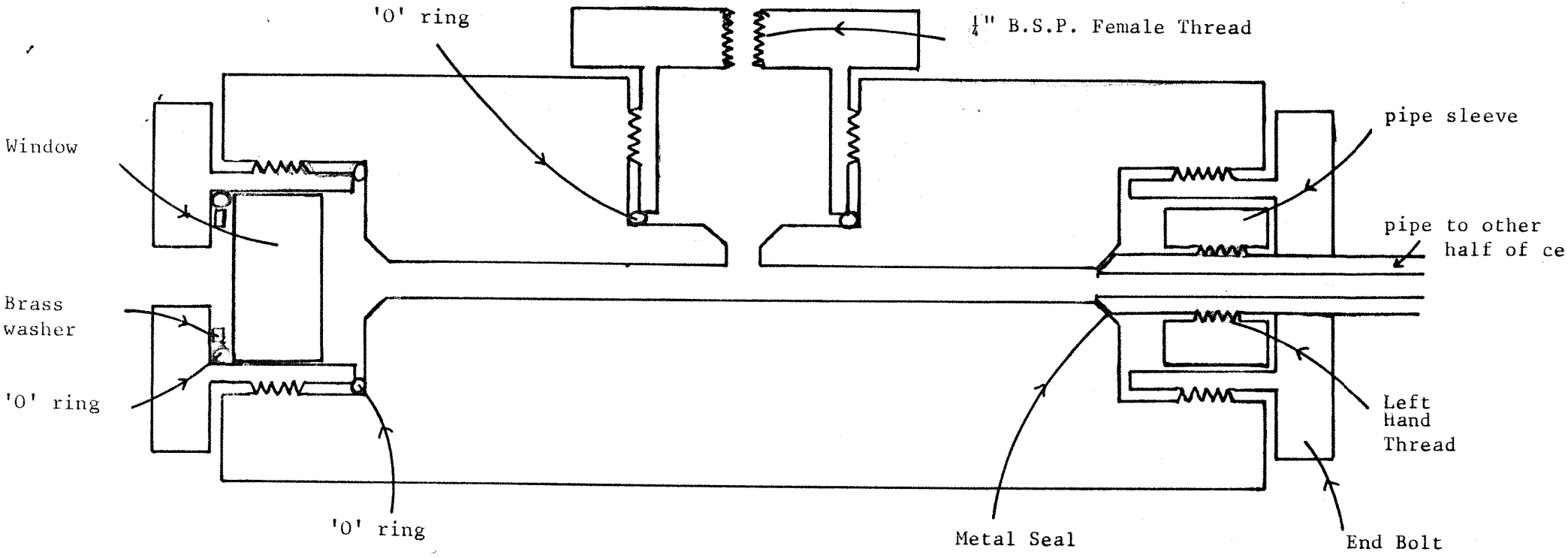


FIGURE 5.3 CONSTRUCTION OF THE GAS CELL (HALF SHOWN)

FIGURE 5.3

The windows used in the Raman cell were 21mm diameter by 12mm thick. As such they should have a safety factor of at least 10 at the gas pressures used. Perhaps the weakest point in the construction of the gas cell is the o-ring used to seal the window. The gas pressure on this O-ring will tend to make it collapse radially. A small brass washer was located inside the O-ring to prevent this.

The use of waveguides complicated the gas cell construction since the capillary must be kept straight and well away from the cell windows to prevent optical damage from tightly focussed beams. The capillary must also not move around when the gas cell pressure is changed. The system used for most of the measurements is shown in figure 5.4. As can be seen the end pieces seal against the thick glass supporting capillary which is itself pressurized and supported in a precision V-groove. Unfortunately the mounting of the end pieces was inadequate with the result that the ends moved under pressure causing capillary bending, misalignment, and sometimes breakage of the thick supporting capillary. Since a theoretical analysis of bending losses showed that large scale bending was not after all a major source of capillary loss, we decided to try a simpler system. Towards the end of the work described in this thesis, a thick supporting capillary was simply wedged against one side of the steel tube used to connect the Aminco 'T' end pieces together. From the few results obtained so far, this latter method would seem far superior to that using the V groove. It is simpler, more reliable, and results in higher capillary transmissions.

### 5.1.3 The beam expanding telescope, Nd: Yag amplifier, and frequency doubler

As was noted in chapter 3 the A.M.L. oscillator was only able to produce a few mJ of energy in the output train. This was not enough for some experiments and so a 3" x 3/8" diameter Yag amplifier was added. The amplifier rod was preceded by a 3 x magnification telescope comprising two lenses which were A.R.

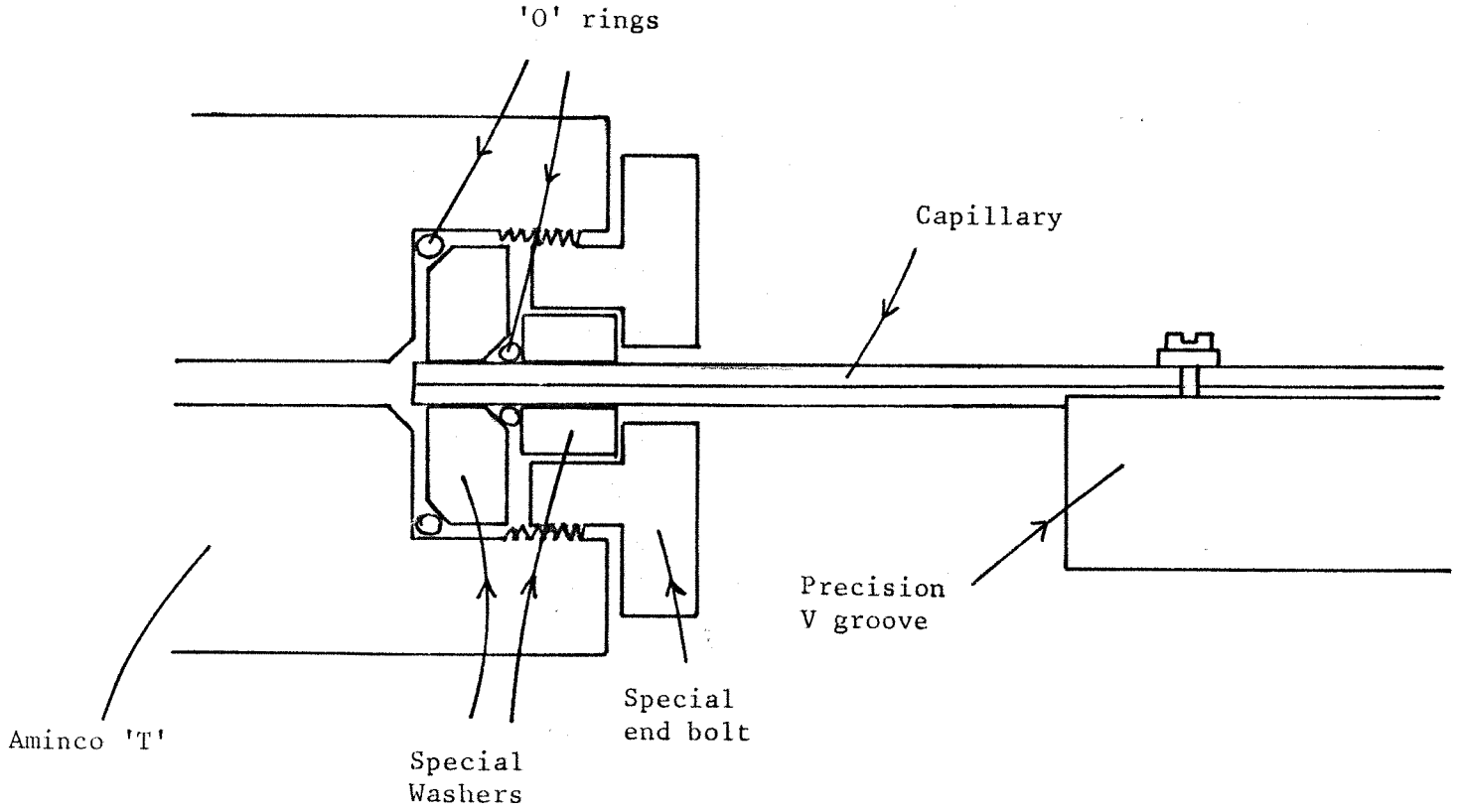


FIGURE 5.4 CONSTRUCTION OF HIGH PRESSURE WAVEGUIDE CELLS

FIGURE 5.4

coated at 1.06. The resulting beam travelling through the amplifier rod had a waist size of about 2mm, compared with a maximum possible size of about 3mm due to the 9mm rod aperture. The maximum output energy without damage was estimated to be at least 50mJ in the pulse train with this beam size. In practise the train energy never exceeded 30mJ but this was with only 60% of the available flashlamp energy.

The telescope and Yag amplifier rod had to be carefully aligned to prevent beam distortions. In particular it was necessary to have the telescope lenses aligned centrally to prevent beam distortions in the far field due to coma. The convex telescope lens was mounted on a translation stage in order to adjust the telescope spacing. This allowed accurate control over the spot size at the Raman cell focusing lens, and hence the focussing conditions, into the Raman cell. In order to know the precise focusing conditions the waist size at the Raman cell focusing lens was measured experimentally with a photodiode array.

Frequency doubling was carried out using a 4cm long crystal of $KD^*P$ mounted in an oven at $40^{\circ}$ centrigrade. The maximum efficiency that was obtained was 3.4mJ of 532nm from 25mJ of 1.06$\mu$m after a system with an overall transmission of only 53%, (turning prisms, dichroic filter, etc). This gives a conversion efficiency for the doubler of 26% which means that the efficiency at the centre of the central pulse will be saturating as discussed in section 3.1.4. With this small degree of saturation however, the relationship between the input and output spot sizes and temporal characteristics will still be given by a factor of ~1.4.

In order to make measurements of Raman threshold it is necessary to vary the amount of energy incident on the Raman cell without altering any other beam parameters. In experiments using the Nd:Yag amplifier this was possible simply by altering the amplifier flashlamp energy. In earlier experiments without the Yag

amplifier, a two plate attenuator was used, (Berry , 1981). This comprised two self compensating glass flats which could be simultaneously tilted in order to vary the loss due to the Fresnel reflection from the four surfaces. For some of the measurements with a very low S.R.S. threshold it was necessary to insert even more attenuation by activating a Pockels cell/polarizer system mounted externally to the A.M.L. oscillator.

## 5.2 Short pulse S.R.S. threshold measurements

Most of the experimental work described in this chapter is associated with investigations of S.R.S. threshold behaviour since this is an important characteristic of the S.R.S. process.

### 5.2.1 General points concerning the interpretation of results

All of the threshold measurements were taken using an energy meter placed immediately before the Raman cell input window. It is the aim of this section to relate this threshold energy to the peak power present at the centre of the central pulse in the pulse train. Each of the pulses in the pulse train is separated by about 7.5nS corresponding to the round trip time of the A.M.L. oscillator. Consequently each pulse can be considered to act independently on the Raman medium since the vibrational lifetime is 280pSec in hydrogen and much less in methane. After 7.5nSec any Raman excitations will have decayed away to a negligible level.

In order to obtain the centre pulse energy is is necessary to consider the width of the pulse train. From measurements on oscillographs of the train profile it was found that the peak pulse energy ($E_{cp}$), the f.w.h.m. of the train profile ($\Delta t$), and the train energy ($E_t$), were related by

$$E_{cp} = 0.94 \cdot E_t \cdot t_R/\Delta t \qquad 5.1$$

where $t_R$ = 7.5nSec, the pulse separation. When making an S.R.S. threshold measurement the pulse train length as well as the train energy was measured in order to eliminate any error that could be induced by a varying pulse train length. The pulse train length varied from day to day due to changes in flashlamp condition, Pockels cell voltage setting and mirror alignment.

When making energy measurements at 1.06$\mu$m it was necessary to compensate for pre-lase energy included in the energy meter readings. Over 5mSec this pre-lase energy can amount to a significant fraction of the energy. The pre-lase energy registered could be measured by blocking the q-switch trigger to the A.M.L. oscillator. A similar problem occured at 532nm but here the problem was due to leakage of 1.06$\mu$m radiation through the dichroic filter. This leakage could be measured by detuning the phase matching angle of the doubler to stop any 532nm generation.

In order to relate the peak pulse power to the centre pulse energy and pulse length we must multiply by a factor 0.94 for Gaussian pulses, i.e. P = 0.94.E/t. This factor corresponds to the $(4 \text{ Ln } (2/\pi))^{1/2}$ term which arises from the integration of the area under a Gaussian pulse. Reflection losses from the gas cell input window meant that the actual threshold power was $(0.96)^2$ times smaller than that measured. Since the cell input window could, in principle, be A.R. coated and essentially loss free, the value for S.R.S. threshold that we give includes an allowance for this cell window loss.

### 5.2.2 Short pulse S.R.S. using tight focussing

The experimental measurements described here of S.R.S. using tight focussing were carried out at two wavelengths, (532nm and 1.06$\mu$m), in the gases Methane and Hydrogen. Additionally measurements were

made in $CH_4$ using a single amplified pulse from a synchronously pumped dye laser operating at 560nm. These results are given separately in section 5.3. The input pulses to the Raman cell consisted of a train of pulses with an approximately Gaussian envelope as discussed in section 5.2.1. Both the pulse length and the train envelope length were monitored throughout the experiments as a check in the performance of the A.M.L. oscillator. At each of the pump wavelengths and in both gases at a pressure of 30 atmospheres the threshold for first Stokes generation was observed. Threshold was measured by varying the incident pump power while observing the first Stokes, either visually or with the pyroelectric energy meter depending on the Stokes wavelength. The results obtained are presented in table 5.5. In all the experiments the cell length to confocal parameter ratio, $L/b_p$, was kept close to 20, large enough to make its exact value unimportant.

The results presented in table 5.5 show good agreement with the theoretically predicted threshold energies also listed in table 5.5, obtained using the procedure given in chapter 4. This agreement confirms that the approximations made in chapter 4 are reasonable. Consequently predictions can now be made for other wavelengths and at other pulse durations.

The effect of pressure on the S.R.S. process was at higher pressures to reduce threshold whereas at lower pressures higher order Stokes and anti-Stokes generation was enhanced. Experimental observations of threshold over the range of 15 to 30 atmospheres showed an approximately linear dependence on pressure, i.e. $E_{th} \propto 1/P$, for both hydrogen and methane.

The enhanced, higher order S.R.S. generation is a result of the smaller phase matching angle required at lower pressures, and hence a longer interaction length for the parametric anti-Stokes

TABLE 5.5

THRESHOLD VALUES FOR S.R.S. IN GASES WITH TRANSIENT PUMP PULSES AND TIGHT FOCUSSING

| GAS | PUMP WAVELENGTH | STOKES WAVELENGTH | PULSE LENGTH | EXPERIMENTAL THRESHOLD | | PREDICTED THRESHOLD POWER |
|---|---|---|---|---|---|---|
| | | | | ENERGY | PEAK POWER | |
| $CH_4$ | 1.06um | 1.544um | 117pS | 0.95mJ | 7.6MW | 6.85MW |
| $CH_4$ | 532nm | 629nm | 83pS | 84uJ | 950KW | 1.17MW |
| $H_2$ | 1.06um | 1.904um | 125pS | 2.3mJ | 17MW | 18MW |
| $H_2$ | 532nm | 683nm | 83pS | 200uJ | 2.3MW | 3.16MW |

generating processes, (see section 4.5: gas dispersion). Details of a brief investigation into the dependence of first anti-Stokes generation on pressure are to be found in section 5.4.

### 5.2.3 Short pulse S.R.S. using capillary waveguides

Capillaries have been used with the Raman process to reduce the threshold power requirement by increasing the interaction length (Berry and Hanna, 1983, 2 papers). This section gives details of an investigation into the use of capillaries as a means of threshold reduction using short pulses. Experiments were carried out at the 2 wavelengths 532nm and 1.06$\mu$m,in the gases methane and hydrogen. The choice of waveguide depends on the degree of threshold reduction that is required and the amount of waveguide loss that can be tolerated, (see figure 4.2). In all the experimental results presented in this thesis an 82cm long capillary with a 200$\mu$m diameter bore was used. The capillaries were made of high quality fused silica and were manufactured by the optical fibre group at Southampton University. This capillary, of outside diameter 300$\mu$m, was supported inside a precision 330$\mu$m diameter bore pyrex capillary of about 6mm outside diameter. This thick walled capillary was held in a V-groove to maintain its straightness as outlined in section 5.1.2. It was necessary to use a combination of two capillaries since a thick wall is required to ease handling but a thick walled, silica precision bore capillary was not available. A fused silica capillary is required because pyrex suffers optical damage at lower intensities than silica. Additionally, its lower transmission will have a slight effect on capillary losses via the $EH_{11}$ mode evanescent wave component.

A practical complication of using a capillary is that the focussing conditions for the pump beam are much more stringent than when a capillary is not used. Abrams, (1972) shows that the free space $TEM_{oo}$ mode and the guided $EH_{11}$ mode couple with a 98% efficiency when the $TEM_{oo}$ spot size, W, equals 0.644 x a where a is the capillary bore radius. Hence, for a maximum capillary

transmission, we require a $TEM_{oo}$ waist at the entrance to the capillary with a 64$\mu$m spot size. In addition to this the spot size at the gas cell window must be large enough to prevent optical damage from occuring at the highest pump powers likely to be used. To meet both of these conditions we need to accurately know the beam focussing parameters. In our work the pump spot size immediately before the focussing lens was measured using a photodiode array. An allowance was then made for the input beam's radius of curvature in selecting the focussing lens.

Having obtained accurate focussing conditions for the pump beam the capillary was positioned for optimum transmission. In our experiments it was found that the lateral alignment tolerances of the capillary were: front end: 5$\mu$m, rear end: 5mm. Additionally the capillary had to be positioned to within about 5mm in a longitudinal direction. Further details of capilliary usage, alignment and suppliers have been presented in Berry, (1984), inconjunction with the steady state S.R.S. capillary measurements mentioned in the introduction to this thesis.

In order to ensure that the capillary is of high quality and correctly aligned, a transmission measurement is made. The value obtained is then used in section 4.2.2 to evaluate an effective capillary length from which a predicted threshold can be obtained. The concept of using an effective length is only valid if the measured losses are close to the predicted losses of figure 4.2. If this is not so then the assumption of an evenly distributed loss may be invalid and slight inaccuracies in the theoretical predictions will result.

Our experimental results are given in table 5.6 together with our predicted thresholds calculated in chapter 4. Comparison of these results with those of table 5.5 indicates that a substantial decrease in the threshold energy has resulted from the introduction of a capillary into the gas cell. Of particular note is our result for methane at 532nm where an experimental

TABLE 5.6

THRESHOLD VALUES FOR S.R.S. USING SHORT PULSES IN A WAVEGUIDE

| GAS | PUMP WAVELENGTH | CAPILLARY TRANSMISSION | EFFECTIVE LENGTH | EXPERIMENTAL ENERGY | PULSE LENGTH (ps) | EXPERIMENTAL THRESHOLD (kw) | PREDICTED THRESHOLD (kw) |
|---|---|---|---|---|---|---|---|
| $CH_4$ | 1.06um | 0.17 | 0.38 | 93uJ | 110 | 750 | 720 |
| $CH_4$ | 532nm | 0.49 | 0.57 | 9uJ | 67 | 125 | 147 |
| $H_2$ | 1.06um | 0.22 | 0.42 | 140uJ | 110 | 1.2MW | 1.27MW |
| $H_2$ | 532nm | 0.3 | 0.48 | 22uJ | 53 | 392 | 467 |

Experimental Conditions: Capillary length = 82cm

Capillary diameter = 200um

Gas pressure = 30 Atmospheres

single pulse threshold energy of only 9$\mu$J was achieved. This result indicated that a number of low energy, short pulse laser sources will now be capable of using S.R.S. in capillaries as a means for extending their wavelength coverage.

From the results presented in table 5.6, it can be seen that the experimental results and theoretical predictions all agree to within about 20%. This is encouraging evidence which gives support to the theoretical analysis as described in chapter 4.

At this point it should be noted that threshold reduction is not an advantage in all cases. Whilst the use of capillaries can bring S.R.S. within reach of low power lasers previously unable to reach threshold, in some cases the S.R.S. threshold can be reduced too far with a resulting decrease in conversion efficiency to some wavelengths. The S.R.S. conversion efficiency is a function of the degree by which the pump power exceeds the threshold power, (see section 5.4 and Von der Linde, 1969). For first Stokes, optimum efficiency is obtained when this factor is around 2 or 3. At higher pump powers very little extra first Stokes is generated. Therefore, to generate the maximum amount of first Stokes it is desirable to have a threshold of about a third of the maximum available pump energy. A lower threshold will result in pump energy being wasted by conversion to higher order Stokes and anti-Stokes weavelengths. A typical example where threshold reduction is not required is when using a J.K. Lasers Synchronously pumped dye laser system. This laser produced over 500$\mu$J of 570nm radiation in a single 50-70pS long pulse. Since the theory of chapter 4 predicts a capillary threshold of around 10$\mu$J, the available pump energy would be 50 times threshold.

### 5.2.4 Synchronously pumped S.R.S.

An alternative to capillaries as a means for reducing threshold is to introduce resonator mirrors so that the Stokes wave undergoes

multiple passes through the gain medium. This reduces the gain required per single pass and therefore the threshold. If this technique is used in conjunction with a capillary then threshold can be reduced even further.

A complication with this technique, is that with 100pS pump pulses, the circulating Stokes pulses must be timed so as to overlap with pump pulses incident on the resonator. This is obtained by adjusting the spacing of the Stokes resonator mirrors to match the A.M.L. oscillator cavity length. Typical threshold reductions that can be obtained are limited to a factor of 2 to 3 in our system due to losses in the Stokes resonator and the limited number of pulses in the mode-locked train. In section 4.2.3 we evaluated the degree of threshold reduction expected theoretically. The most important result of this section is that the amount of threshold reduction obtained is not very dependent on the amount of Stokes losses. This is fortunate since the Stokes resonator invariably has a large number of elements which all contribute to the round trip Stokes loss. These factors are; Stokes mirror and cavity component losses, incorrect focussing of the circulating Stokes wave and inaccurate synchronism between the Stokes and pump pulses. In our system these losses were estimated to result in a combined Stokes attenuation factor of exp(-4). If a capillary is employed as well as the resonator then an additional loss will also be present corresponding to the double pass capillary attenuation. In our system using a capillary resonator we estimated the total round trip Stokes attenuation factor to be exp(-7).

The Stokes feedback mirrors must be chosen to have a high transmission at the pump wavelength and yet reflect the required amount of first Stokes. The mirrors used in our experiments were selected from a large stock of locally produced mirrors. These mirrors were non-ideal and transmitted only 88% at 532nm while having approximately 50% transmission at the first Stokes frequencies, (630 & 690nm).

The resonator configuration used in the experiments is shown in figure 5.7. Both of the lenses used were uncoated and so contributed a loss as did the cell windows. As in previous threshold measurements our values for threshold are corrected to allow for these pump losses. Hence the value for threshold given is that which would be obtained if fully A.R. coated components were employed.

The following threshold values were obtained both with, and without the Stokes resonator mirrors aligned. The results with the mirrors mis-aligned correspond to the single pass results given in section 5.2.2.

| Threshold (mJ) | Single Pass | Oscillating |
|---|---|---|
| Hydrogen | 1.2 | 0.5 |
| Methane | 0.5 | 0.19 |

The energies given here correspond to that in the whole pump train which had a roughly Gaussian envelope with a f.w.h.m. of 50nS, i.e. 7 pulses. The pulse length in all cases was 80pS, all measurements being taken at 30 Atmospheres with a pump wavelength of 532nm.

The use of an oscillator with a capillary and synchronous pumping represents a considerable alignment problem. This is a consequence of the need to efficiently couple the Stokes radiation into an out of the capillary at both ends whilst maintaining efficient coupling into the capillary for the pump. As noted

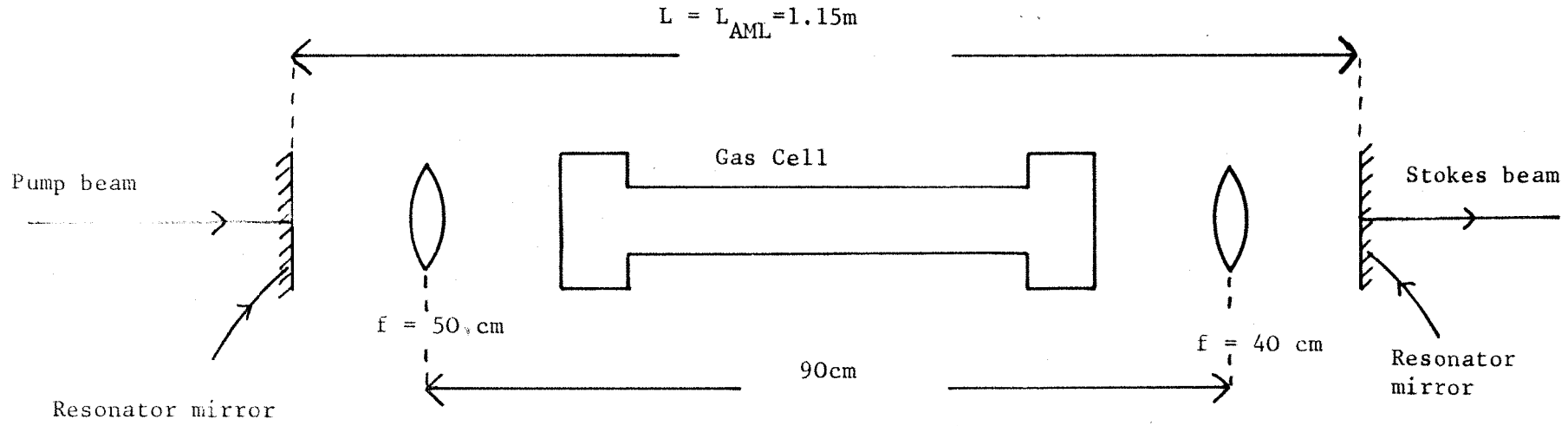


FIGURE 5.7 SCHEMATIC DIAGRAM OF THE RESONATOR USED FOR SYNCHRONOUSLY PUMPED S.R.S.

FIGURE 5.7

earlier our prediction for the round trip Stokes attenuation factor was exp(-7) which gives an expected threshold reduction of about 40% for our pump train, (see section 4.2.3). Experimentally a threshold reduction of 33% was obtained which agrees reasonably well with that expected theoretically.

No results are presented in this section for threshold measurements using a 1.06$\mu$m pump. This is not due to difficulty in aligning the Stokes mirrors but due to feedback of the pump radiation from the Stokes mirrors into the A.M.L. oscillator. This feedback, whilst assisting with alignment of the Stokes mirrors, resulted in disturbance to the mode locking process. This occurred even with extremely small amounts of feedback. A simple quarter-wave plate/polarizer isolation technique (see figure 2.7), was attempted but the amount of feedback was still large enough to disturb the A.M.L. oscillator mode locking process.

## 5.3 S.R.S. using the tunable, synchronously pumped dye laser

The predicted threshold for S.R.S. in methane at 570nm using 70pS pulses, 30 atmospheres pressure and tight focussing is given in table 4.6 as 1.76MW or 130$\mu$J in a single pulse. The synchronously pumped dye laser, (SPDL), recently developed by J.K. Lasers Ltd, produces a single tunable pulse containing upto 1mJ of energy. This PhD programme was carried out partly with the assistance of J.K. Lasers Ltd. in the form of a CASE award and therefore a visit to J.K. Lasers was arranged in order to attempt S.R.S. in methane with the S.P.D.L. The production of coherent, tunable, picosecond, near infrared, high energy, bandwidth limited radiation was of interest to J.K. Lasers Ltd. as a product.

The S.P.D.L constructed and used in these experiments has been described in section 3.3 of this thesis. The laser actually produced upto 600$\mu$J which was sufficiently above threshold for single pass S.R.S. in methane using tight focussing.

The use of a waveguide with the S.P.D.L. would have reduced 1st Stokes S.R.S. efficiency since threshold would be much lower allowing more higher order Stokes generation. This would reduce the conversion efficiency into lower order Stokes wavelengths.

The output from the dye amplifier stage was focussed using a 20cm focal length lens into a 35cm long cell giving a resulting value for $L/b_p$ of about 10. After the cell, a collimating lens and two prisms were used to separate the various Stokes orders.

Table 5.8 shows the conversion efficiencies into the various Stokes and anti-Stokes orders, taking into account any losses introduced as a result of the prisms or non A.R. coated optics. The energy measurements were made with a J.K. Lasers energy monitor which was based around a Plessey SC102 silicon photodiode. This had only been calibrated at 532nm and 1.06$\mu$m and so had to be recalibrated at 570nm and at each of the Stokes and anti-Stokes wavelengths. This was done using a rather insensitive disc calorimeter which means that our calibrations are rather inaccurate, possibly by as much as 50%.

Whilst making the measurements given in table 5.8, a set of threshold results were taken at the three pressures, 30, 20 and 15 atmospheres, the results being 120$\mu$J, 170$\mu$J and 200$\mu$J respectively. The value at 30 atmospheres agrees fairly well with that predicted in section 4.4.2 of 130$\mu$J. The lower pressure values also follow the inverse dependence on pressure which is to be expected with highly transient pulses from equation 5.2.

It can be seen from table 5.8 that conversion efficiencies of 10%, 10% and 5% can simultaneously be achieved for the first, second and third Stokes wavelengths respectively. At pump energies slightly higher than 600$\mu$J, a higher efficiency for 3rd Stokes is expected. This is because at 600$\mu$J, 3rd Stokes was barely above its threshold. Since the A.M.L. should produce upto 1mJ, better performance for 3rd Stokes than that achieved here should be possible.

| Input Energy ($\mu$J) | Pressure (Atm) | $E_{S1}$ ($\mu$J) | $E_{S2}$ ($\mu$J) | $E_{S3}$ ($\mu$J) | $E_{A1}$ ($\mu$J) | $E_{A2}$ ($\mu$J) |
|---|---|---|---|---|---|---|
| 640 | 30 | | 60 | 20-40 | | |
| 510 | 30 | 50 | 50 | 12-25 | 20 | 2 |
| 400 | 30 | 32 | 27 | 2-10 | | |
| 300 | 30 | 25 | 10 | 1 | | |
| 185 | 30 | 15 | 5-10 | | | |
| 130 | 30 | 5-15 | 1 | | | |
| 550 | 20 | 50 | 45 | 30 | | |
| 450 | 20 | 32 | 27 | 2-10 | 5-10 | 1 |
| 320 | 20 | 27 | 7-17 | | 5-7 | |
| 220 | 20 | 10-20 | 2 | | | |
| 550 | 15 | 50 | 27 | 10 | | |
| Wavelength: (Pump = 568nm) | | 681nm | 849nm | 1.13um | 487nm | 427nm |

TABLE 5.8: S.R.S. PERFORMANCE OF METHANE PUMPED BY THE S.P.D.L.

## 5.4 Observations on Conversion efficiency

Throughout the threshold measurements on short pulse, S.R.S. in gases, observations were made on the conversion efficiency into the various Stokes and anti-Stokes orders. This section collects together this work involving tight focussing, waveguides and resonators to give an idea of how efficiency varies with different configurations. The conversion efficiency measurements on the synchronously pumped dye laser were discussed in that section as all the work on the S.P.D.L. stands alone to some extent. All the conversion efficiency measurements given in this thesis have been corrected to allow for window, prism, lens and filter losses.

A complication in making conversion efficiency measurements is that the value obtained depends on the degree by which the incident pump exceeds the threshold power. For first Stokes this conversion efficiency tends to a maximum when the incident pump is around twice threshold. For higher Stokes and anti-Stokes orders maximum efficiency occurs at higher pump powers.

Typical conversion efficiencies into the first and second Stokes was 10% in a single pass unguided configuration. When a waveguide was employed this conversion efficiency dropped, as a consequence of waveguide transmission losses, to around 5%. The conversion efficiency values obtained for the anti-Stokes wavelengths were generally much smaller, around 1% to 1st anti-Stokes and 0.1% into 2nd anti-Stokes. Hydrogen generally performed better than methane at anti-Stokes generation as long as its higher first Stokes threshold was reached. This better performance is likely to be as a consequence of hydrogen's smaller dispersion (see equation 4.60 and associated text). This dispersion gives rise to a phase mismatch which is about 3 times larger for methane than hydrogen.

The use of Stokes oscillator mirrors had a peculiar effect on the conversion efficiency into the various wavelengths. This

manifested itself as a increase in first Stokes generation efficiency but a reduction in efficency to all other orders. This however only applied when the incident pump energy was well above the threshold intensity. At low pump powers the lowering of threshold by the Stokes feedback resulted in an increased conversion efficiency to all orders.

Table 5.9 shows this effect for first anti-Stokes generation. At lower pressures with no feedback, the incident pump power is barely above threshold with the consequent reduction in conversion to anti-Stokes. The increase in anti-Stokes at lower pressures despite a fixed input power is a consequence of better phase matching for the parametric processes as discussed in section 4.5.

Table 5.9

First anti-Stokes generation as a function of pressure and Stokes feedback

| Pressure | No Feedback | oscillating |
|---|---|---|
| (Atmospheres) | ($\mu$J) | ($\mu$J) |
| 30 | 8 | 3 |
| 20 | 10 | 6 |
| 15 | 7.5 | 9 |

Incident pump energy = 1mJ
Incident pump wavelength = 532nm
Raman medium = methane
pulse length ≃ 70pS
train length ≃ 6 pulses

## 6. Concluding Remarks

The theoretical and experimental work presented in this thesis is concerned with two separate aspects; Nd: laser oscillator development and the application of the A.M.L. laser to an investigation of Stimulated Raman Scattering (S.R.S.) , as a process for converting radiation to new wavelengths. Accordingly our conclusions on these two aspects are discussed separately.

The final stages of the work on the single longitudinal mode, (SLM), oscillator presented in the early part of chapter 2 of this thesis provided an effective, practical method for producing a single frequency, high output energy, Nd: Yag laser. The theoretical work presented on Fabry-Perot etalons predicts the losses of these devices as a function of tilt angle which agrees well with our experimental measurements. This theory can therefore be used to give an estimate of etalon losses in future resonator designs. If these losses are too large then the technique allowing insertion of the etalon at normal incidence can be used as a method for virtually eliminating etalon insertion losses. Our work on Nd: Glass showed this material to be unsatisfactory for our purposes. Although some tunability was obtained, performance was severely limited by thermally induced birefringence losses. This problem may be largely eliminated with the development of slab geometry laser systems which are currently under investigation in a number of laboratories.

Having concluded our work on S.L.M. lasers our investigations turned to the development of an actively mode locked, (A.M.L.), Nd: Yag laser with the aim of carrying out short pulse S.R.S. characterization experiments. This work on the A.M.L. oscillator confirmed the theories of Kuizenga, (1981), and succeeded in producing short, (~100pS), pulses with Fourier transform limited bandwidths. All of the resonator configurations examined produced a Gaussian transverse profile which is necessary for accurate comparisons between S.R.S. theory and experiment.

Our work on characterizing S.R.S. in gases using short (~100pSec) pulses involved the development of a theory describing transient S.R.S. under a variety of conditions. These included, tight focussing, using a waveguide and using Stokes resonator mirrors. Under all of these conditions the pump transverse profile is a near Gaussian. The theory presented combines the plane wave, transient S.R.S. equations with an analysis considering gain focussing of the Stokes beam. The approximations made in the theory include the Stokes beam being smaller than the pump and hence experiencing the on-axis pump gain. This is not necessarily the case, (the Stokes and pump beams being fairly close in size), and so a more rigorous theory is ideally required. This theory is however difficult and not available at the present time. Despite our theoretical approximations, our predictions show reasonable agreement with experimental results. Another factor requiring attention is the question of losses in capillary waveguides. In this and previous work, a continuously distributed capillary loss has been assumed. A significant proportion of the capillary loss may be due to inaccurate launching which will have the effect of slightly increasing the threshold power.

Our conclusions on the practical aspects of S.R.S.using short pulses indicate that very low threshold energies can be achieved with the use of capillary waveguides, (i.e. 9$\mu$J in a 67pS duration pulse at 532nm). This result brings S.R.S. in methane within reach of mode-locked, C.W. dye lasers amplified using pulses from a copper or gold vapour laser. This will result in a new route for the generation of tunable infra-red radiation of high peak and average power. A secondary advantage of gold and copper vapour lasers are their very high repetition rates which can be very useful in spectroscopic experiments where signal averaging is used to improve signal-to-noise ratios.

The threshold reduction obtained by using capillaries is not always an advantage. In particular, when threshold can easily be reached in a single pass, unguided arrangement, the use of a capillary can reduce conversion efficiency into the near Stokes wavelengths.

Due to the low threshold now obtainable with S.R.S. in gases, it should be possible to obtain short pulse, tunable, infra red radiation out to wavelengths of 4$\mu$m and longer, even using pump lasers with a very modest output energy. Experiments with this aim in mind are continuing in the laser group at Southampton University.

REFERENCES

R.L.ABRAMS. IEEE Jnl. QE-8(11), (1972), 838-843

M.J.ADAMS "An introduction ot Optical Waveguides", Wiley, Chicester (1981)

J.A.ARNAUD, A.A.M.SALEH, J.T.RUSCIO. IEE Trans MTT-22, (1974), 486-493

A.J.BERRY, Ph.D. Thesis. Univ. of Soton. 1984

A.J.BERRY, D.C.HANNA. Optics commun, 45(5), (1983), 357-360

A.J.BERRY, D.C.HANNA, C.G.SAWYERS. Optics commun, 40, (1981), 54-58

M.BORN, E.WOLF, "Principles of optics", 6th edition, Pergamon press, 1980

G.D.BOYD, W.D.JOHNSON, I.P.KAMINOV. IEEE Jnl. QE-5 (1969) 203-206

P.N.BUTCHER. "Nonlinear optical phenomena", Bulletin 200, Exg.exp. Station. Ohio State University, 1965

R.L.BYER. IEEE Jnl. QE-12, (1976), 732-733

R.L.CARMAN, F.SHIMIZU, C.S.WANG, N.BLOEMBERGEN. Phys Rev A,2 (1970), 60-72

M.J.COLLES. Appl. Phys Lett; 19(2), (1971), 23-25

D.COTTER, D.C.HANNA, R.WYATT. Appl. Phys. 8, (1975), 333-340

W.DEMTRODER, "Laser spectroscopy", Springer series in chemical physics, Vol 5, Springer verlag, 1981

R.DUNSMUIR. Jnl. electron control. 10, (1961), 453

V.EVTUHOV, A.E.SIEGMAN. Appl. Opt. 4, (1965), 142-143

K.R.GERMAN, Appl Optics, 20(18), (1981), p3168

H.GRAENER, A.LAUBEREAU. Optics. commun., 37(2), (1981), 138-142

F.GRAF, C.LOW, A.PENZKOFER. Optics commun., 47(5), (1983), 329-334

A.Z.GRAZIUK, I.G.ZUBAREV. Appl. Phys. 17,(1978), 211-232

D.C.HANNA, Y.W.KOO. Optics commun., 43 (1982), 414-418

D.C.HANNA, Y.W.KOO, D.J.PRATT. Optics commun., 44,(1983), 188-191

D.C.HANNA, M.A.YURATICH, D.COTTER, "Non-linear optics of free atoms and molecules", Springer series in optical sciences, Vol 17, 1979.

D.C.HANNA, B.LUTHER-DAVIES, R.C.SMITH. Electron lett., 8, (1972), 269-270

D.C.HANNA, B.LUTHER-DAVIES, R.C.SMITH. Opto-electronics, 4,(1972), 249-256

D.C.HANNA, D.J.PRATT. Paper presented at Electro-Optics/Laser International, Brighton, 1984

D.C.HANNA, D.J.POINTER, D.J.PRATT, Accepted for publication, IEEE.Jnl.Quant.elect. September 1985

W.HARTIG, W.SCHMIDT. Appl.phys. 18, (1979), 235-241

E.HECHT, A.ZAJAC. "Optics", Addison-Wesley, 1974

D.HERRIOT, H.KOGELNIK, R.KOMPFNER. Appl.optic. 3(4), (1964), 523-526

M.C.IBISON. "Minithesis", University of Southampton, (1982)

W.KAISER, M.MAIER. In "Laser handbook", F.T.ARRECHI, E.O.SCHULTZ-DUBOIS, Eds. North Holland, Amsterdam, (1972), 1077-1150

W.KEOCHNER. In "Solid state laser engineering", Springer series in optical sciences, Vol 1, Springer-Verlag, 1976

K.KERL. Zeitschrift fur Physicalische chemie, Bd-129, (1982), 129-148

D.J.KUIZENGA. IEEE.Jnl.Quant.elect. QE-17(9), (1981), 1694-1708

D.J.KUIZENGA. Optics commun. 22(2), (1977), 156-160

D.J.KUIZENGA, A.E.SEIGMAN. IEEE. Jnl. Quant. elect. QE-6(11), (1970), 694-708

W.R.LEEB. Appl. Phys. 6, (1975), 267-272

W.H.LOWDERMILK, G.I.KACHEN. Appl.Phys.lett,27, (1975), 133-135

L.A.LOMPRE, G.MAINFRAY, J.THEBAULT. Jnl.Appl.Phys.48, (1977), 1570-1575

B.LUTHER-DAVIES, V.DEL PIZZO. Optics commun. 30, (1979), 403-407

E.A.J.MARCATILI, R.A.SCHMELTZER. Bell Sys. Tech. Jnl, 43, (1964), 1783-1809

A.DE MARTINO, R.FREY, F.PRADERE, IEEE.Jnl.Quant.elect. QE-16, (1980), 1184-1191

A.D.MAY, M.A.HENESIAN, R.L.BYER, Can.Jnl.Phys. 56, (1978), 248-250

P.MAY, W.SIBBETT. Appl.phys.lett. 43(7), (1983), 624
M.W.McGEOCH. Optic commun. 17(2), 1973), 116-120
J.MORELLEC, D.NORMANS, G.PETITE. Appl.Optics, 18, (1979), 141-142
J.R.MURRAY, A.JAVAN. Jnl.mol.spect 42, (1972), 1-26
R.PARTRIDGE. NPL, Private communication, 1984
E.R.PECK, S.HUANG. J. Opt.Soc.Amer. 67, (1977), 1550-1554
A.PENZKOFER, A.LAUBEREAU, W.KAISER. Prog.Quant.Elect. 6, (1979), 55-140
G.PETITE. Jnl.Appl.Phys, 46(8), (1975), 3462-3464
R.H.PIERSON et al. Analt.Chem. 28, (1956), 1218-1239
D.J.POINTER, Private communication, 1984
P.RABINOWITZ, A.KALDOR, R.BRICKMAN, W.SCHMIDT. Appl. Optics 15(9), (1976), 2005-2006
C.G.SAWYERS. PhD. Thesis, University of Southampton, 1981
H.W.SCHROTTER, H.W.KLOCKNER. In "Raman spectroscopy of Gases and liquids", A.WEBER, Eds. Springer, Berlin, 1979, 123-164
A.E.SIEGMAN, D.J.KUIZENGA. Opto-electronics. 6, (1974), 43-66
H.STATZ, G.A.MARS, D.T.WILSON, Jnl.appl.phys.30(5),(1965), 1510
O.SVELTO. "Principles of Lasers", 2nd edition, Plenum, 1982
Y.TAIRA, K.IDE, H.TAKUMA. Chem.phys.lett, 91(4), (1982), 200-302
W.R.TRUTNA, R.L.BYER. Appl.optics. 19(2), (1980), 310-312
K.URE. University of Southampton. "minithesis", (1984)
D.VON DER LINDE, K.F.ROGERS. Optics.commun. 18(1), (1973), 91-94
D.VON DER LINDE, M.MAIER, W.KAISER. Phys.Rev. 178(1),(1969), 11-17
A.WATANABE, H.L.WELSH, Can.Jnl. Phys. 43(5), (1965), 818-828
A.WOKAUM. P.F.LIAO, P.R.FREEMAN, R.H.STORZ. Opt.lett. 7, (1982), 13-15
A.YARIV "Quantum electronics", 2nd edition, Wiley, 1975

## ACKNOWLEDGEMENTS

The author would like to take this opportunity to thank all those people who have assisted him during the period of this work. In particular he would like to thank :

My supervisor, Dr D.C.Hanna for his invaluble ideas and advice during the research work and guidance during the preparation of this thesis.

I should also like to thank Ken Ure for his assistance and advice during the period of work carried out at J.K.Lasers and Dr Clive Ireland for arranging the loan of various small items of laser hardware from J.K.Lasers.

I should like to thank the S.E.R.C. for providing a studentship with which to sustain myself and also produce this thesis.

Lastly, but not leastly, the author would like to thank the rest of the laser group at Southampton University for their advice and friendship. In particular, I would like to thank Ian Carr, Andy Berry, Dave Pointer, Marcos Pacheco, K.H.Wong, Graham Smith, Dave Hearn, Mike Ibison and Ruth Hodder. I should also thank Dr Mike Yuratich for getting me into this in the first place !

# Q-100

# A SUPER-GAIN LASER GLASS

from

KIGRE, INC.

# Q-100 Super-Gain Laser Glass

## ackground

Following the development of Q-98, a vastly improved athermal phosphate laser glass, Kigre, Inc. continued their efforts to develop a derivitive of Q-98 especially suited for military and industrial applications. Our goal was to increase the gain of Q-98 by increasing the neodymium doping level to the maximum permitted....all the while adjusting the composition to maintain its athermal and other desirable properties.

The result of this effort we decided to call Q-100.

## ıtroduction

Initial test results on Q-100 have been most gratifying. So much so in fact, that several customers are considering Q-100 as a direct replacement for YAG. The following pages describe various test results on Q-100. Some of the tests were performed by customers in their respective systems...others were performed at Kigre. Each data plot is identified as to source, operational parameters and configuration.

The final page lists the pertinent properties of Q-100 plus our entire family of laser glasses. We invite inquiries regarding operational parameters of Q-100 and our other glasses,...Q-88, Q-98 and Q-246.

## pplication Notes

Since the gain of Q-100 laser glass is comparable to YAG, one must take the same precautions to suppress parasitic lasing and other performance degrading phenomena. For example, Q-100 laser rod barrels should, in general, not be polished. In air-cooled or static-cooled systems, samarium cavity filters are recommended.

1. Dye Q-switched systems....Q-100, like YAG, requires that anti-reflection coatings be applied to the faces of the laser rod to eliminate the 4% Fresnel reflections, when used with dye Q-switches. The 4% Fresnel reflection is sufficient to cause parasitic lasing during the pump pulse....thereby depleting the stored energy and preventing "bleaching" of the dye.

2. Maximum average power....When run for extended periods of time, the maximum average power loading for Q-100 is approxiamtely 100 watts per inch of length. One will notice no change in beam divergence when increasing average power....even up to the point of rod breakage.

3. Stress-induced birefringence....The onset of significant birefringence occurs at a pumping leve; of approximately 40 watts per inch of length. Between 40 watts per inch and 70 watts per inch, the output will decrease about 20 percent when used with a polarizing cavity element. The relationship is linear to the point of breakage.

4. Athermal properties....The athermal property of Q-100 is determined by the following relationship:

$$\alpha\,(n-1) = -dn/dt$$

Where:

$\alpha$ = Thermal expansion

$n$ = Index of refraction @ 1.054 microns

$dn/dt$ = Change in index with temperature

This relationship dictates a constant optical path length regardless of temperature when utilized with external mirrors. Mirrors that are vapor deposited upon the rod will negate the athermal or "constant beam divergence" property of Q-100. TIR's or roof prisms fabricated directly on Q-100 laser rods are the exception and can be used without disturbing the athermal character of Q-100.

Q-100

Test Data

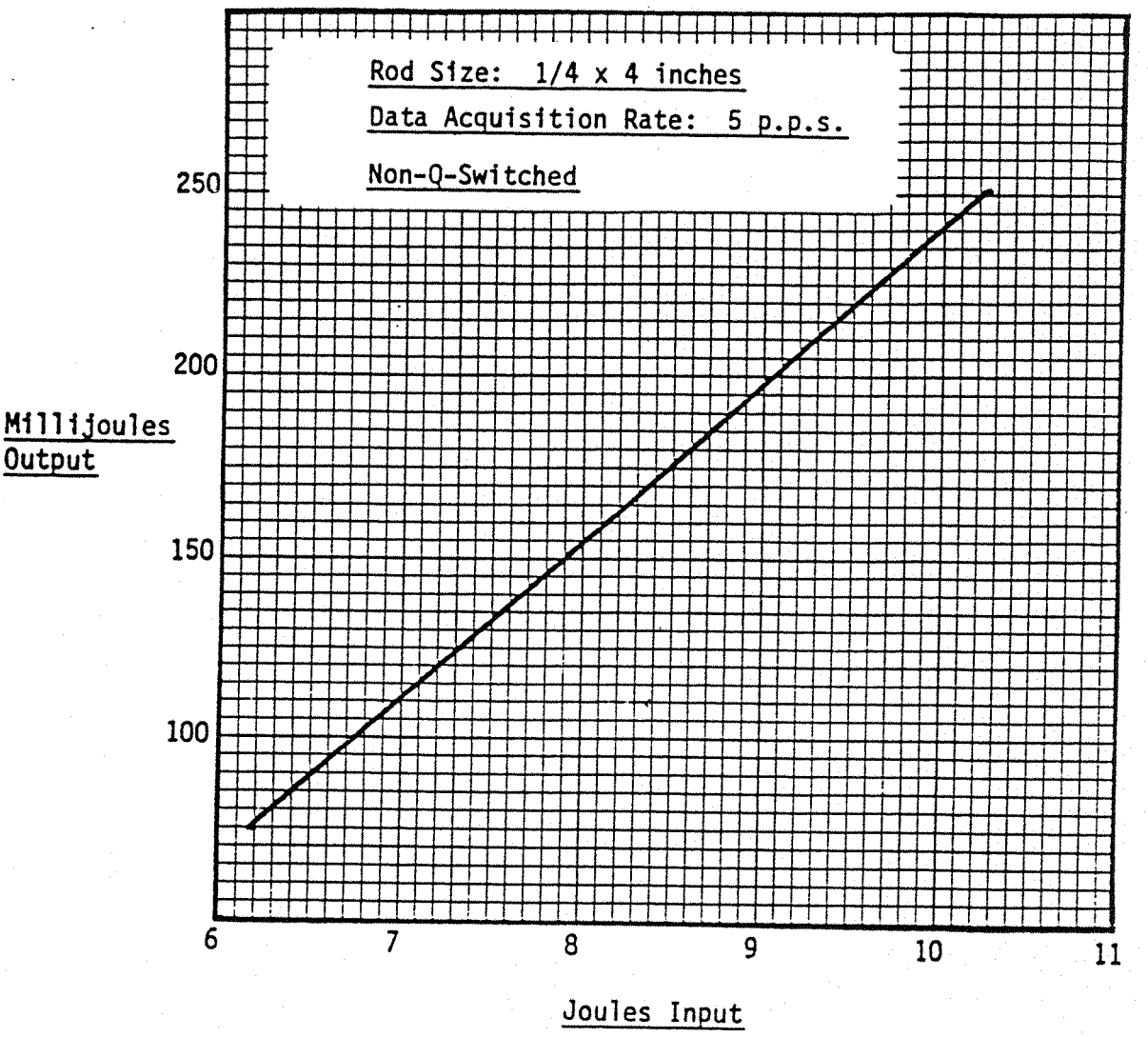


ROD: 1/4 x 4", No Coatings

Output: 85% Reflector

Cavity: ILS "YAG" Cavity

Coolant: Liquid

Q-100

Test Data

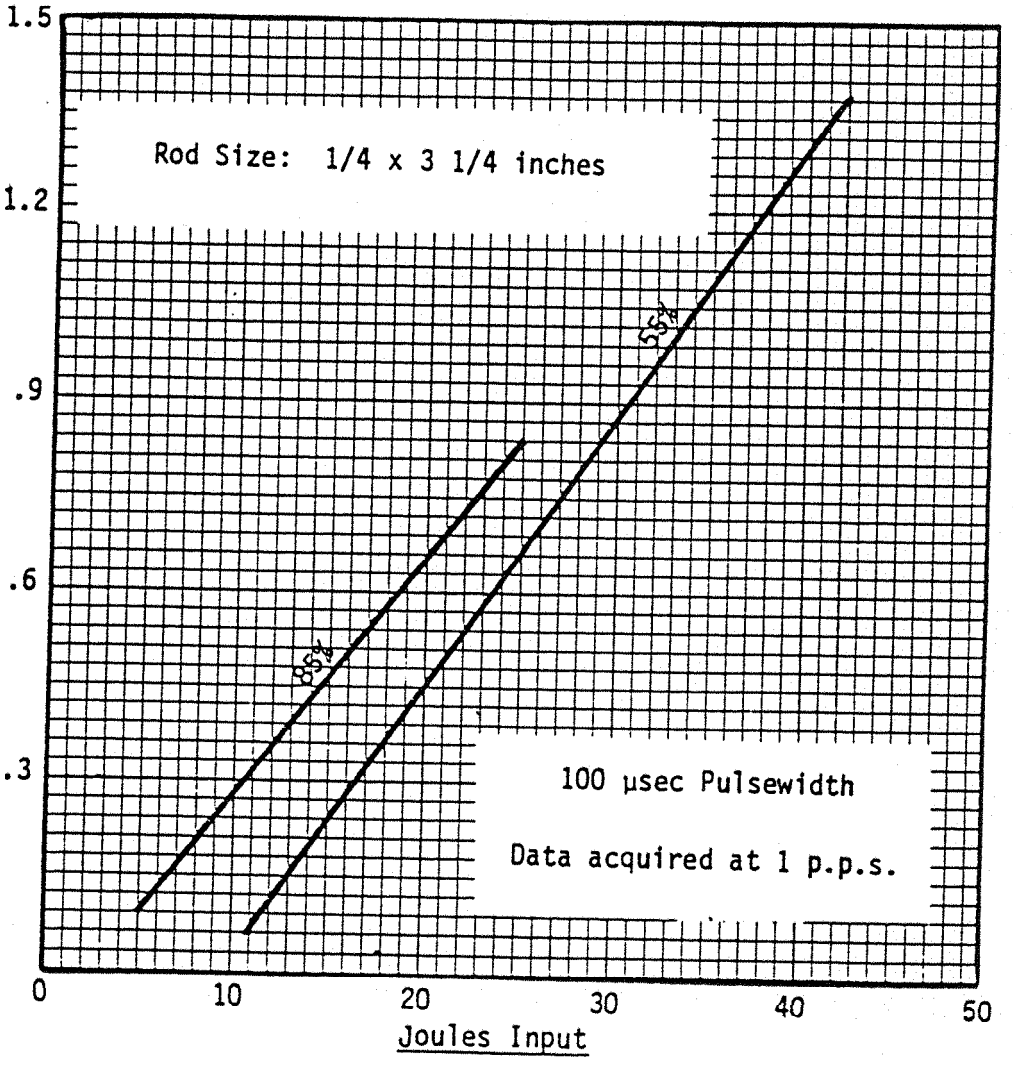


ROD: 1/4 x 3 1/4, No Coatings

Output: 55% & 85% Reflectors

Cavity: Kigre, Silver-Coated Ellipse

Coolant: $H_2O$

## Properties of Kigre Laser Glasses

| Glass Type | Q-246 Silicate | Q-88 Phosphate | Q-98 Athermal Phos. | Q-100 Athermal Phos. |
|---|---|---|---|---|
| **Spectroscopic Properties** | | | | |
| Peak Wavelength (nm) | 1062 | 1054 | 1053 | 1054 |
| Cross Section ($x10^{20}cm$) | 2.9 | 4.0 | 4.5 | 4.4 |
| Fluorescent Lifetime (μsec) | 340 | 330 | 350 | 190 |
| Radiative Lifetime (μsec) | 370 | 326 | 308 | 357 |
| Linewidth (nm) | | | | |
| FWHM | 27.7 | 21.9 | 21.1 | 21.2 |
| Effective | 34.0 | 26.3 | 25.5 | 25.1 |
| Loss @ Lasing Wavelength ($cm^{-1}$) | .002 | .0008 | .0008 | .0008 |
| **Optical Properties** | | | | |
| Density (gm/cc) | 2.55 | 2.71 | 3.099 | 3.204 |
| Index of Refraction ($N_d$) | 1.568 | 1.545 | 1.555 | 1.555 |
| Nonlinear Index $n_2$ ($10^{-13}$esu) | 1.4 | 1.1 | 1.2 | 1.2 |
| Abbe No. | 57.8 | 64.8 | 63.6 | 62.1 |
| dn/dt ($10^{-6}/^oC$) ($20^o$-$40^oC$) | 2.9 | -0.5 | -4.5 | -4.6 |
| Thermal Coefficient of Optical Path ($20^o$-$40^oC$) ($10^{-6}/^oC$) | +8.0 | +2.7 | 0±.5 | 0±.5 |
| **Thermal Properties** | | | | |
| Softening Point $^oC$ | 580 | 384 | 467 | 470 |
| Transformation Point $^oC$ | 518 | 367 | 450 | 452 |
| Annealing Point $^oC$ | 455 | 350 | 433 | 435 |
| Thermal Expansion ($10^{-7}/^oC$) ($20^o$-$40^oC$) | 90 | 104 | 99 | 96 |
| Thermal Conductivity (w/m·k) | 1.30 | 0.84 | 0.82 | 0.82 |
| Specific Heat (J/g·k) | 0.93 | 0.81 | 0.80 | 0.80 |
| **Chemical Properties** | | | | |
| Dw ($H_2O$ $100^oC$ 1 hr) wt% loss | 0.04 | 0.20 | 0.08 | 0.08 |
| **Other Properties** | | | | |
| Knoop Hardness | 600 | 418 | 556 | 558 |
| Young's Modulus ($kg/mm^2$) | 8570 | 7123 | 7210 | 7150 |
| Poisson's Ratio | 0.24 | 0.24 | 0.24 | 0.24 |
| Damage Threshold (1 ns) $J/cm^2$ | >20 | >25 | >25 | >25 |
| Solarization Resistance | ----------Excellent, No Protection Needed---------- | | | |

[illegible] at time of publication.

Appendix 3

A step by step alignment procedure for the A.M.L. oscillator

These alignment notes should be read in conjunction with the diagram showing the component layout.

a) Align the He-Ne so as to follow the intended 1.06$\mu$m beam. In our work this was exactly 2.5 inches above the table in order to pass through the centre of all resonator components.

b) Insert the end mirror, centralize and align the reflected He-Ne beam. Both reflected He-Ne beams should co-incide unless the mirror is wedged. The transmitted He-Ne beam should be undeviated. The end mirror should be removable despite the close proximity of the mode locker.

c) Insert the mode locker close to the end mirror, centralize and align to ensure both reflected beams lie in a horizontal plane and are equally spaced.

d) Insert the Rod/flashlamp assembly and centralize, if the rod is unwedged then deliberately add a tilt to suppress etalon effects. About 10mRads is sufficient with a 6mm diameter, 3" long rod.

e) Insert the Pockels cell and Polarizer. Align the Pockels cell using the malteze cross principle, (Sawyers, 1981). Roughly align the polarizer.

f) Insert the cavity length adjusting blocks, aligned at Brewsters angle. This corresponds to 5mm on the micrometer scale.

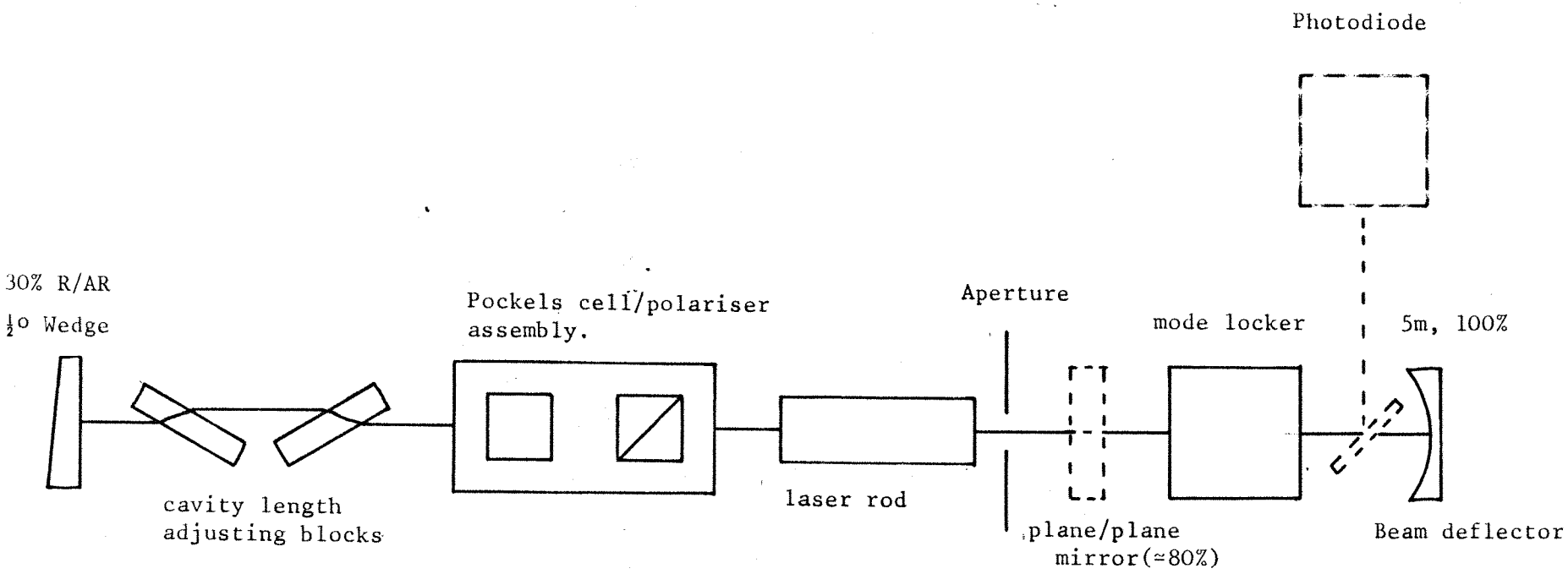


FIGURE A3 THE A.M.L. OSCILLATOR WITH ALIGNMENT COMPONENTS (SHOWN DASHED)

FIGURE A3

g) Insert the end mirror (30% R/A.R, plane 1/2° wedge) at the correct cavity length. This is found from the R.F. oscillator frequency, allowing also for the refractive index of the Yag rod, mode locker, Pockels cell, polarizer and cavity length adjusting blocks.

h) Obtain laser action by adjusting the recently inserted end mirror. Optimize by monitoring with a photodiode and minimizing the delay to the occurrance of the first relaxation oscillation spike.

i) Insert an aperture close to the rod, between it and the mode locker. Optimize the alignment of this and the polarizer using the technique given in h.

j) Insert a plane/parallel mirror of about 70% reflectivity, between the aperture and the mode locker. Block off or remove the end mirror (100% reflectivity, 5m radius of curvature) and align the new mirror to obtain as low a lasing threshold as possible.

k) Apply R.F. to the acousto-optic mode locker and use a small area photo-detector to monitor the transmitted beam. By delaying the pulsed on application of the R.F., it should be possible to see the magnitude of the diffraction efficiency. Optimise this by careful alignment of the Bragg angle/mode locker height. A diffraction efficiency of over 50% should be obtained.

l) Re-insert the end mirror, remove the temporary plane/parallel mirror and align/optimise the end mirror again.

m) Optimise the cavity length using the threshold reduction technique indicated at h) above. Near the optimum cavity length a sudden change in the pre-lase characteristics will be noted. The cavity length must be set to the clean region of pre-lase between the two regions where the relaxation oscillations are undamped. If the cavity length adjusting blocks are no longer close to Brewsters angle then the cavity mirror, (100%, 5m), should be moved. A 4mm change on the cavity length adjusting micrometer corresponds to a cavity length change of half that, i.e. 2mm.

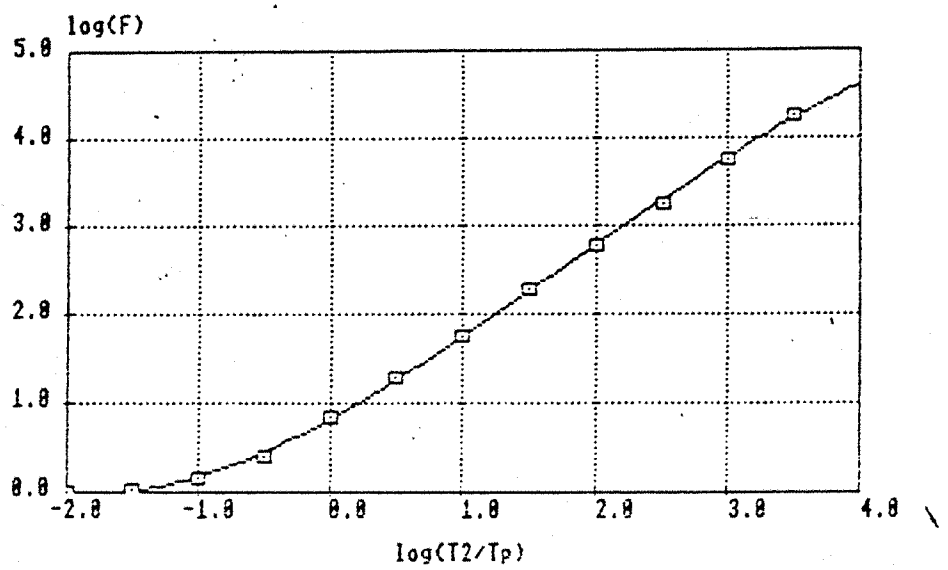
log(F)
5.0
4.0
3.0
2.0
1.0
0.0
-2.0
-1.0
0.0
1.0
2.0
3.0
4.0
log(T2/Tp)

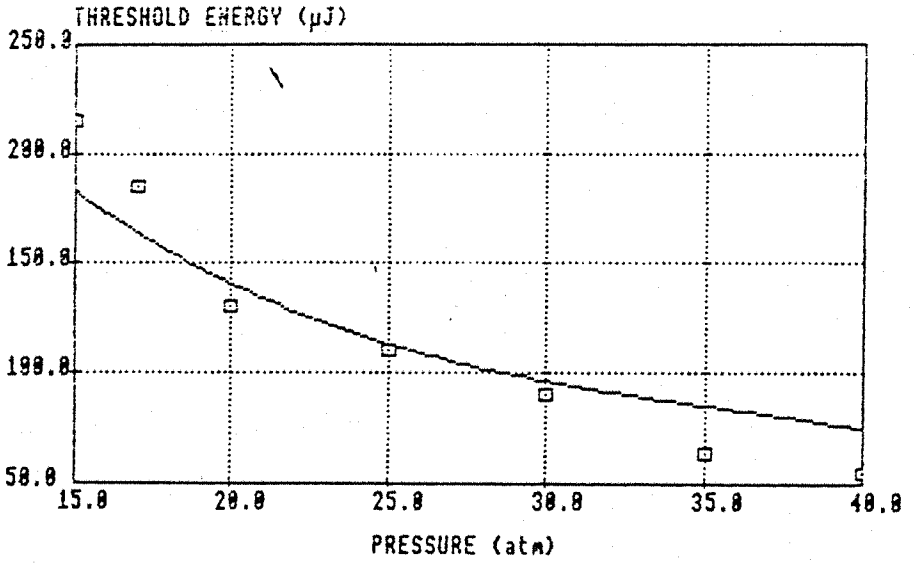
THRESHOLD ENERGY (μJ)
250.0
200.0
150.0
100.0
50.0
15.0
20.0
25.0
30.0
35.0
40.0
PRESSURE (atm)

The following published papers were included in the bound thesis. These have not been digitised due to copyright restrictions, but the links are provided.

https://doi.org/10.1016/0030-4018(83)90198-0

https://doi.org/10.1109/jqe.1986.1072945

**LOW THRESHOLD STIMULATED RAMAN SCATTERING IN GAS-PILLED CAPILLARY WAVEGUIDES. D.C. Hanna and D.J. Pratt. Department of Physics University of Southampton Southampton. S09 5NH.**